A SYSTEMS ANALYSIS OF BIOMASS DENSIFICATION PROCESS

by

SUDHAGAR MANI

M. Tech., Indian Institute of Technology, India, 2000
B. E., Tamil Nadu Agricultural University, India, 1998

A THESIS SUBMITTED IN PARTIAL FULFILLMENT
OF THE REQUIREMENTS FOR THE DEGREE OF

DOCTOR OF PHILOSOPHY

in

THE FACULTY OF GRADUATE STUDIES

(Chemical & Biological Engineering)

THE UNIVERSITY OF BRITISH COLUMBIA

September 2005

ABSTRACT

Pelletizing is a method of densifying biomass. Pellets have low moisture content (about 8% wet basis) for safe storage and a high bulk density (more than 500 kg/m^3) for efficient transport. Biomass pellets that are usually up to 6 mm in diameter and 12 mm long, are uniform in moisture content. They can be handled, transported and fed to boilers and furnaces easily. Manufacturing of pellets involves energy intensive drying, grinding, and pelleting processes. In a typical operation, manufacturing one ton of dried pellets may use 300-3500 MJ for drying, 100-180 MJ for grinding, and 100-300 MJ for densification. The present study investigates the entire densification process using the systems analysis approach and on finding out the best alternative fuel source for biomass drying application with the lowest cost, emissions and energy consumptions.

In this study, biomass drying, size reduction and compaction were studied in detail theoretically and experimentally. Drying of biomass is performed in a direct contact, co-current type rotary drum dryer. Single and triple pass rotary dryers were modeled using the lumped parameter approach. The developed models predicted the temperature and moisture profiles of hot flue gas and biomass particles and the results were in agreement with commercial rotary dryer outlet conditions. Five heating fuel sources for the dryer were compared: natural gas, coal, wet sawdust, dry sawdust and wood pellets. The combustion of fuels was modeled to predict the hot flue gas compositions and fuel requirement for the given dryer inlet conditions. A series of experiments were conducted where biomass samples were ground using a laboratory hammer mill at different screen sizes and moisture contents. Specific energy consumption of grinding biomass was estimated and used to develop the relationship between hammer mill screen size and specific grinding energy data. The laboratory hammer mill energy data were compared with commercial hammer mill data. The ground samples were analysed for particle size distribution, geometric mean particle size, bulk density and particle density.

Biomass grinds were compacted into pellets using a single pelleter unit. Compression data from the experiment were analyzed using several compaction models. Particle rearrangement and elastic and plastic deformation were the predominant compaction mechanisms during the pelleting process. Particle interlocking or local

ii

melting of constituents could have occurred at high pressures and temperatures during compaction, although this phenomenon was not examined in detail. The force-displacement data were collected and analyzed to estimate the specific energy required to compress and extrude biomass materials. It was found that more than 60% of the total energy spent during the extrusion of pellet was to overcome the wall friction. The pelleting energy could be reduced if some processing aids are used without losing the quality of compacted pellets. Or a new compaction unit may be designed and developed to eliminate the friction energy consumed during the compaction process.

To conduct a systems analysis of the entire biomass densification process, a typical wood pelleting plant was chosen to evaluate the total energy consumption, environmental emissions and cost of pellet production using different alternative fuels. The process models developed in the thesis were used to predict the energy consumption and emissions during combustion process. Average emission factors were used from published literature sources to estimate the emissions of trace metals and toxic pollutants. The environmental impacts of the emissions were evaluated based on greenhouse gases, acid rain formation, smog formation and human toxicity impact potentials. A detailed engineering cost analysis was conducted to estimate the pellet production cost using different process options and fuel sources. A multi-criteria decision making method, Preference Ranking Organization Method for Enrichment Evaluation (PROMETHEE) was used to rank fuel alternatives. The best fuel source was selected based on the four main criteria – energy, environmental impacts, economics and fuel quality. It was found that wood pellet or dry sawdust may be the best alternative to natural gas followed by coal and wet sawdust, if all the criteria are weighed equally. The ranking was changed to: 1) coal; 2) dry sawdust; 3) wet sawdust; 4) wood pellet; and 5) natural gas, when the weighting factor for cost was doubled.

TABLE OF CONTENTS

LIST OF TABLES

LIST OF FIGURES

ACKNOWLEDGEMENT

Finally, I would like to extend my special thanks to my parents and relatives for their love and continuous support during my course of study. Many thanks to my beloved wife, Dr. S. Jaya for her understanding, support and motivation during the course of study.

CHAPTER 1

INTRODUCTION

Biomass is described as all organic (plant and animal) matter of both live and dead biological organisms on the earth's surface. It is considered as a form of stored solar energy, which is captured through the process of photosynthesis in plant growth. It also includes field and forest residues, waste products from the wood processing industries, animal manures and other sources. Biomass can substitute fossil fuel resulting in a net reduction in greenhouse gas emissions. This renewable energy can be recovered by combustion process or by conversion of biomass into usable form, for example, ethanol, electricity, bio-oils or producer gases. The net energy available from biomass ranges from about 20 MJ/kg for dry plant matter to 55 MJ/kg for methane, as compared with about 27-32 MJ/kg for coal (Twidell, 1998; Demirbas, 1998a; Demirbas, 1998b).

At the time of its collection, biomass may have a moisture content ranging from 10 to 75% (wb) depending on the type of biomass and harvesting time (Pordesimo et al., 2004). Transportation and storage of high moisture biomass are difficult for complete utilization. High moisture biomass is susceptible to mold growth and spoilage. The elevated moisture content in biomass not only reduces net energy but also increases the size of the equipment required to convert biomass energy into useful form (Kinoshita, 1988). Therefore, drying of biomass is an important operation of any biomass conversion process.

Biomass has low bulk density. This causes major problem during storage, handling and transportation for further processing. The lowest bulk densities are around 40 kg/m³ for loose straw and bagasse; the highest levels are around 250 kg/m³ for some wood residues (Tripathi et al., 1998). Thus gain in bulk densities of 2-10 times can be expected from densification. Densification involves the use of some form of mechanical pressure to reduce the volume of biological matter, which is easier to handle, transport and store than the original material.

1

1.1 Description of a Densification Process

A typical layout of biomass densification system is shown in Figure 1.1. A biomass densification system consists of three major unit operations namely, drying, size reduction and densification (pelleting). The high moisture biomsss is first dried in a rotary drum dryer to a moisture content of about 10% (wb). The drying medium is the flue gas from the direct combustion of natural gas or other fuel sources. A typical rotary dryer consists of a cylindrical shell that rotates along its longitudinal axis. The dryer inside is normally equipped with lifting flights in order to enhance the transport of the material continuously and to increase the contact surface area between the material and the drying medium. Inside the dryer, there are three main transport phenomena occurring simultaneously: transport of wet materials by cascading, heat transfer between the hot gas and the material and moisture transfer from the solids to the drying medium.
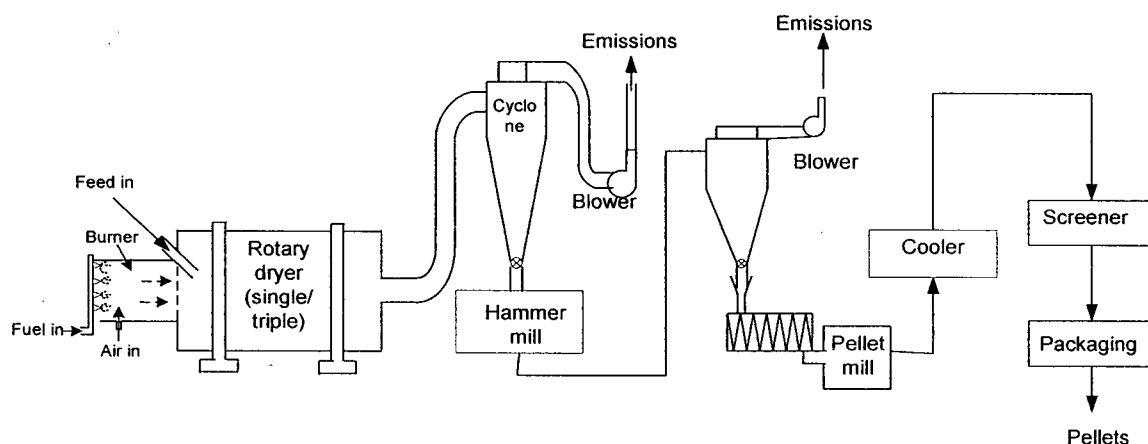
Figure 1.1 Layout of a biomass densification system.

After drying, the biomass is ground in a hammer mill to reduce the particle size suitable for pelleting operation. A hammer mill screen size of 6.4 or 3.2 mm (¼ or 1/8 in) is normally used for size reduction of biomass and compacted into pellets. Biomass pellets are usually up to 6 mm in diameter and 10-12 mm long. In some operations, the ground material is treated with super-heated steam at temperatures above 100°C before pelleting. Steam conditioning of ground biomass is done to supply heat and moisture. It promotes starch gelatinization, releases and activates the natural binders present in the biomass, increases the moisture content and improves the pellet quality (Robinson, 1984). Pellets coming out of the pellet mill are usually at about 70-90°C due to the frictional heat

2

generated during extrusion and material pre-heating. So, pellets are cooled to within 5°C of the ambient temperature. The cooled pellets are conveyed from the cooler to storage areas using mechanical or pneumatic conveying systems. Pellets may be passed over a screen to have fines removed, and weighed before being packed or stored.

1.2 Problem Statement

Poor operation of the rotary dryer would result in high energy consumption and the reduction in product quality. In this system, the fuel burner and the rotary dryer are the major energy intensive units that are directly contribute to emissions from the system. If the biomass has various components (fibers, leaves and stems), the drying rate for each fractions differs. Although many rotary dryer models have been proposed (Sharples et al., 1964; Kamke and Wilson, 1986a, b; Douglas et al., 1993; Wang et al., 1993), little information is available on modeling of rotary dryers. There is not a general theory to describe the mechanism of rotary drying and it seems that specific models for dryers and materials are more useful than any general models. In existing Canadian industries, both single pass and triple pass rotary dryers are often used to dry biomass and forages. A mathematical model representing triple pass rotary dryer is limited in the literature. In this study, an attempt is made to develop a general rotary dryer model and to apply it to triple pass dryer with two biomass fractions. Development of a rotary dryer model can be used to predict the temperature and moisture profiles of hot flue gases and the feed material along the dryer length.

In most rotary dryers used in North America, hot flue gas from direct burning of natural gas is used. But due to the increase in natural gas price in recent years, there is a need to use alternative energy sources suitable for rotary drying operation. Such fuel sources should be capable of satisfying the existing cost factor, environmental regulations and product quality. Coal and biomass can be potential candidates for use as fuel in rotary drying operation. When compared with the cost of natural gas ($8/GJ), coal ($2-3/GJ) and biomass ($2-2.5/GJ) are cheaper (all prices are estimates for 2004).

Hot flue gases from the combustion of coal and other biomass sources may be suitable for direct drying application. However, control of emissions from these sources

3

is important to maintain product quality and environmental regulations. No published literatures are available in direct drying application of hot flue gases from coal or biomass combustion. Simulation of flue gas compositions from coal and biomass sources is essential for exploring the possible application of these fuels.

The grinder and the pellet mill are merely mechanical units and operate with electricity. The hammer mill is used to grind biomass to the particle sizes less than 3 mm. The ground materials are compacted to a density close to the particle density of the material using a pellet mill. Grinding and pelleting operations are also energy intensive operations. NOVEM (1996) reported that energy consumption for grinding and pelleting of biomass would be 100-180 MJ/t and 100-300 MJ/t, respectively. Energy consumption of the grinding operation increases with increasing fineness of biomass particles. During pelleting, the material is compacted into a solid form (pellets) by the application of mechanical force. It is important to undersand the mechanism of biomass compaction process, as it is required to design and develop energy efficient compaction equipment. Although less emphasis is given to modeling aspects of grinding and pelleting operations, they are studied to understand the mechanics of the processes and to estimate the energy requirement.

Biomass densification system also encounters emissions namely, greenhouse gases, particulates and volatile organic compounds from the dryer. In the context of cleaner production, it is important to estimate the emissions from a biomass drying system while using alternative fuel sources. In order to assess and select the best alternative fuel source for the densification process, an environmental systems assessment technique can be used. Environmental Systems Assessment (ESA) technique is a useful tool for quantifying and assessing the environmental impacts from any system (Burgess and Brennan, 2001a and b). Knowledge of environmental and health impacts due to the emissions is also essential to meet the local environmental regulations/standards for the industry. Along with the emission estimates, energy and economic analysis can also be included to analyze the suitability of the system.

By keeping the above critical factors in mind, the present research focuses on the systems analysis approach to model biomass densification process with alternative fuel sources and conduct simulation analysis to assess the energy usage, cost of operation and

4

emissions from the biomass densification system using alternative fuel sources - natural gas, biomass and coal.

1.3 Objectives

The overall objective of this research is to conduct a detailed systems analysis of biomass densification process using alternate fuels by considering technical feasibility, cost, and environmental impacts. The specific tasks of the research are:

1. to develop a mathematical model for a co-current rotary drum dryer to dry biomass fractions and validate the model with industrial data for single and triple pass rotary dryers, to predict the temperature and the moisture profiles of the hot flue gases and the feed material along the length of the dryer and to find out the effect of various process parameters on the dryer model output.

2. to develop a combustion model for natural gas, coal and biomass to predict flue gas compositions and to integrate the combustion model with the drying model to analyze biomass and forage drying system with respect to fuel use and overall emissions;

3. to develop an empirical model to predict the specific energy consumption for biomass grinding using a laboratory hammer mill, and to determine the physical properties of ground biomass namely, particle size distribution, geometric mean diameter, bulk density and particle density.

4. to investigate the compaction mechanism of biomass particles during the pelleting process using different compaction models and to experimentally determine the specific energy required to compress and extrude biomass to produce densified products.

5. to assess the feasibility of using flue gases generated from combustion of different biomass and coal for drying biomass to replace natural gas using the systems analysis approach and to rank the fuel sources based on energy consumption, environmental impacts and economics of producing pellets using the preference ranking organization method for enrichment evaluations (PROMETHEE).

1.4 Scope of this Thesis

The present research focuses on modeling of biomass densification processes using alternative fuel sources and conduct analysis of the entire densification process with respect to energy efficiency, cost and emissions. Equipment and material considered in this research are as follows:

Dryer – rotary drum with single or triple pass arrangement

Grinder – hammer mill

Pellet mill - rotary die 6 mm diameter holes die length 70 mm

Fuels - biomass (sawdust, pellets), coal, natural gas

1.5 Thesis Organization

This thesis is organized in four main chapters followed by conclusions and recommendations. Chapter 2 presents the overview of biomass drying process and rotary dryer modeling approach including the burner model. The burner model calculates the fuel requirement and flue gas composition of the given rotary dryer inputs. Rotary dryer model validation with the industrial and published drying data is discussed. The sensitivity of various process parameters on the model output is also investigated.

Chapter 3 describes the biomass grinding experiments, specific energy consumption for grinding using a laboratory hammer mill and the physical properties of the ground samples. Specific energy requirement of a laboratory hammer mill and the commercial hammer mills are also discussed.

Chapter 4 investigates the compaction mechanism of biomass grinds under different process variables. The chapter also investigates different compaction models, which better explains the compaction mechanism and the pressure-density relationship. Specific energy required for compression and extrusion of biomass grinds are experimentally investigated and discussed.

Chapter 5 describes the environmental systems analysis of the entire biomass densification process to estimate total energy, emissions and cost associated with the production of densified products. Information from the rotary dryer and burner models, specific energy requirement for grinding and compaction are used to calculate the overall

energy and emission inventories. Different scenarios of densification process using alternative fuels are discussed and compared based on the energy, emissions and cost of production. Emission inventory data are further analysed to assess the environmental impacts of using alternative fuels and process modifications. Ranking of different scenarios based on energy, environmental impacts, economics and fuel quality is performed by Preference Ranking Organization METHod for Enrichment and Evaluations (PROMETHEE) using 'Visual Decision Lab' software.

CHAPTER 2

MODELING OF BIOMASS DRYING PROCESS

2.1 Introduction

The moisture content of biomass after harvest is usually high but may decrease during field drying as harvest season progresses. The moisture content of wood-based biofuels (bark, forest residues, and waste wood) typically varies between 50 and 60% (wb). Typical moisture content of the agricultural residues and energy crops vary from 10 to 75% (wb). In order to process biomass into densified products, the feedstock moisture content must be below 15% (wb). In densification plants, direct contact co-current type rotary drum dryers are often used for drying biomass. They are well known to produce uniform product quality because they are characterized by long residence time and relatively good mixing compared with other types of dryers.

As in any dryer, simultaneous heat and mass transfer processes occur in a rotary dryer. Although the mechanism is similar to other drying operations, it is further complicated because of the cascading movement of the materials through the dryer. The cascading cycle of the materials consists of the cascading periods and the resting in flight periods. During the cascading periods, the materials are subjected to heat and mass transfer processes. But in the resting period, the process slows down. Transport of wet material to the dryer exit is achieved, when it is lifted by the flights during the rotating movement, dislodged and falling back as it cascades through the hot air stream. The total amount of heat and mass transferred during the passage of material through the dryer largely depends on the surface area and the contact time between the two phases (Throne and Kelly, 1980; Kelly, 1995). So, knowledge of residence time of the material is important. The heat and mass transfer processes also depend upon the physical properties of the material and the dryer configurations. It is also difficult to describe the heat and mass transfer processes using mathematical equations as it involves not only the properties of feed materials and the drying gases but also the design and operating characteristics and configuration of the rotary dryer (Kelly, 1995; Mujumdar, 2000). However, there are heat and mass transfer models published in literature specific to dryer configurations and materials.
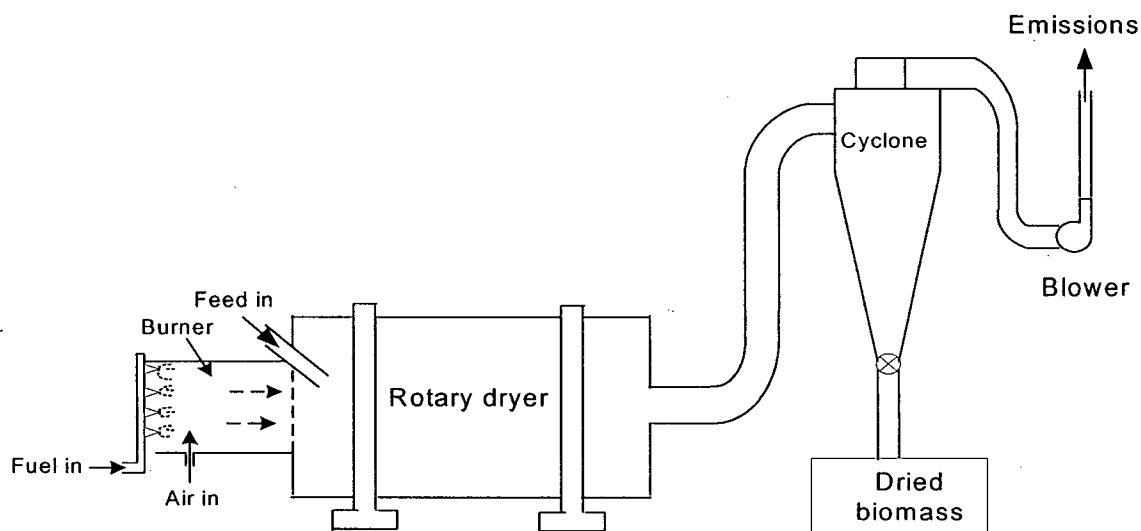
Figure 2.1 Schematic diagram of a rotary drum dryer.

Rotary dryers have been used for many years, but relatively few studies on dynamic modeling and simulation of rotary drying of biomass have been published (Kamke and Wilson, 1986b; Shene et al., 1996; Iguaz et al., 2002; and Iguaz et al., 2003); and are summarized in Appendix I. The objective of this study is to develop a biomass rotary drum drying model that can best predict the dryer outlet conditions with less computational time, so that the model can be used to develop an integrated process systems analysis, apart from its application in the dryer control system design.

Rotary dryers are usually operated with flue gases from direct combustion of natural gas or other solid fuels. The dryer inlet gas temperature and gas flow rate are usually controlled at the burner inlet depending upon the properties of the feed material. This chapter describes the modeling aspects of the solid fuel combustion in the burner and the rotary drum dryer (both single and triple pass system) for drying biomass, solution procedure and model validation. Sensitivity of different dryer operating conditions on the outlet gas temperature and feed moisture content are also analyzed and discussed.

2.2 Combustion Model Development

Solid fuel combustion is a complicated process, which involves drying, pyrolysis and oxidation of pyrolysis gases and carbon. The combustion performance of many biomass fuels has been studied by several researchers (Payne, 1984; Stanzel, 1994; Li et al., 2001). In this work, a simple model representing combustion of various fuels is developed to predict the flue gas temperature and its composition and the fuel requirement. The model can be used in systems analysis to explore usability, emission control options and fuel cost in the rotary drying operation.

A simple combustion reaction model is developed for solid fuels with the following assumptions.

1. Solid fuel is completely combusted into carbon dioxide, water vapor and sulfur dioxide.

2. Nitrogen and other compounds (ash, trace elements) in the fuel are small and they do not affect the oxidation reaction.

Complete combustion of fuels can be represented as

$$
\begin{aligned}
C + O_2 &\rightarrow CO_2 \\
2H + 0.5O_2 &\rightarrow H_2O \\
S + O_2 &\rightarrow SO_2
\end{aligned}
\tag{2.1}
$$

The combustion model is developed based on the heat and mass balance equations to calculate the stoichiometric air requirement, flue gas composition, fuel required for a rotary dryer to dry biomass and drying cost per tonne of water evaporated. The solid fuels considered for this analysis are wood pellets, wet sawdust, and coal. The typical composition of coal, sawdust and wood pellets are shown in Table 2.1. Stoichiometric analysis of natural gas was also performed to compare with combustion characteristics of solid fuels. It was assumed that natural gas contained only methane. The composition of flue gas and the fuel requirement are calculated by assuming a complete combustion process.

In an ideal combustion system, heat released from fuel combustion is completely converted to gaseous products enthalpy, which determines the flue gas temperature. In actual combustion process, there are some energy losses due to incomplete combustion of carbon in the ash, heat loss from ash and fly ash, radiation and convective losses from the

burner (Li et al., 2001). These additional heat losses account for about 10-40% of the fuel heat content depending on the fuel moisture content and type of fuel. In other words, combustion efficiency (recoverable heat) varies from 90-60%. Combustion efficiency is the ratio of recoverable heat to available heat in the fuel.

Table 2.1 Composition of various solid fuels used in the burner.

Composition	Bituminous coal[†]	Sawdust[*]	Wood pellet[*]
Carbon	75.8	49.00	49.50
Hydrogen	5.0	6.72	6.68
Oxygen	7.4	43.70	43.43
Nitrogen	1.5	0.10	0.10
Sulfur	1.6	0.01	0.01
Ash	8.7	0.57	0.38
HHV (MJ/kg)	29.0	19.00	19.40

[†] source: Nevers (2000).

[*] Measured data based on the ASTM standards for solid fuels.

The stoichiometric air fuel ratio (AF_s) can be estimated as:

$$AF_s = \frac{1}{mf_O}\left[\left(\frac{M_{CO_2}}{M_C}-1\right)[C]+\left(\frac{M_{H_2O}}{M_H}-1\right)[H]+\left(\frac{M_{SO_2}}{M_S}-1\right)[S]-[O]\right] \qquad (2.2)$$

where, mf_O is the mass fraction of oxygen in the air, M_i is the molecular weight of component i, and [i] is the mass fraction of component i, in the fuel.

If the fraction of excess air, ϕ is known, actual air-fuel ratio (AF_a) can be estimated as:

$$AF_a = AF_s(1+\phi) \qquad (2.3)$$

It was assumed that the enthalpy contributions from air humidity and flue gas humidity are negligible. If the fuel has a moisture content of m_{fm}, the overall energy balance for the complete combustion of the burner can be written as:

$$m_{fuel}(1-m_{fm})c_{pf}\Delta T_f + m_{fuel}(1-m_{fm})\eta_c LHV + m_{fuel}m_{fm}c_{pm}\Delta T_f + m_{fuel}(1-m_{fm})AF_s(1+\phi)c_{pa}\Delta T_a$$
$$= m_{fuel}m_{fm}c_{pm}\Delta T_{fg} + [[m_{fuel}(1-m_{fm})-[A]]+ AF_s(1+\phi)]c_{pfg}\Delta T_{fg} + [A]c_{pA}\Delta T_A$$
$$----- \qquad (2.4)$$

11

where, m_{fuel} is the mass flow rate of the fuel consumed in the burner in kg/hr; m_{fm} is the moisture content of the fuel in dry basis; η_c is the overall combustion efficiency in fraction, which accounts for heat loss from the burner system; LHV is the lower heating value of the fuel in kJ/kg; c_{pf} is the specific heat of the dry fuel, c_{pw} is the specific heat of water, c_{pfg} is the specific heat of flue gas; c_{pa} is the specific heat of ash in kJ/kg°C; ΔT_f, ΔT_a, ΔT_A, ΔT_{fg} are the temperatures of fuel, air, ash and flue gas respectively in °C; and, [A] is the ash content of the fuel in mass fraction.

It was assumed that the flue gas contains nitrogen, water vapor, oxygen, carbon dioxide and sulfur dioxide. Specific heat of flue gas mixtures is a function of flue gas temperature and can be obtained from Perry and Green (1999). A MATLAB program (The MathWorks Inc., Natick, MA) was written to predict the flue gas composition and fuel requirement of the given solid fuel by specifying the dryer inlet gas temperature and flow rate.

2.3 Rotary Dryer Model Development

Rotary dryers can be modeled as either a distributed parameter system or a lumped parameter system. Distributed parameter systems are defined by partial differential equations. In this case, the system variables depend on both time and space. Distributed parameter models are discretized into differential and/or algebraic equations and the algebraic equations are solved numerically. The distributed parameter model requires high computational time and is difficult to solve. In contrast, lumped parameter systems can be described by ordinary differential equations and the solution can be easily obtained with less computational time.

In this work, a lumped parameter approach is used to develop a rotary dryer model. In the densification industry, both the single and triple pass rotary dryers are commonly used. So, both the single and triple pass rotary drum dryer models are developed. A single pass dryer is first modeled and the model is extended to a triple pass rotary dryer. In both cases, a co-current type direct-fired rotary dryer was considered in modeling the dynamic behavior of the dryer.

2.3.1 Heat and mass balances

In order to develop a mathematical model, the whole dryer is divided into n number of control volumes (Figure 2.2). Heat and mass balance equations are developed for each control volume (Figure 2.3) with the following assumptions:

1. Heat transfer between the hot gas and feed material is by convection. Other heat transfer modes namely conduction and radiation are assumed negligible.

2. Drying of feed materials takes place in the falling rate period, when the initial feed moisture is below the critical moisture content.

3. The angle of repose for biomass particles inside the dryer is assumed constant throughout the drying process.

The moisture balance in the feed and hot gas and heat balance for the feed and hot gas are developed for a given control volume. The mass and heat balance was developed based on the work from Kelly (1995). The developed equations are further extended to other control volumes.

The mass balance in the feed can be written as:

$$\frac{d(m_f)}{dt} = G_{fi} - G_{fo} \tag{2.5}$$

Moisture balance in the feed can be written as:

$$\frac{d(m_f X)}{dt} = m_f \frac{dX}{dt} + X \frac{dm_f}{dt} = G_{fi} X_i - G_{fo} X - R_w m_f \tag{2.6}$$

Moisture balance in the air can be given as:

$$\frac{d(m_a H)}{dt} = m_a \frac{dH}{dt} + H \frac{dm_a}{dt} = G_{ai} H_i - G_a H + R_w m_f \tag{2.7}$$

since the mass flow rate of dry air does not change within the control volume,

$G_{ai} = G_a$.

Heat balance in the product:

$$\frac{d(m_f C_{pf} T_f)}{dt} = m_f C_{pf} \frac{dT_f}{dt} + m_f T_f \frac{dC_{pf}}{dt} + C_{pf} T_f \frac{dm_f}{dt} = G_{fi} C_{pf} T_{fi} - G_{fo} C_{pf} T_f$$
$$+ U_v a V \Delta T_m - R_w m_f \lambda - R_w m_f C_{pv} (T_a - T_f) - Q_l \tag{2.8}$$

Heat balance in the air:

$$\frac{d\left(m_a C_{pa} T_a\right)}{dt} = m_a C_{pa} \frac{dT_a}{dt} + m_a T_a \frac{dC_{pa}}{dt} + C_{pa} T_a \frac{dm_a}{dt} = G_{ai} C_{pa} T_{ai} - G_a C_{pa} T_a$$
$$- U_v aV\Delta T_m + R_w m_f C_{pv} T_a \qquad (2.9)$$
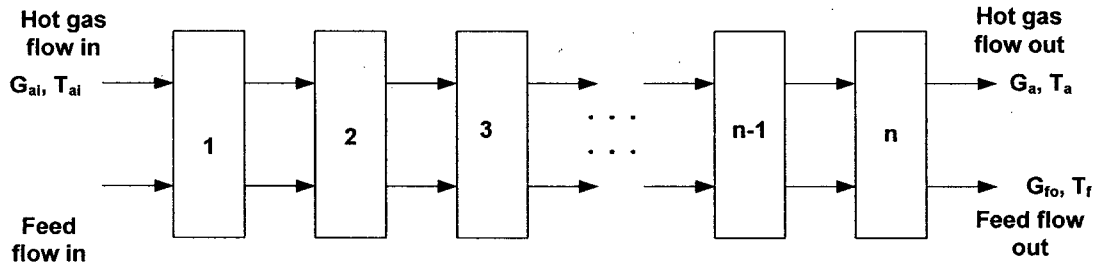
Figure 2.2 Representation of rotary drum dryer sections.
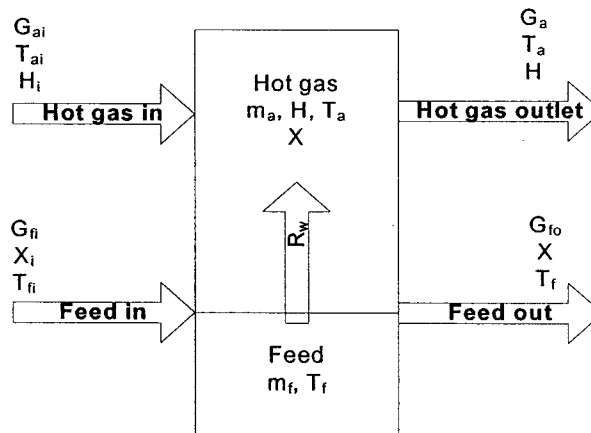
Figure 2.3 Heat and mass balance in a control volume

A set of heat and mass balance equations for each control volume in the dryer was developed. In the case of a triple pass rotary dryer, the entire dryer was stretched outside as shown in Figure 2.4. The heat and mass balance equations were applied to each section of the dryer for analysis. The inner section of the dryer is similar to the single pass dryer. The conductive heat transfer between passes in the triple pass dryer was ignored.

14
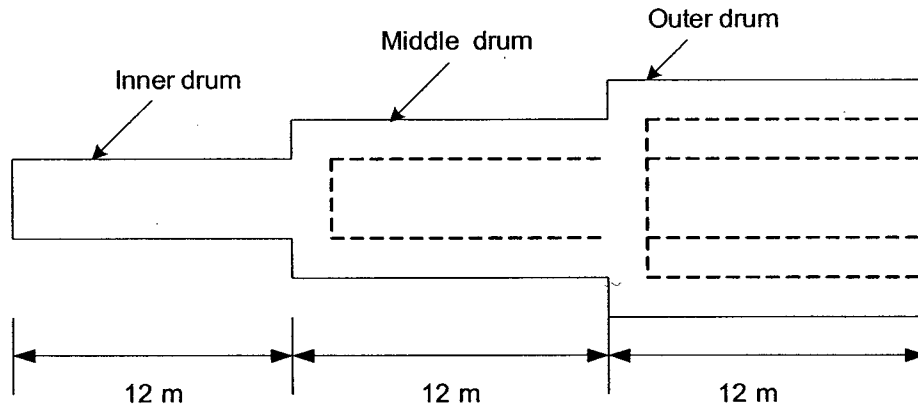
Figure 2.4 Exploded view of a triple pass rotary dryer.

2.3.2 Residence time model

Residence time of particles in the rotary drum is an important parameter in the development of a rotary dryer model. Transport of particles along the length of the dryer takes place by means of cascading action. While cascading, particles travel along the length of the drum in two phases: air borne phase and dense phase. In the air borne phase, particles travel along the drum due to the gravity and hot gas flow. In the dense phase, particles travel by sliding, bouncing and rolling along the drum, which may occur at the bottom of the drum. Even though many studies (Friedman and Marshall, 1949a; Saeman and Mitchell 1954; Schofield and Glikin, 1962; Baker, 1992; Kamke and Wilson, 1986a; Matchett and Baker, 1987, 1988; Matchett and Sheikh, 1990; Sherritt et al., 1993, 1994; Renaud et al., 2000) were carried out to develop a mean residence time model or residence time distribution, the residence time is still determined experimentally in many cases (Alvarez and Shene, 1994b; Renaud et al., 2001). In pilot plant drums, the feed material is stopped suddenly, the drum is unloaded and the material is weighed to experimentally determine the residence of the particles. Knowing the feed rate, the mean residence time can be calculated from equation 2.10. The quantity of material in the drum during steady state operation is called drum holdup, H_d. For a fixed material feed rate f, the mean residence time,τ of the material is given as:

$$\tau = \frac{H_d}{f}$$ (2.10)

Where, τ is the mean residence time in s; H_d is the drum hold up in kg; and, f is the feed rate of the material in kg/s.

In the present study, the drum slope is zero and particles are transported only in the air borne phase. The mean residence time for a rotary dryer having the drum length, L, can be written as

$$\tau = \frac{L}{(\text{Cascade length})_{ave}}(\text{Cascade time})_{ave} \tag{2.11}$$

where (cascade length)$_{ave}$ is the distance along the drum; the average particle progresses with each cascade (m); and, (cascade time)$_{ave}$ is the time taken by the average particle for each cascade (s). The development of the residence time model for the biomass particles is given below.

2.3.2.1 Single pass rotary drum dryer

Cascading length of a particle can be determined by force balance of the particle in the drum (Schofield and Glikin, 1962; Kamake and Wilson 1986a; Baker, 1992). Figure 2.5 shows the cascading motion and forces acting on a single spherical particle.
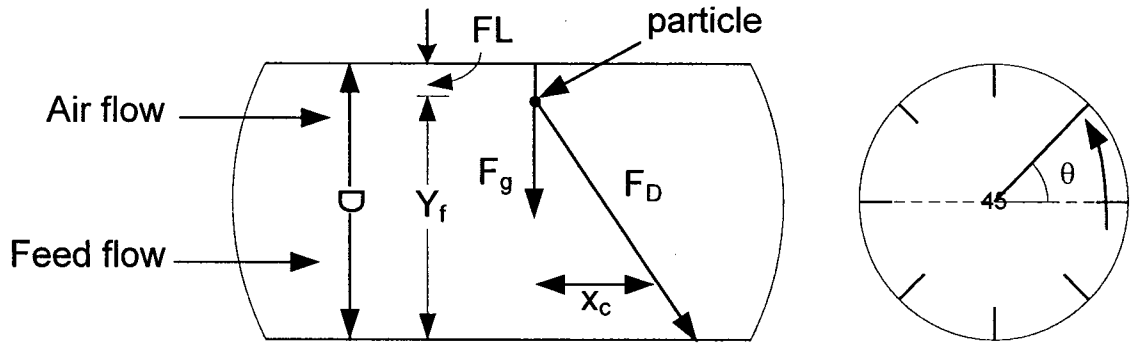
Figure 2.5 Cascading of single pass rotary dryer.

The forces acting on the individual particles are the gravitational force, F_g acting vertically downward and the drag force, F_D, acting in a drum axial direction. Applying Newton's second law of motion to the particle in the axial direction yields:

$$F = ma = F_D \tag{2.12}$$

$$V_p \rho_p \left(\frac{d^2 x_c}{dt^2} \right) = C_D \rho_a A_p \left(\frac{\left(v_a - v_{px} \right)^2}{2} \right)$$
(2.13)

where, V_p is the volume of the particle in m^3, Ap is the particle surface area in m^2, C_D is the drag coefficient, ρ_p is the particle density in kg/m^3, ρ_a is the particle density in kg/m^3 v_a is the hot gas velocity in m/s, and v_{px} is the particle velocity in the axial direction in m/s. Particle velocity (v_{px}) along the axial direction is usually negligible when compared with the gas velocity. So, the relative velocity between gas and particles can be approximated by the gas velocity in the axial direction (v_a-v_{px} $\approx v_a$). For a spherical particle, the equation can be reduced to:

$$\frac{\pi}{6} d_p^3 \rho_p \left(\frac{d^2 x_c}{dt^2} \right) = C_D \rho_a \frac{\pi}{4} d_p^2 \left(\frac{\left(v_a \right)^2}{2} \right)$$
(2.14)

where, d is the diameter of the particle in m. The above equation was integrated twice to yield an equation for determining the cascading length (x_c) of the particle for each cascade, by assuming C_D is independent of v_{px}.

$$x_c = \frac{1}{2} K t_f^2 v_a^2$$
(2.15)

$$\text{where, } K = \frac{3}{4} C_D \frac{\rho_a}{d_p \rho_p}$$
(2.16)

Sawdust particles are irregularly shaped particles and are represented by their geometric mean particle diameter determined by ASAE standard S319.3 (ASAE, 2001b). The drag coefficient for spherical particles is a function of particle Reynolds number (Re_p), is defined as:

$$Re_p = \frac{\rho_a d_p \left(v_a - v_p \right)}{\mu_a} \cong \frac{\rho_a d_p v_a}{\mu_a} \qquad \text{Since, } v_a >> v_p$$
(2.17)

where, Re_p is the particle Reynold's number, μ_a is the viscosity of air in Pa s and v_p is the particle velocity in m/s.

For spherical particles, the drag coefficient can be obtained from the following relationship (Haider and Levenspiel, 1989):

$$C_D = \frac{24}{Re}\left[1 + 0.1858\,Re^{0.6529}\right] + \left(\frac{0.4373}{1 + \dfrac{7185}{Re}}\right) \qquad Re < 260,000 \qquad (2.18)$$

Cascading time of particles is equal to the time spent by the particle in the flight and the time required to fall from the flight to the drum base. The angle of particle fall from the flight occurs approximately at the angle of repose of the material. Kamke (1984) used a photographic technique to study the kinetic angle of repose for sawdust and found it to be around 82.6°. In this study, the kinetic angle of repose for sawdust was assumed as 80°. The time required for the particle to travel, t_r in the flight can be represented by the following:

$$t_r = \frac{90 + \theta}{360N} \qquad (2.19)$$

Where θ is the kinetic angle of repose of the material, in degree; N is the drum speed in rpm. Assuming the vertical drag force is negligible, the time required for the particle to fall from the flight to the drum base due to gravity can be represented as:

$$t_f = \sqrt{\frac{2Y_f}{g}} \qquad (2.20)$$

where Y_f is the length of fall of particles and g is the acceleration due to gravity (9.81 m/s^2). The length of fall of a particle is given as:

$$Y_f = \frac{D}{2} + \left(\frac{D}{2} - FL\right)\sin(\theta) \qquad (2.21)$$

The cascading time of the particle is equal to:

$$t_c = t_r + t_f = \frac{90 + \theta}{360N} + \sqrt{\frac{2Y_f}{g}} \qquad (2.22)$$

The mean residence time for a rotary dryer having a drum length, L, can be written as:

$$\tau = \frac{L}{\dfrac{KY_f v_a^2}{g}}\left(\sqrt{\frac{2Y_f}{g}} + \frac{90 + \theta}{360N}\right) \qquad (2.23)$$

2.3.3.2 Triple pass rotary drum dryer

In the case of a triple pass dryer, the rotary drums are concentrically arranged as shown in Figure 2.6. The movement of particles was considered separately for each drum section. Two types of particle shapes were considered, a disk and and a cylinder in order to simulate the shape of alfalfa leaves and stems, respectively. The drag force equations were modified for each particle shape accordingly. The drag coefficients for the cylindrical and disk shaped particles were obtained from Cooper and Alley (2002). For the inside drum section, equation 2.23 can be used to estimate the residence time of particles, as it is similar to a single pass drum. For the middle and outer drums, the cascading length and cascading time equations were modified based on the drum dimensions, hot gas velocity, type of particles and particle cascading patterns.

The travel pattern of particles between the inner and middle drum is represented in Figure 2.7. Similar pattern of particle transport is also assumed between the middle and the outer drum. The cascading length and time for both leaves and stems are summarized in Appendix II.
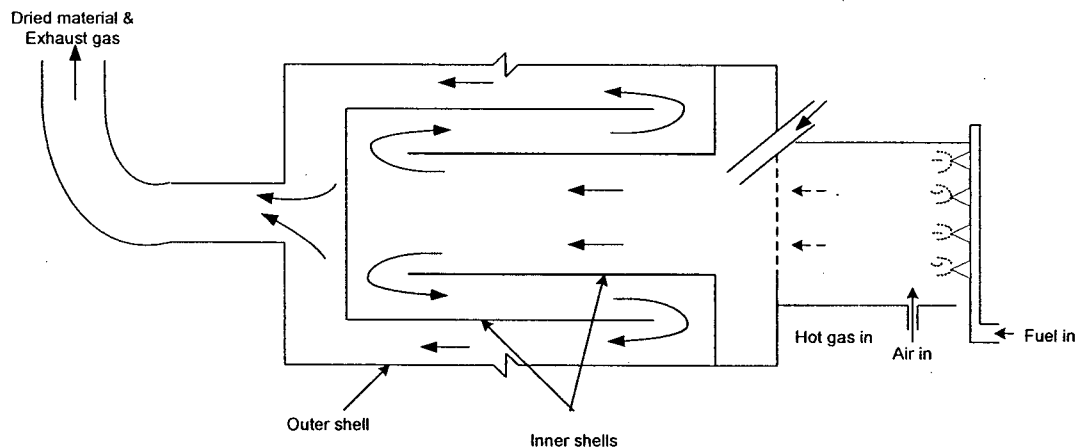
Figure 2.6 Schematic diagram of a triple pass rotary dryer.
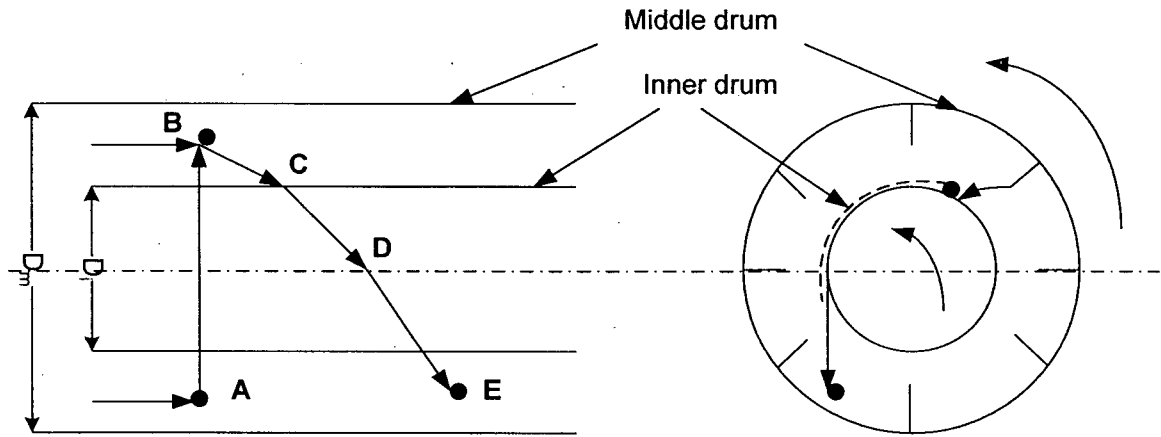
Figure 2.7 Pathway of particle transport in the middle drum.

2.3.3 Volumetric heat transfer coefficient

Heat transfer to the particles is mainly by convection from hot gases. Although the heat that may be transferred indirectly through the drum and flights is neglected in this study, it can be calculated, if the properties of the biomass and the temperature information are known. The mode of heat transfer by conduction may be significant, if a large amount of particles is in contact with the rotary drum as in the case of rotary kilns where, the conduction and radiation mode of heat transfer may be very significant (Boateng and Barr, 1996). In the case of rotary dryers, due to low flue gas temperature and high gas to solid ratio, conduction and radiation modes of heat transfer are less dominant. The rate of heat transfer between the air and the particles is defined by the equation:

$$Q = hA_s \Delta T_m \tag{2.24}$$

where, A_s is the total surface area of all the particles in contact with the gas; h is the convective heat transfer coefficient between the particle and the hot gas. The total surface area of the particles in the gas stream of the dryer is difficult to measure due to the irregularity of particle shape and wide range of particle size distribution. So, the heat transfer coefficient for the rotary dryer is often defined by the overall volumetric heat transfer coefficient, U_{va} (W m^{-3}K^{-1}), which is defined as the rate at which heat is transferred in a unit volume of the drum under a unit temperature difference driving

20

force. The relationship between the volumetric heat transfer coefficient and the convective heat transfer coefficient can be described as:

$$U_{va} = \frac{hA_s}{V}$$

(2.25)

Many relationships for the volumetric heat transfer coefficient were found in literature (Friedman and Marshall, 1949b; McCormick, 1962; Myklestad, 1963a; Kamke and Wilson 1986b; Alvarez and Shene, 1994a; Iguaz et al., 2003). A simple relationship given by Myklestad (1963a) is widely used to model rotary dryers.

$$U_{va} = kG^n$$

(2.26)

Constants k and n had the values of 423 and 0.8 respectively. This equation, fitted for well for air mass velocity range of 4000 – 8000 kg/m² h, which was used in the current simulation. It is important to point out that the correlation was obtained considering dryers working in underload conditions. The correlation gives satisfactory results for steady state consideration, but it does not reflect the dynamic behavior of the heat transfer rate in a rotary dryer when the rotational speed of the drum and holdup changes. A recent study by Alvarez and Shene (1994a, b) concluded that the volumetric heat transfer coefficient depends on the gas mass rate density mainly for both heating and drying situations.

2.3.4 Drying kinetics

Drying of highly moist materials takes place in two stages: constant rate period and falling rate period. During the constant rate period, free water is evaporated from the surface of the material. During the falling rate period, water evaporation rate is controlled by diffusion mechanism. The inner moisture is first transported to the particle surface by diffusion and evaporated. In this study, the falling rate period of drying is considered. The falling rate of drying can be described by a transient state diffusion equation based on Fick's second law.

$$\frac{\partial X}{\partial t} = \frac{\partial}{\partial z}\left(D_L \frac{\partial X}{\partial z}\right)$$

(2.27)

Where, D_L is the diffusivity of moisture in the solids. The above equation can be applied successfully for the defined solid co-ordinates. For the sake of simplicity, the following drying model has been used for biological materials (Sokhansanj et al., 1993), in which the rate of drying is assumed to be proportional to the difference between the moisture content and equilibrium moisture content of the particles:

$$R_w = k_d (X - X_e)$$ (2.28)

where, R_w is the moisture evaporation rate in kg of water evaporated/s. The drying constant, k_d, and the equilibrium moisture content, X_e, are functions of the drying gas temperature. The above equation has been successfully used for many agricultural and forage materials (Nellist, 1976; Jayas and Sokhansanj, 1989; Sun and Woods, 1994; Sokhansanj and Patil, 1996). The drying constant k_d can be usually correlated with drying gas temperature by the Arrhenius equation as follows:

$$k_d = a_0 \exp\left(-\frac{b_0}{T_a + 273} \right)$$ (2.29)

where, k_d is the drying constant in 1/s, T_a is the gas temperature in °C and a_0 and b_0 are constants.

2.3.5 Industrial data collection and analysis

Validation of the rotary dryer models was performed using the industrial drying data collected from the commercial rotary drum drying plants. Single pass dryer model was validated with sawdust drying data collected from the Princeton Wood Pellet Plant, Princeton, BC. Since the biomass drying data for the triple pass rotary dryer was not available, previously collected alfalfa drying data was used for model validation. The drying data were collected from the Tisdale Alfalfa Pellet Plant, Tisdale, SK.

2.3.5.1 Single pass rotary dryer

In order to solve and validate the single pass rotary dryer model, sawdust drying data from the commercial rotary dryer was used. The plant dries sawdust from about 40% to10% (wb) moisture content using a single pass rotary drum dryer. The dryer dimensions and the inlet conditions were given in Table 2.2. Sawdust samples were collected both at the dryer inlet and outlet for moisture content, bulk density, particle size measurements.

The gas temperatures at the dryer inlet and outlet and gas flow rate were also measured for model validation.

Table 2.2 Specifications of the single pass rotary dryer and inlet conditions.

Specifications	Values
Dryer diameter (m)	3.8
Dryer length (m)	12.8
Drum speed (rpm)	8.75
Drum slope (degree)	0
Feed flow rate (kg/s)	1.16
Hot gas flow rate (m^3/s)	16.5
Hot gas inlet temperature (^{o}C)	255
Feed moisture (% db)	67

Samples collected from the Princeton Pellet Plant were analyzed for moisture content, particle size distribution, mean particle size and bulk density. Moisture content of sawdust was determined according to ASAE standard S358.2 FEB 03 for forages (ASAE, 2001c). A sample of 25 g was oven dried for 24 h at 105 ± 3°C. The moisture content was reported in percent wet basis. For bulk density measurement, a four-litre volume container was filled with sawdust and the top surface was levelled. The material mass was measured on an electronic balance. Bulk density was calculated as the mass of the sample over the volume of the container and expressed in kg/m^3. Particle size distribution of the sawdust sample was determined based on the sieve analysis method. The particle size was determined according to ANSI/ASAE standard S319.3 JUL 97 (ASAE, 2001b). The geometric mean diameter (d_{gw}) of the sample and geometric standard deviation of particle diameter (S_{gw}) were calculated according to the aforementioned standard. The properties of sawdust and moisture relationships used in the dryer validation are given in Table 2.3. The specific heat and drying rate of sawdust used in the dryer simulation were also reported in Table 2.3.

Table 2.3 Summary of material properties used in the rotary dryer simulation.

Properties	Formulae or values	Sources
For sawdust		
Bulk density (kg/m^3)	180	Measured
Particle size (mm)	1.5 mm	Measured
Specific heat (kJ/kg C)	$C_{ps} = \dfrac{C_{drywood} + 4.19X}{1+X}$ $C_{drywood} = 1130*(1+0.0043T)$	
Equilibrium moisture content, X_e (db)	$RH = \exp\left[-0.0304(\exp(5.0))^{\left(1-\frac{X_e}{0.304}\right)}\right]$	Nelson (1983)
Drying constant	$k_d = 10\exp\left(\dfrac{-400}{T_a}\right)$	Plumb et al. (1978)
For alfalfa leaves		
Bulk density (kg/m^3)	$\rho_{bl} = 40.64\exp(0.737X)$	Sokhansanj & Patil
Particle shape	Disc	(1996)
Particle size (mm)	22x12x0.5 (axbxt)	
Drying constant	$k_d = 0.09*\exp\left(\dfrac{-197}{T_a}\right)$	Wood & Sokhansanj (1990)
For alfalfa stems		
Bulk density (kg/m^3)	$\rho_{bs} = 63.98\exp(0.38X)$	Sokhansanj & Patil
Particle shape	Cylindrical	(1996)
Particle size (mm)	30x3 (lxd)	
Drying constant	$k_d = 0.074*\exp\left(\dfrac{-236}{T_a}\right)$	Wood & Sokhansanj (1990)
Equilibrium moisture content	$X_e = \dfrac{X_m Ca_w}{(1-RH)[1+(C-1)RH]}$ $X_m = 3.9229\text{x}10^{-4}\exp\left(\dfrac{1858.8}{T_a}\right)$ $C = 323.177\exp\left(\dfrac{974.55}{T_a}\right)$	Guthrie & Collins (1965); Iguaz et al. (2002).

2.3.5.2 Triple pass rotary drum dryer

The triple pass rotary drum dryer model was validated with the alfalfa drying data, collected at an alfalfa pelleting plant, located in Tisdale, Saskatchewan. The plant has a triple pass rotary drum dryer for drying chopped alfalfa. The dryer is attached with a natural gas burner, which produces about 600°C hot flue gases. The dryer dimensions and inlet conditions are given in Table 2.4. The physical properties and the drying kinetics of alfalfa leaves and stems used in the simulation are given in Table 2.3.

Table 2.4 Specifications of the triple pass rotary dryer.

Specifications	Values
Outer drum diameter (m)	2.5
Middle drum diameter (m)	1.75
Inner drum diameter (m)	1
Dryer length in each pass (m)	12
Drum speed (rpm)	8
Air flow rate (m³/s)	16.67
Feed rate (kg/s)	1.2

2.3.6 Solution procedure

The set of differential equations for each control volume was extended to n number of control volumes. The number of control volumes used in the simulation model was set at 10, as it was adequate to predict the results. A single pass rotary dryer (SPRD) simulation model program was written using a MATLAB programming tool. The simultaneous differential equations were solved by variable step numerical method (Fourth order adaptive Runge-Kutta method). The program first calculates the flue gas compositions and fuel requirement for the given dryer conditions. The residence time of the particle is calculated for the given dryer dimensions and particle properties. Finally, the flue gas and feed temperatures, feed moisture content and flue gas humidity were predicted along the dryer length. The drying kinetics of the material and volumetric heat transfer coefficients was calculated from function files and incorporated into the main program for temperature and moisture profile predictions. In the case of a triple pass

25

rotary dryer model, the entire dryer was divided into 12 control volumes and the set of differential equations were solved for each control volume to predict the results. A separate triple pass rotary dryer (TPRD) model program was written with two different particle shapes. The MATLAB program codes for single and triple pass rotary dryers are given in Appendix III.

2.4 Results and Discussions

This section presents the simulation results for the burner and single pass rotary drum dryers and discusses the rotary dryer model validations. The effect of process parameters on the rotary dryer outputs was also discussed. The simulation results obtained from the triple pass rotary dryer models were validated with the industrial drying data.

2.4.1 Single pass rotary dryer

Single pass rotary dryer model was integrated with the combustion model to predict the fuel requirement, flue gas compositions and the temperature and moisture profiles of the hot flue gas and the biomass material along the length of the dryer. First of all, the combustion model results for various fuel sources were provided and the dryer model results were discussed.

2.4.1.1 Combustion model results

The heat and mass balance equations for the combustion process was solved using a root finding method using MATLAB software. The ultimate analysis of the solid fuels given in Table 2.1 was used to predict the flue gas composition and fuel requirement for the given dryer conditions. In the case of natural gas as the fuel, a separate program was written to calculate the air requirement, flue gas composition and fuel requirement. The higher heating value of solid fuels drops as the moisture content of the fuel increases. So, the effect of moisture on fuel heating value was taken into consideration. Table 2.5 shows the stoichiometric air requirement for various fuels, fuel flow rate, fuel cost, and flue gas composition. The results were obtained for drying sawdust at the rate of 7.8 t/h with 255°C gas temperature. The flue gas composition for bituminous coal was closely similar to the flue gas composition of Pittsburgh bituminous coal. The ultimate analysis of the

coal was also similar (Senior et al., 2000). In the current analysis, the bituminous coal has a sulphur content of 1.6%. However, the sulphur content of bituminous coal in Canada is in the range of 0.2 to 1.2% (Walker, 2000). Most of the thermal coals mined in Western Canada have very low sulphur content of 0.4 to 0.5% (Grieve et al., 1996). If the sulphur content of coal is assumed as 0.4%, the flue gas would have contained about 35 ppm of sulphur dioxide for the given dryer inlet gas temperature. Thermal coal produced in Western Canada may be utilized for direct process heating applications. However, application of flue gas from direct combustion of coal should not be recommended without any detailed research on potential emission of toxic elements and the toxicity of the material after drying.

Table 2.5 Results from combustion simulation of various fuels.

Conditions	Natural gas	Bituminous coal	Saw dust	Wood pellet
Fuel moisture content (% wb)	---	2	40	6
Stoichiometric air- fuel ratio (wt)	17.4	10.2	3.7	5.9
Actual air –fuel ratio (wt)	186	97	35	68
Flue gas temperature (°C)	255	255	255	255
Combustion efficiency (%)	90	80	60	80
Fuel required (kg/hr)	223	428	1187	605
Fuel cost ($/t)	8.5/GJ	60	20[*]	120[*]
Drying cost ($/t of water evaporated)	40	10	10	30
Flue gas composition				
Carbon dioxide (vol %)	1.33	2.1	2.2	1.8
Oxygen (vol %)	18.1	18.4	17.8	18.6
Nitrogen (vol %)	77.0	77.5	75.3	76.8
Water vapor (vol %)	3.5	2.0	4.7	2.7
Sulfur dioxide (ppmv)	0	150	2	0

*Price quote is from Princeton co-generation pellet plant.

In this system, the burner produces the flue gas with the temperature of 255°C, which may be an insufficient way of obtaining such a low flue gas temperature to dry biomass. One of the alternative ways to obtain such a low temperature is using the flue

gases released from the cogeneration systems. Cogeneration plants usually releases the flue gases from the power turbines at about 200 to 300°C, which may be utlized for drying biomass. Since the biomass densification plant also consumed electricity to run hammer mill, pellet mill and other handling equipment, a cogeneration system may be the right choice to utilize both the power and heat energy.

2.4.1.2 Rotary dryer model validation

The dryer inlet conditions and dimensions summarized in Table 2.2 were used to run the SPRD model. The model predicted both the temperature and moisture profiles of the hot gas and feed materials, respectively along the entire dryer length. Figure 2.8 shows the moisture profile of the feed material and hot gas. At the inlet section of the dryer, the drying rate is high due to the high inlet gas temperature and heat transfer rate. Within the 2-m length of the dryer, more than 50% of the water is evaporated from the feed material and it tends to decrease afterwards. Figure 2.9 shows the temperature profile of the hot gas and feed material along the dryer length. The heat transfer rate is at maximum at the inlet because of the great difference between the hot gas and feed temperatures. As a result, the feed material temperature also increases. As the material moves forward, the heat transfer rate decreases and the material heating slowed down.

Simulation model results were validated with the experimental data collected in the sawdust drying plant. Since the temperature and moisture data along each section of the dryer is difficult to measure, the dryer outlet conditions are used for comparison, as done previously by other researchers to validate the rotary dryer model (Wood and Sokhansanj, 1990; Douglas et al., 1993). Table 2.6 shows the predicted and measured exit conditions of the rotary dryer. The predicted outlet feed moisture was slightly lower than the measured feed moisture, while the predicted outlet gas temperature was slightly higher than the measured temperature. Feed temperature at the dryer outlet was not measured in the industrial plant. However, it is expected that the feed temperature at the dryer outlet would be 10-20°C lower than the outlet gas temperature (Nonhebel and Moss, 1971). The dryer model predicted a feed temperature of about 75°C at the outlet. The predicted model results were in reasonable agreement with the measured sawdust drying data. So, the model can be successfully used to predict the temperature and moisture profiles.
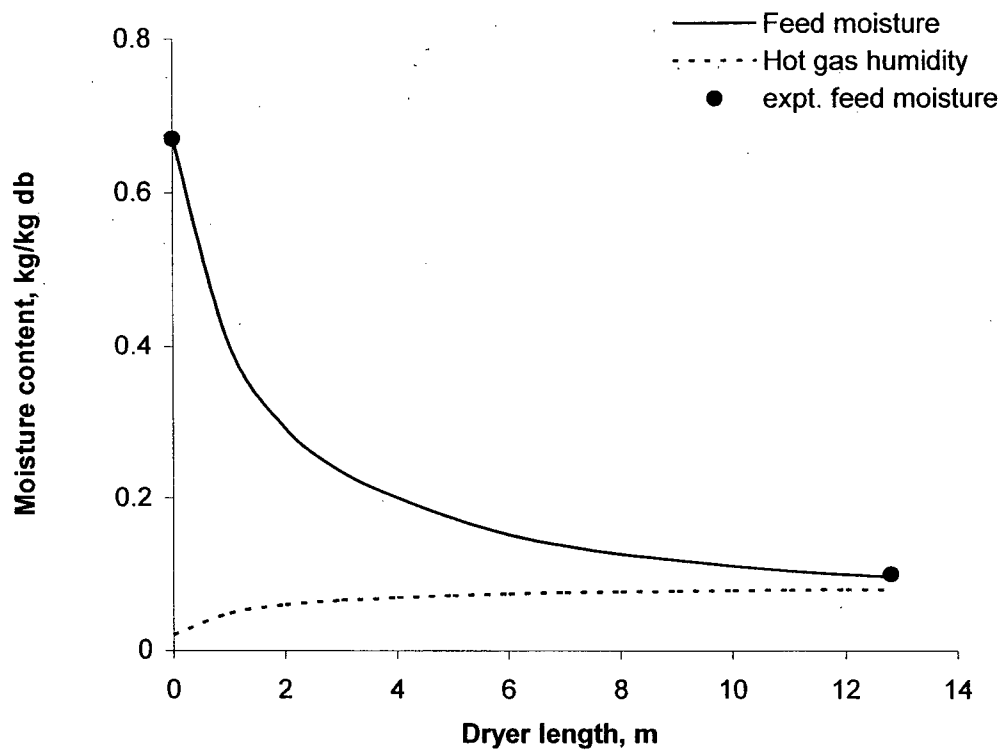
Figure 2.8 Moisture profiles of sawdust and hot gas along the dryer length.
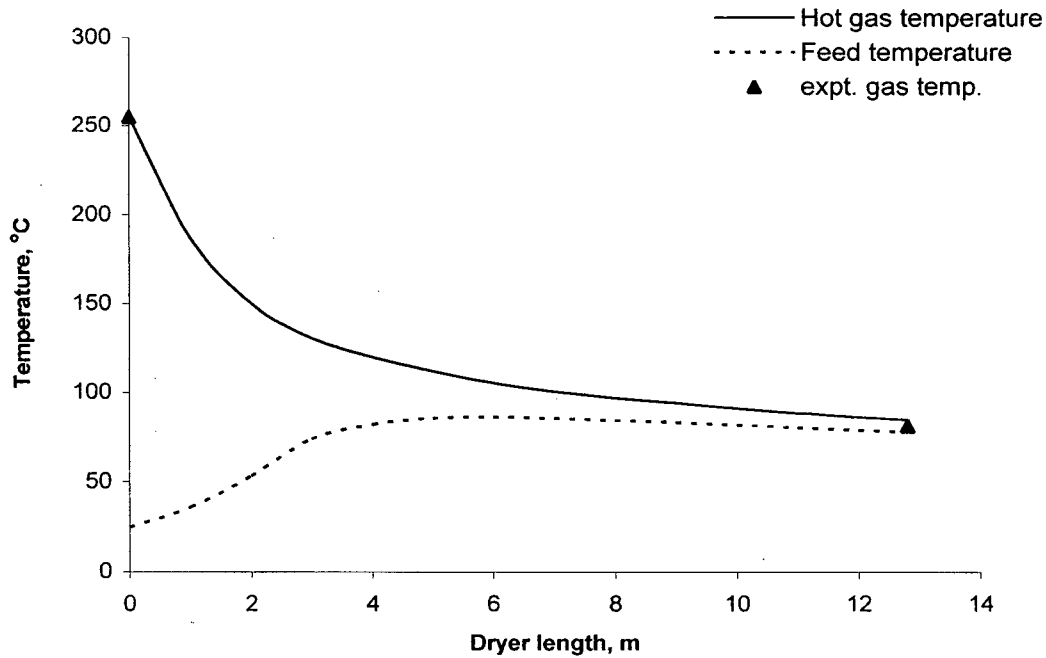
Figure 2.9 Temperature profiles of hot gas and feed material along the length of the dryer.

Table 2.6 Inlet and outlet conditions of the rotary dryer.

Conditions	Inlet conditions	Outlet conditions	
		Predicted	Measured
Hot gas temperature (°C)	255	84	82
Feed moisture (kg/kg)	0.67	0.09	0.1

2.4.1.3 Sensitivity analysis

The dynamic behavior of a rotary dryer is influenced by the feed initial moisture content, feed rate, hot gas temperature and hot gas flow rate, drum length, drum diameter, drum slope, drum speed and heat loss from the drum. In order to further study the effect of operating conditions on the feed moisture and gas temperature at the dryer outlet, each operating parameters: the gas flow rate, gas temperature, inlet feed moisture, drum speed was varied by 40% below and above the base condition, while all other parameters were kept constant. Table 2.7 shows the summary of rotary dryer parameters used in developing Figures 2.10 and 2.11. The results showed that the inlet gas temperature has the highest effect on both exit feed moisture and gas temperature followed by gas flow rate, inlet feed moisture and drum speed. It is observed that an increase in inlet air temperature increases the outlet gas temperature and decreases the moisture content of the feed material considerably. Similar dryer behavior was reported by Kamke and Wilson (1986b) and Iguaz et al., (2003). A decrease in hot gas flow rate increases the outlet feed moisture content due to the low volumetric heat transfer rate. Volumetric heat transfer coefficient for the rotary dryer is directly related to the gas flow rate. So, an increase in hot gas flow rate increases the volumetric heat transfer coefficient and vice versa.

Table 2.7 Summary of rotary dryer parameters used in the sensitivity analysis.

Parameters	-40% from the base value	Base value	+40% from the base value
Inlet gas temperature (°C)	153	255	357
Hot gas flow rate (kg/s)	7.8	13	18.2
Inlet feed moisture (kg/kg)	0.40	0.67	0.94
Drum speed (rpm)	5.25	8.75	12.25
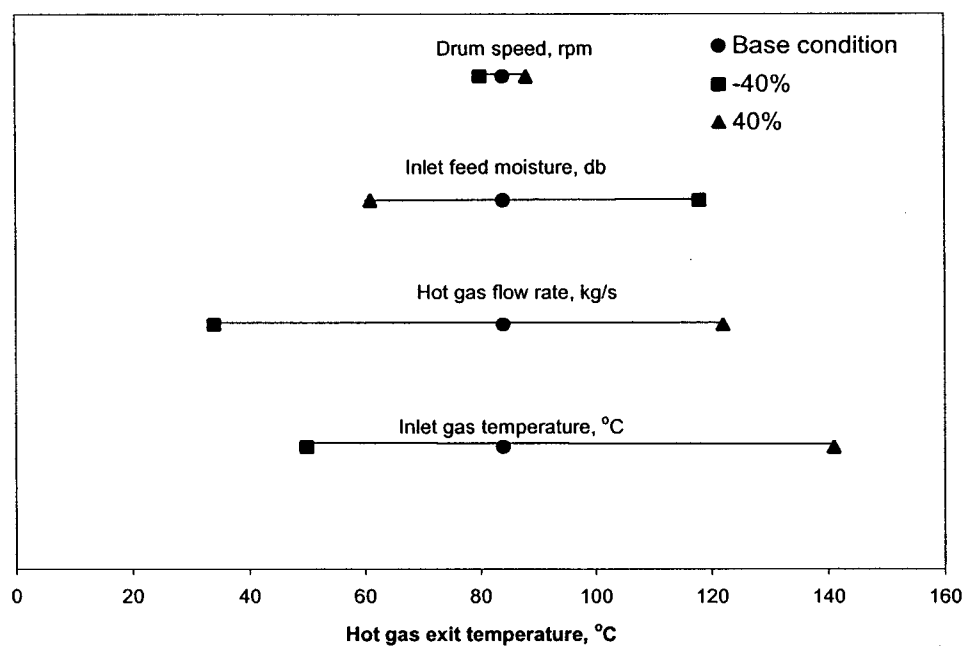
Figure 2.10 Effect of variations of operating parameters for the rotary dryer by 40% above or below the hot gas exit temperature.
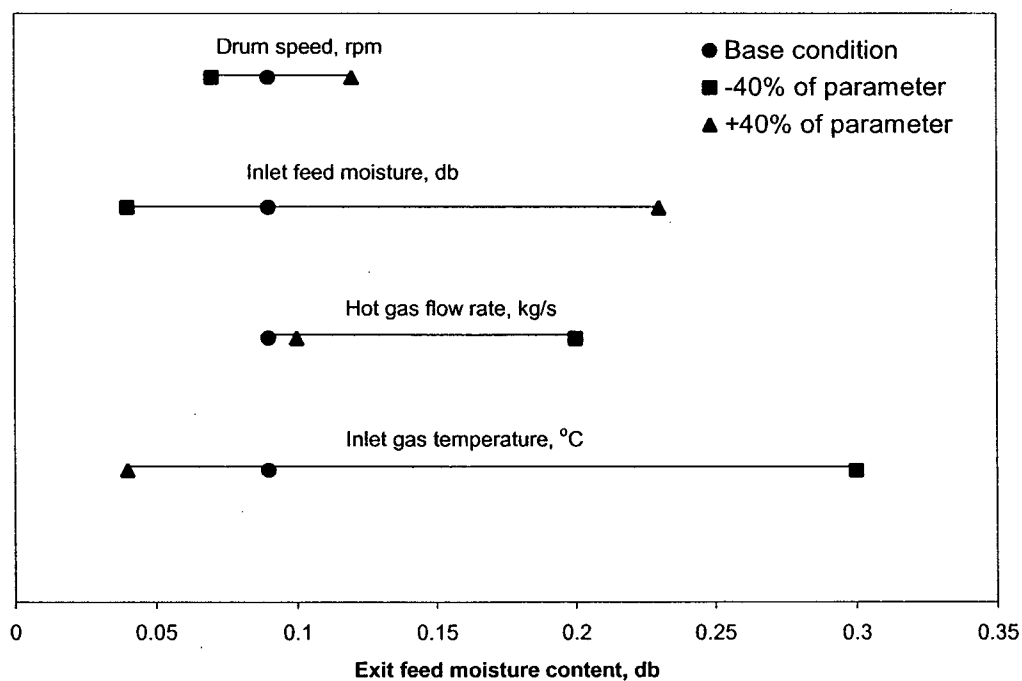
Figure 2.11 Effect of variations of operating parameters for the rotary dryer by 40% above or below the exit feed moisture content.

2.4.2 Triple pass rotary dryer

Triple pass rotary dryer model was validated with the alfalfa drying data due to the non-availability of biomass drying data. Two particle fractions- stems and leaves were considered in the analysis.

2.4.2.1 Model validation

The SPRD model equations were extended to a TPRD and a separate MATLAB program was written to predict residence time and temperature and moisture profiles of hot gas and feed materials. Residence time for both alfalfa leaves and stems in each section were estimated and integrated to the heat and mass transfer models. The program was used with known inlet conditions to predict the outlet conditions. The simulation results were compared with the experimental data. The shape of the alfalfa leaves was assumed as elliptical disks, and stems were assumed as cylinders. For both leaves and stems, the model was used to predict the outlet feed moisture content, and feed and hot gas temperature. Experimental data were collected for drying alfalfa stems and leaves in a triple pass rotary dryer. The drying kinetics of the alfalfa stems and leaves were obtained from Sokhansanj and Patil (1996). The physical properties and drying kinetics of both the leaves and stems are given in Table 2.3.

Figure 2.12 shows the moisture profile of alfalfa leaves and stems in a (TPRD) triple pass rotary dryer. Alfalfa leaves dried faster than the stems. The residence time of leaves was about 70 s, whereas it was about 200 s for stems. Figure 2.13 shows the temperature variation of alfalfa stems and hot gas in a (TPRD) triple pass rotary dryer. Hot gas temperature dropped at a faster rate in the inner section of the dryer. The gas temperature was slowly reduced afterwards. The feed temperature increased slowly in the inner drum and other sections. Table 2.8 shows the simulation and experimental results for exit condition of gas temperature and leaf and stem exit moisture content. The simulation results showed lower moisture content for leaves than stems consistent with experimental results. The predicted outlet gas temperature was also in close agreement with the experimental results. However, further validation of the dryer model needs to be done by conducting the laboratory experiment and measuring the moisture and temperature profiles at each section of the dryer. Since the dryer uses the hot flue gas

32

temperature of about 600°C, radiation mode of heat transfer may be significant and must be included in the dryer model as it was not considered in this study.

Sensitivity analysis of process parameters for the triple pass dryer model was not presented, as it is similar to the one obtained for the single pass rotary dryer. The effects of various process parameters on the dryer output applies to triple pass rotary dryer model as well.

Table 2.8 Inlet and exit conditions of a triple pass rotary dryer.

Conditions	Predicted	Measured
Hot gas inlet temperature (°C)	--	600
Hot gas exit temperature (°C)	110	120
Exit leaf moisture (kg/kg)	0.085	0.09
Exit stem moisture (kg/kg)	0.11	0.12
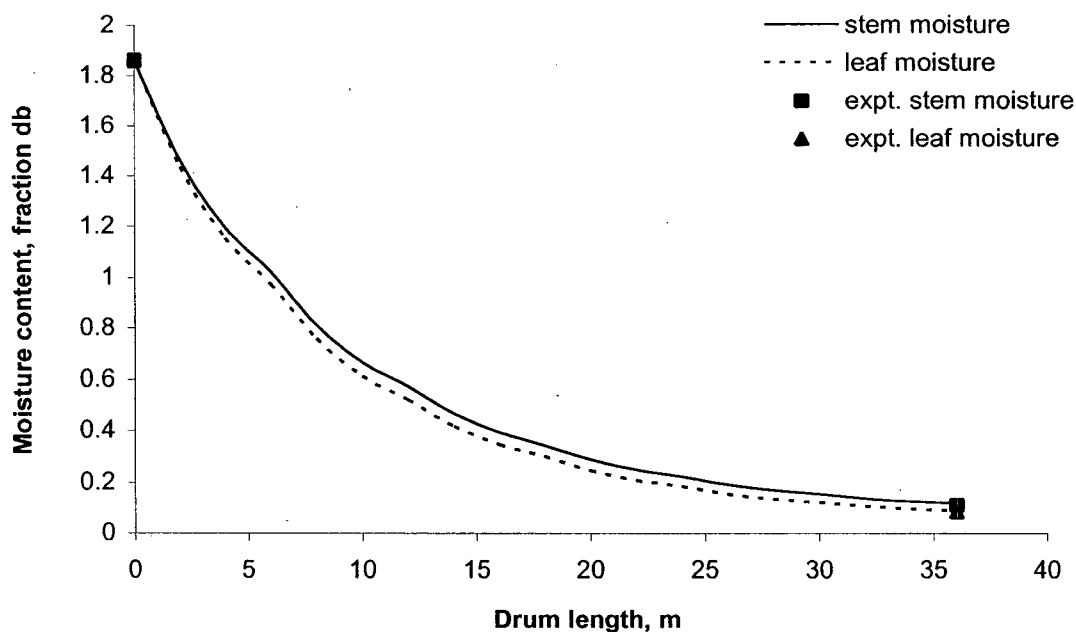
Figure 2.12 Moisture profiles of alfalfa fractions in a triple pass rotary dryer.
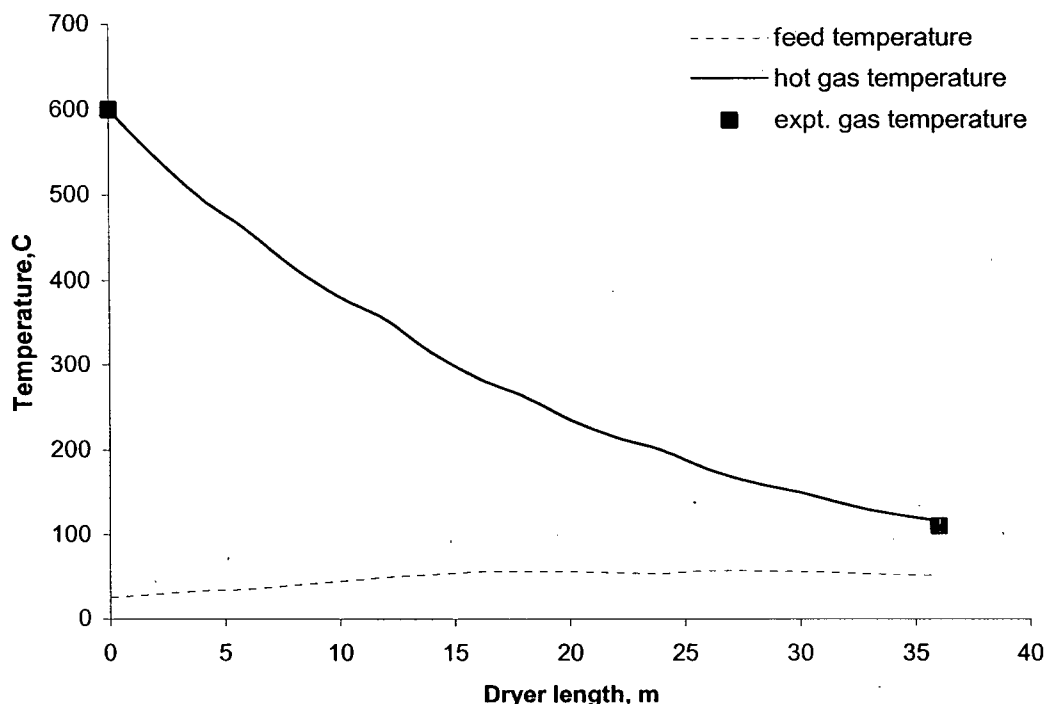
Figure 2.13 Temperature profiles of alfalfa and hot gas in a triple pass rotary dryer.

2.5 Summary

A modeling and analysis of the rotary drying process with fuel burner was performed in terms of heat and mass transfer and residence time. The single pass rotary dryer model was simulated and validated with the sawdust drying data. The validation of the drying model may be further enhanced by measuring feed moisture and temperature data at each section of the dryer. The effect of process variables namely hot gas flow rate, gas inlet temperature, feed flow rate and feed moisture on the outlet feed moisture was analyzed. Within the range of variables studied, the hot gas temperature had the highest effect on the predicted outlet feed moisture and gas temperature followed by the gas flow rate and inlet feed moisture.

The single pass rotary dryer model was extended to a triple rotary dryer and validated with alfalfa drying data of two fractions: stems and leaves. The predicted results were in close agreement with the experimental data and the model can be used in developing an integrated biomass densification process model to perform systems

34

analysis. The developed rotary dryer model may be used as a tool for better understanding of the rotary drying process. In the dryer model, the volumetric heat transfer coefficient was predicted from the empirical relationship. Further research is required to validate this relationship for biomass drying process. The combustion model was developed and integrated with the dryer model to estimate various alternative fuels required for the dryer.

CHAPTER 3
GRINDING STUDY

3.1 Introduction

Grinding of biomass is an important unit operation in the densification process. For example, in the production of fuel pellets and briquettes, the feedstocks have to be ground before transformation into final product. The grinding process increases the total surface area of the material and the number of contact points for inter-particle bonding during the compaction process, apart from the reduction in the pore volume (Drzymala, 1993). Reduction of pore volume of ground biomass is achieved, due to the generation of small particles, which fills between the pores of large particles. As a result, the bulk density of the ground biomass increased to some extent.

Grinding is a complex process and no general law exists to represent the process or to predict the energy consumption. Mathematical modeling of the grinding process is generally limited to either the prediction of energy requirement or the prediction of the size distribution of the products. A number of classical laws of grinding have been reported to describe the functional relationship between a characteristic parameter of the ground particles and the input energy. In general, these laws are not applicable to fibrous biological materials, which are unlikely to follow the classical theories that have been developed for homogenous materials namely, coal, limestone and glass. Therefore, energy required for grinding biomass and biological materials is usually determined by experimental procedures (Fang et al. 1998; Pasikatan et al., 2001).

In the forage industry, the hammer mill is widely used for grinding alfalfa chops to produce densified pellets. Hammer mills are relatively cheap, easy to operate and produce wide range of particles, which is needed for the densification of ground materials (Lopo, 2002). A hammer mill was used by many researchers (Rypma, 1983; Hill and Pulkinen, 1988; Grover and Mishra, 1996; Samson et al., 2000) in studies on grinding of forage crops, grains and biomass materials for making densified masses. Arthur et al., (1982) investigated the performance of tub grinder and hammer mill with crop and forest residues to evaluate their potential for use in a biomass energy conversion system. Datta (1981) reported that coarse reduction (0.6-0.2 mm) of hardwood chips required 20-40

kWh/t, whereas for size reduction range of 0.15 - 0.3 mm required 100-200 kWh/t grinding energy. However, he did not report the moisture content of the feedstock, type of mill and particle size distributions. Hammer mills reduce the particle size of biomass materials using both shear and impact action and produce particles of wider particle size distributions. The energy requirement for grinding biomass can be determined experimentally. However, it depends on the physical and mechanical properties of the material and hammer mill parameters: hammer tip speed, grinding rate, screen size and the clearance between the hammer and the screen. The performance of a hammer mill is measured by energy consumption and geometric mean particle diameter and particle size distribution of the ground product. Geometric mean particle diameter and particle size distribution of biomass grinds are important factors that affect the binding characteristics of biomass particles during densification and are useful information in the design of pneumatic conveyors and cyclones.

In the present work, the specific energy consumption of a hammer mill for grinding different biomass was determined and was compared with the commercial mill energy data. The physical properties of the ground biomass: particle size distribution, bulk density and particle density were determined and compared.

3.2 Materials and Methods

3.2.1 Materials

Wheat and barley straws in square bales were obtained from an experimental farm near Saskatoon, Saskatchewan, Canada. The bales were of standard dimension of 1.00 x 0.45 x 0.35 m with moisture contents of 8.3 % (wb) for wheat and 6.9 % (wb) for barley. Corn stover was collected in the form of whole plant without cobs from a sweet corn variety grown in Saskatoon with moisture content of 6.2% (wb). Switchgrass var 'Pathfinder' was received at 5.2% (wb) moisture content from Resource Efficient Agricultural Production (REAP), Montreal, QC.

3.2.2 Chop size

The corn stover and switchgrass were chopped manually to the size equivalent to the size from a tub grinder (25 mm to 50 mm) and the chop size was determined using a chopped forage size analyzer specified in ASAE Standard S424.1 MAR 98 (ASAE, 2001a). A sample of 4 liter cut biomass was taken and fed into the top screen of the screen shaker. The material was screened for 5 minutes and the mass retained on each screen was weighed to determine the geometric mean size of the chopped material.

3.2.3 Conditioning of biomass

Conditioning the materials to the required moisture content was done by spraying water uniformly into the chopped material. The wetted material was placed in a plastic bag and stored in a room at 22°C for 72 h for moisture equilibration prior to grinding.

3.2.4 Grinding test apparatus

Figure 3.1 is a schematic diagram of the hammer mill used for grinding biomass in this work. Hammer mills reduce particle size of solid materials by shear and impact action. The hammer mill used in this study consisted of 22 swinging hammers, attached to a shaft powered by a 1.5 kW electric motor. The shaft rotated at a speed of 3600 r/min. Perforated metal screens covering the discharge opening of the mill retained coarse materials for further grinding while allowing the properly sized materials to pass as finished product. To avoid dust generation during grinding, the ground product was collected through the ground material collection system, which consisted of a cyclone with an air-lock, an exhaust fan and a ducting assembly (Figure 3.1). The power drawn by the hammer mill motor was measured using a wattmeter (Ohio Semitronics International, Hilliard, OH). The meter was connected to the data logging system (LABMATE Data Acquisition and Control System, Sciemetric Instruments, Ottawa, ON). The data logger was connected to a desktop computer where the time-power data was stored.

Three hammer mill screen sizes, 3.2, 1.6 and 0.8 mm were used in grinding the biomass. To start grinding, the exhaust fan was switched on followed by the air-lock delivery system (star wheel) of the ground material collection system. The hammer mill

was started. A known quantity of straw was manually fed into the hammer mill and the time required to grind the straw was recorded every 6 s along with the power drawn by the hammer mill motor. The power required to run the hammer mill empty was measured before the material was introduced. This allowed determining the net power required to grind the material. The specific energy required for grinding was determined by integrating the area under the power demand curve for the total time required to grind the sample (Balk, 1964). Each test was repeated three times.

3.2.5 Particle size analysis

A sample grind of 100 g was placed in a stack of sieves arranged from the largest to the smallest opening. The sieve series selected were based on the range of particles in the sample. For the grinds from 3.2 mm hammer mill screen opening, Canadian series sieve numbers 10, 14, 16, 18, 20, 30, 40, 50, 70, 100, 140 and 200 (sieve sizes: 2.0, 1.4, 1.2, 1.0, 0.85, 0.59, 0.43, 0.30, 0.21, 0.15, 0.11 and 0.08 mm, respectively) were used. For grinds from 1.6 mm hammer mill screen opening, the sieve numbers used were 20, 30, 40, 50, 70 and 100 (0.85, 0.59, 0.43, 0.30, 0.21 and 0.15 mm, respectively). For the fine grinds from 0.8 mm hammer mill screen opening, the sieve numbers used were 30, 40, 50, 70, 100, and 140 (0.59, 0.43, 0.30, 0.21, 0.15 and 0.11 mm, respectively). The set of sieves was placed on the Ro-Tap sieve shaker (Tyler Industrial Products, Mentor, OH). The duration of sieving was 10 min, which was previously determined through trials to be optimal. This time duration was sufficient for straw grinds, because of their fluffy and fibrous nature. After sieving, the mass retained on each sieve was weighed. Sieve analysis was repeated three times for each ground sample. The particle size was determined according to ANSI/ASAE standard S319.3 JUL 97 (ASAE, 2001b). The geometric mean diameter (d_{gw}) of the sample and geometric standard deviation of particle diameter (S_{gw}) were calculated according to the aforementioned standard.

2.2.6 Moisture content

Moisture content of a sample was determined according to ASAE standard S358.2 DEC 98 for forages (ASAE, 2001c). A sample of 25 g was oven dried for 24 h or until no change in weight at 105 ± 3°C. The moisture content was reported in percent wet basis.
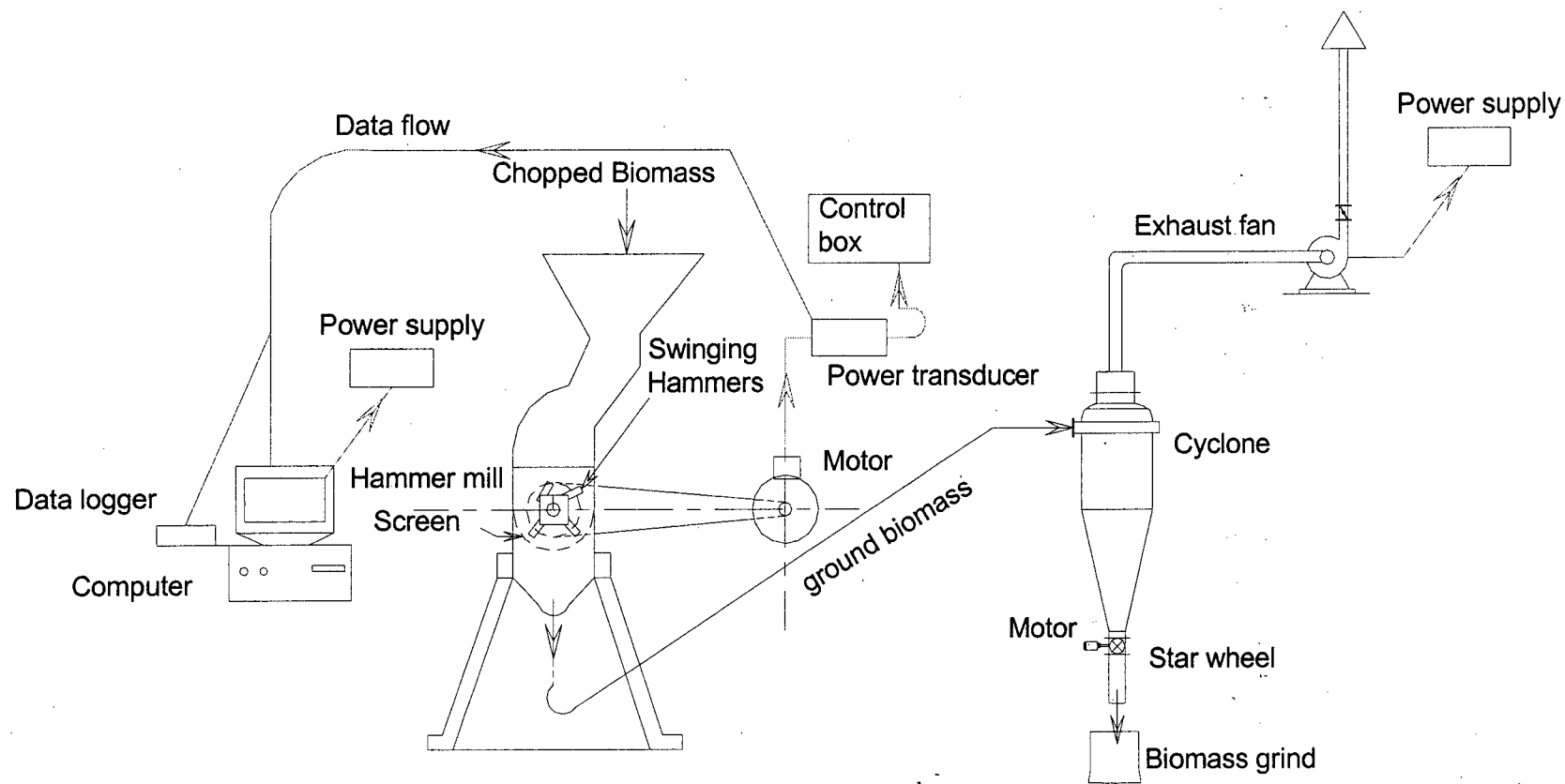
Figure 3.1 Complete flow chart for grinding test.

2.2.7 Bulk density and particle density of grinds

Bulk density of ground samples was measured using the grain bulk density apparatus. The grinds were placed on the funnel and dropped at the center of a 0.5 L steel cup continuously. Since the grind was fluffy and did not flow down readily through the funnel, it was stirred using a wire in order to maintain a continuous flow of the material. The cup was levelled gently by a rubber coated steel rod and weighed. Mass per unit volume gave the bulk density of the grinds in kg/m^3.

Particle density of the grind was measured using a gas multi-pycnometer (Quantachrome Corporation, FL) by measuring the pressure difference when a known quantity of nitrogen under pressure is allowed to flow from a previously known reference volume (V_R) into a sample cell (V_c) containing the ground material. The true volume of the sample (V_p) was calculated from Equation. 3.1. The particle density of the sample is its mass divided by V_p and was expressed in Mg/m^3. Each bulk and particle measurement was repeated five times on the same sample.

$$V_p = V_c - V_R \left[\frac{P_1}{P_2} - 1 \right]$$

(3.1)

Where, V_p is the volume of ground biomass in m^3, V_c is the volume of sample cell in m^3, V_R is the reference volume in m^3, P_1 is the pressure reading after pressurizing the reference volume in Pa and P_2 is the pressure after including V_c in Pa.

2.2.8 Commercial hammer mill energy consumption

In an industrial operation, hammer mill energy consumption is usually determined by measuring the current (amperage) drawn by the hammer mill motor. The total power (P_H) consumed by the mill can be calculated as below (Payne, 1997).

$$P_H (kW) = \frac{Current * Voltage * 1.73}{1000} f_p$$

(3.2)

Where, f_p is the power factor, which is usually assumed as 0.93.

Once the total power drawn from the mill is known, energy consumption of the mill for a particular material can be calculated as below.

$$E_H = \frac{P_H}{C_H}$$
(3.3)

Where, E_H is the specific energy consumption of a hammer mill (kWh/t); and C_H is the mill capacity, (t/h). In order to develop a relationship between the hammer mill power and its capacity, commercial hammer mill users and manufactures are contacted for data collection and analysis.

3.3 Results and Discussions

Specific energy required for grinding biomass depends on physical properties of the material and machine variables. This section presents the specific energy required for grinding selected biomass using a laboratory hammer mill and the physical properties of the ground materials and the results were discussed.

3.3.1 Energy requirement for grinding

The average specific energy consumption for grinding selected biomass using the hammer mill with three different screen sizes at two moisture contents is summarized in Table 3.1. The specific energy consumption for grinding wheat straw with the hammer mill screen sizes of 0.8, 1.6 and 3.2 mm were 51.6, 37.0 and 11.4 kWh/t respectively, at 8.30% (wb) moisture content. Energy consumption to reduce corn stover to particle sizes 0.8, 1.6 and 3.2 was 22.0, 14.8 and 7.0 kWh/t, respectively. The specific energy consumption for wheat straw and corn stover was similar to the results reported by Cadoche and Lopez (1989), who tested a knife and hammer mill for milling hardwood chips, wheat straw and corn stover at 4-7% moisture content. The results were also comparable with the work of Himmel at al. (1985), who milled wheat straw (36 kWh/t for 1.6 mm screen size) at 4% moisture content and corn stover (10 kWh/t for 3.2 mm screen size) at 7% moisture content.

Figure 3.2 represents the specific energy requirement for grinding biomass as a function of screen size at moisture content of 8% (wb) or lower. The smaller the screen size, the higher is the specific energy for grinding biomass samples. In other words, fine grinding requires high specific energy.

42

Table 3.1 Specific energy requirements for grinding of biomass residues and switchgrass using hammer mill.

Material	Moisture content (% wb)	Geometric mean chop size (mm)	Hammer mill screen opening (mm)	Average specific energy consumption (kWh/t)
Wheat straw	8.3	7.67	0.8	51.55 (2.93)†
	8.3		1.6	37.01 (6.65)
	8.3		3.2	11.36 (1.02)
	12.1		0.8	45.32 (0.98)
	12.1		1.6	43.56 (1.80)
	12.1		3.2	24.66 (1.82)
Barley straw	6.9	20.52	0.8	53.00 (2.66)
	6.9		1.6	37.91 (4.51)
	6.9		3.2	13.79 (0.18)
	12.0		0.8	99.49 (7.35)
	12.0		1.6	27.09 (1.59)
	12.0		3.2	N/A*
Corn stover	6.2	12.48	0.8	22.07 (0.32)
	6.2		1.6	14.79 (0.54)
	6.2		3.2	6.96 (0.75)
	12.0		0.8	34.30 (1.47)
	12.0		1.6	19.84 (3.47)
	12.0		3.2	11.04 (0.97)
Switchgrass	8.0	7.15	0.8	62.55 (0.63)
	8.0		1.6	51.76 (0.96)
	8.0		3.2	23.84 (0.63)
	12.0		0.8	56.57 (1.91)
	12.0		1.6	58.47 (1.86)
	12.0		3.2	27.63 (1.07)

* Data not available; † Number enclosed in parenthesis are standard deviations for n = 3
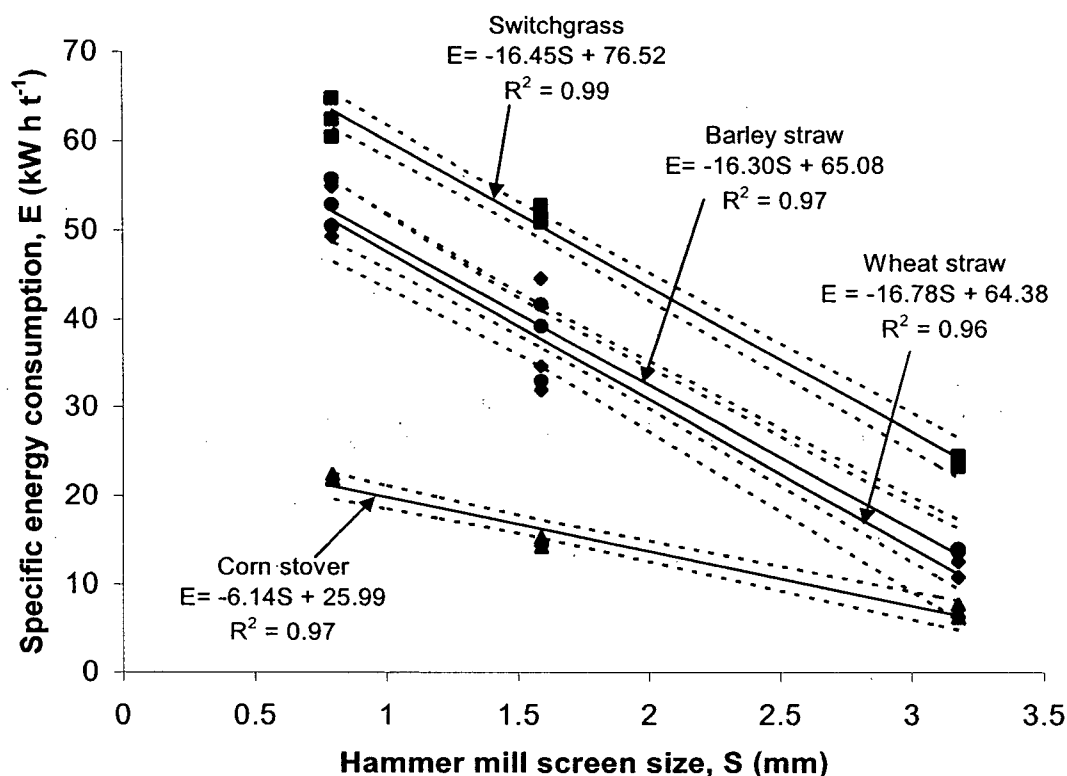
Figure 3.2 Specific energy requirements for grinding of selected biomass at 8% (wb) moisture content or lower.

Figure 3.3 shows the relationship between the specific energy requirement of biomass residues and hammer mill screen sizes at 12% (wb) moisture content. Corn stover consumed the least specific energy of 11 kWh/t with hammer mill screen size of 3.2 mm at 12% moisture content. It was expected that corn stover would consume less energy due to its lower fiber content and the presence of more spongy vascular tissues in the stem. At high moisture, barley straw grind used the highest energy of 99.5 kWh/t with the screen size of 0.8 mm. The high energy consumption may be caused by the larger mean chop size of the barley feed. The geometric mean chop size of switchgrass (7.15 mm) was the least among the biomass tested and consumed the highest specific energy due to the fibrous nature of switchgrass. The data did not show much difference in the specific energy requirement for switchgrass as observed at both moisture levels except for the largest screen size (3.2 mm). Among the four materials studied, switchgrass used the highest specific energy to grind in all hammer mill screen sizes, whereas corn stover required the least specific energy.
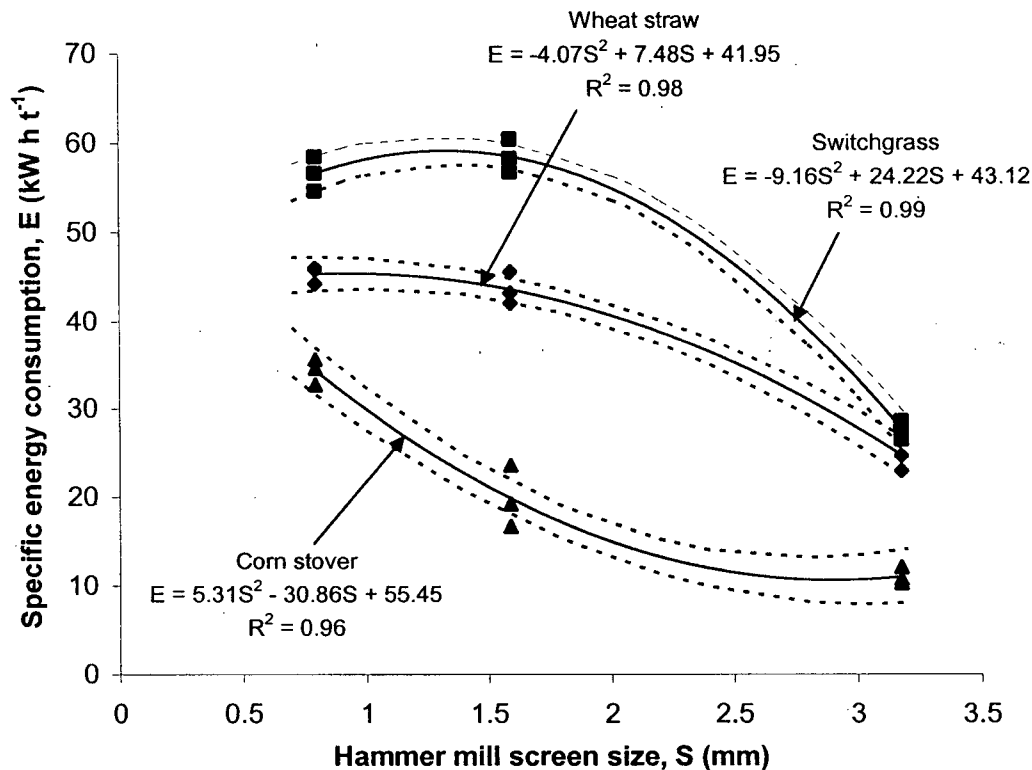
Figure 3.3 Specific energy requirements for grinding of selected biomass at 12% (wb) moisture content.

A regression analysis was performed to correlate the specific energy requirement for grinding of biomass with the hammer mill screen sizes ranging between 3.2 mm and 0.8 mm. At low moisture content (less than 8%), a simple linear model fitted well with the experimental data (Figure 3.2) for all biomass samples with coefficient of determination (R^2) values ranging from 0.96 to 0.99. At higher moisture content (12%), a second order regression model fitted well for wheat straw, corn stover and switchgrass (Figure 3.3) with higher R^2 values. The 95% confidence bounds (dotted lines) for the regression models (solid lines) showed the statistical significance of the developed models. In Figures 3.2 and 3.3, some experimental data points were located outside the 95% confidence region. Although R^2 values for the models were high, the predicted results from the model may not be precise in that region.

From Figures 3.2 and 3.3, it can be observed that hammer mill screen size was negatively correlated with specific energy consumption. The larger the hammer mill

45

screen size, the lower was the specific energy consumption. This is in agreement with the results for grinding alfalfa stem reported by Sitkei (1986). He reported a second-order polynomial relationship between the specific energy requirement and the mean particle size for alfalfa stems with a R^2 value of 0.99. Similarly, Holtzapple et al. (1989) reported the relationship for grinding energy with the sieve openings. They also concluded that grinding energy increased greatly as the particle size is reduced.

Moisture is also an important factor to be considered during hammer milling of biomass. Moisture content had a positive correlation with specific energy consumption. The higher the moisture content, the higher was the specific energy consumption. It can be explained by the fact that an increase in moisture content of straw samples would increase the shear strength of the material, although shear strength decreases with decomposition of straw samples (Annoussamy et al., 2000). So, biomass demands more specific energy to hammer mill at high moisture content. This result agrees with the results reported by Balk (1964). He reported that for alfalfa grinding, moisture content had a positive correlation with specific energy consumption. Schell and Harwood (1994) studied the milling performance of hammer mill, disc mill and shredder to mill wood chips at about 60% moisture and switchgrass and paper wastes at 10% moisture content. They reported that dry wood chips are easier to mill than wet wood chips.

3.3.2 Commercial mill energy requirement for grinding

The energy consumption of a commercial hammer mill can be calculated once the mill power is known using equation (3.3). This energy consumption is the total input energy to the hammer mill. Jannasch et al. (2001) reported a specific energy of 55.9 kWh/t for the commercial hammer mill screen sizes of 5.6 mm and 2.8 mm for switchgrass. This was twice higher than the energy required for switchgrass in this study.

Energy requirement of a commercial hammer mill unit was calculated based on the survey of hammer mills used in British Columbia densification plants and hammer mill manufacturer (Bliss Industries, 2003). The mill capacity and its horse power data were analyzed. The data produced a simple relationship between the hammer mill capacity and mill power.

$$P_H = 24.44C_H - 4.88 \qquad\qquad R^2 = 0.93 \qquad\qquad (3.4)$$

Where P_H is the hammer mill power, kW and C_H is the mill capacity in t/h.

Table 3.2 summarizes the specific energy requirement for grinding different biomass using the laboratory and commercial hammer mills. For pelleting operation, screen sizes of 6.4 or 3.2 mm are often used for particle size reduction. Hard wood chips required the highest amount of specific energy compare to other biomass species. Most of the wood pellet plants use either 6.4 mm or 3.2 mm hammer mill screen size. It can also be noticed in Table 3.2 that commercial hammer mills consumed 1.5 to 2 times higher specific energy than that of laboratory hammer mills. The reason for the higher energy consumption of commercial mills is not clear at this stage. However, it is hypothesized that commercial hammer mills may draw large amount of energy in order to overcome the friction between the hammers and large particles. The inlet and outlet particle size distribution of material during grinding must also be taken into consideration while comparing the performance of laborotary and commercial hammer mills. The difference in energy consumption between laboratory and commercial mills needs to be addressed in the future by investigating the scale up effect based on mathematical models.

Table 3.2 Specific energy requirement for grinding biomass using a hammer mill (2.8 - 3.2 mm screen sizes)

Materials	Specific energy requirement (kWh/t)	Sources
Straws	24.7[a]	Mani et al (2004)
	37-45[b]	Miles and Miles (1980)
Corn stover	11.0[a]	Mani et al (2004)
Switchgrass	27.6[a]	Mani et al (2004)
	44.9 – 55.9[b]	Samson et al (2000) & Jannasch et al (2001)
Wood chips	40-150[b]	Cadoche and Lopez (1989) & NOVEM (1996)

[a] Laboratory mill

[b] Commercial mill

Holtzapple et al. (1989) reported the specific energy requirement of wood chips using a conventional method of mechanical size reduction. The energy requirement for grinding wood chips was estimated by equipment manufacturers and was correlated to the size of the material that would just fit through the sieve openings by:

$$E = -203.06 \log(S_s) + 206.11 \tag{3.5}$$

where, E is the grinding energy, kWh/t and S_s is the sieve opening size, mm.

3.3.3 Physical properties of biomass grinds

Figure 3.4 shows a typical particle size distribution of wheat grind from three different hammer mill screen sizes. The graphs depict the skewness of the distribution for wheat straw at 3.2 mm screen size, which was similarly reported for alfalfa grinds (Yang et al., 1996), wheat straw, and corn stover (Himmel et al., 1985). The grinds from screen size of 3.2 mm had a large size distribution with a geometric mean particle diameter of 0.64 mm for wheat straw grind and 0.69 mm for barley straw grind. The geometric mean diameter for corn stover and switchgrass grinds was 0.41 and 0.46 mm, respectively; which were finer than wheat and barley straw grinds.
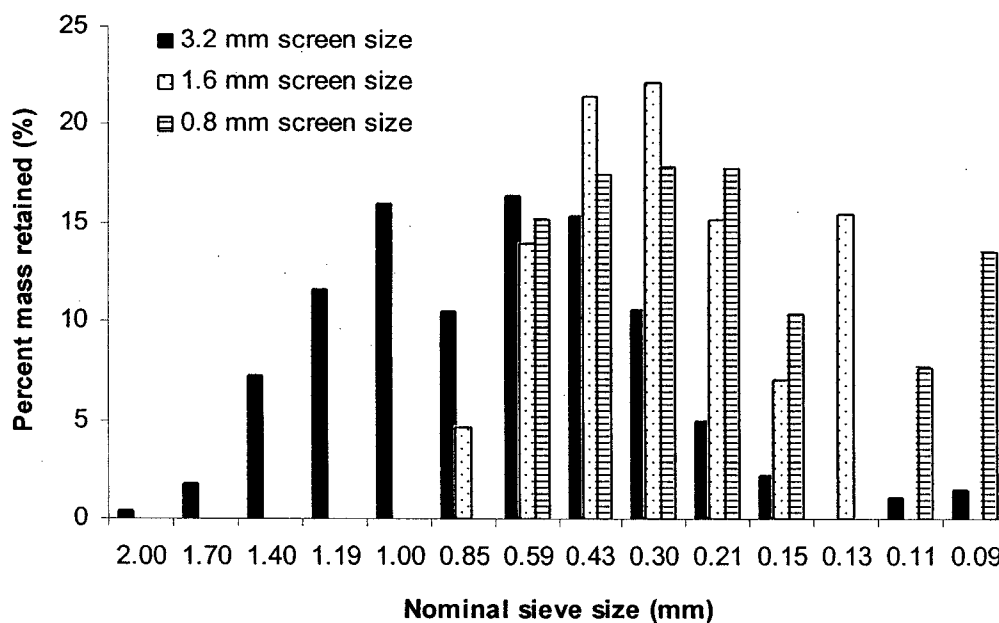
Figure 3.4 Typical particle size distributions of wheat straw grinds at various screen sizes.

Grinds from the hammer mill screen size of 1.6 and 0.8 mm were distributed in narrow range (Figure 3.4) and produced particles with geometric mean particle diameter of 0.34 and 0.28 mm, respectively for wheat straw grinds and 0.38 and 0.32 mm, respectively for barley straw grinds. Similar results were also observed for corn stover and switchgrass grinds. Wider particle size distribution is suitable for compaction (pelleting or briquetting) process. During compaction, smaller (fine) particles are rearranged and filled in the void space of larger (coarse) particles producing denser and durable compacts (Mani et al, 2003; Tabil, 1996; Tabil and Sokhansanj, 1996). Coarse particles are also suitable feed for boilers and gasifiers. Narrow range particle size distribution with more fines is suitable for enzymatic hydrolysis of lignocelluloses due to the generation of more surface area and pore spaces during fine grinding. But fine grinding of biomass requires high energy (Himmel et al., 1985). Knowledge of particle size distribution requirement for various conversion processes is not available. An ideal particle size distribution remains to be determined for each bioconversion process.

For the same hammer mill screen size, geometric mean particle diameter of wheat straw grind was slightly smaller than that of barley straw grind. This might be due to the difference in mechanical properties of wheat and barley straws. Grinds from corn stover were the finest among the biomass tested. Corn stover had the lowest moisture content among the materials used. It was observed that corn stover was easier to grind than the other biomass.

Geometric mean particle diameter, bulk and particle densities of biomass grinds from different hammer mill screen sizes are given in Table 3.3. The larger the screen openings, the lower were the bulk and particle densities. Grinds from the smallest screen size (0.8 mm) produced highest bulk and particle densities of 121 kg/m^3 and 1340 kg/m^3, respectively for wheat straw and 112 kg/m^3 and 1250 kg/m^3, respectively for barley straw. Bulk and particle densities of wheat straw grind were slightly higher than that of barley straw grinds. Switchgrass grinds had the highest bulk density of 182 kg/m^3 when passed through hammer mill screen size of 0.8 mm. Among four biomass grinds, corn stover grinds had the highest bulk and particle densities due to the smallest geometric mean particle diameter of the grind from the hammer mill screen sizes of 3.2 and 1.6 mm.

49

Table 3.3 Physical properties of biomass grinds.

Biomass grinds	Moisture content (% wb)	Hammer mill screen size (mm)	Geo. mean particle diameter (mm)	Geometric standard deviation (mm)	Bulk density (kg/m^3)	Particle density (kg/m^3)
Wheat straw	8.30	3.175	0.639	0.306	97.37 (0.78)*	1026.57 (6.39)*
		1.588	0.342	0.196	106.73 (1.02)	1258.45 (7.91)
		0.794	0.281	0.201	121.29 (1.32)	1344.07 (1.92)
Barley straw	6.98	3.175	0.691	0.364	80.99 (0.71)	887.34 (6.57)
		1.588	0.383	0.222	101.44 (0.50)	1178.05 (6.69)
		0.794	0.315	0.217	112.13 (0.74)	1245.36 (7.51)
Corn stover	6.22	3.175	0.412	0.261	131.37 (2.25)	1169.91 (4.54)
		1.588	0.262	0.447	155.64 (2.15)	1330.78 (4.24)
		0.794	0.193	0.308	157.73 (1.54)	1399.16 (3.89)
Switch grass	8.00	3.175	0.456	0.255	115.4 (1.31)	945.97 (4.60)
		1.588	0.283	0.391	156.20 (1.99)	1142.36 (4.79)
		0.794	0.253	0.438	181.56 (1.17)	1172.75 (2.71)

*Number enclosed in parenthesis are standard deviations for n = 5.

3.4 Summary

Corn stover consumed the least specific energy during hammer mill grinding of all biomass tested. Switchgrass used the highest specific energy requirement for grinding at both moisture levels and all screen sizes due to the fibrous nature of the material. Commercial hammer mill energy consumption was about 1.5 to 2.0 times higher than that of laboratory hammer mill energy consumption data. Further research is required to address the reason for higher energy consumption of commercial hammer mills. The physical properties of biomass grind: particle size, particle size distribution, bulk and particle densities are useful data for storage and handling of biomass grinds in the energy conversion system. The physical properties of biomass grinds also influence the final quality of the densified products.

CHAPTER 4

DENSIFICATION STUDY

4.1 Introduction

Densification is the process of compacting ground biomass into pellets and briquettes. Densification process increases the density of the feed materials in the order of 2 to 10. Among different densified products, pellets are often preferred as a fuel for heating and energy application due to its uniform physical properties and ease of feeding and handling. Figure 4.1 shows a schematic diagram of a typical pelleting unit consisting of a series of circular die and roll assembly. When the ground material is introduced into the housing where internal rollers press the material against the die opening, the material is densified and extruded through the die holes in a step-wise fashion. A doctor blade attached to the outside housing cut the extruded material to the required length (Sokhansanj et al., 1993).
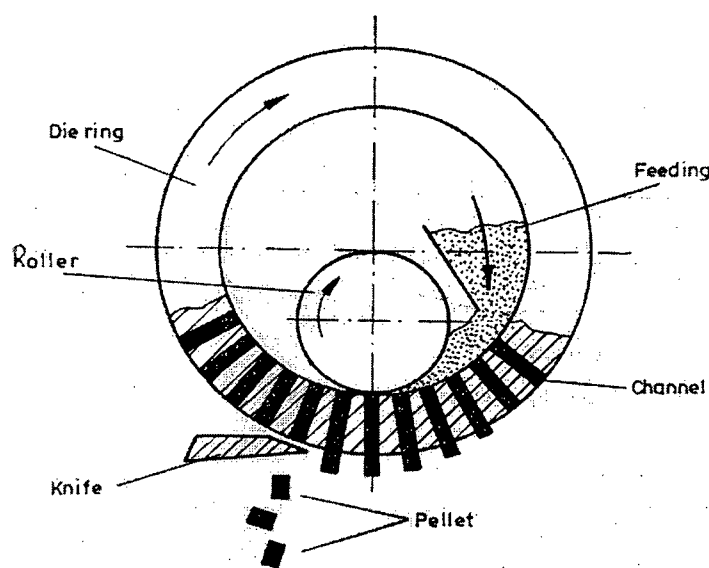
Figure 4.1 Pelleting process (Sitkei, 1986).

Energy required for pelleting biomass depends on the three main critical factors namely moisture content of the feed, temperature of the feed, and die size (Sitkei, 1986). Since pelleting is an extrusion process, more energy is being exploited by frictional

energy developed between the metal surface and the material. Energy required for compacting biomass is often less than extruding it. However, these energy components vary with biomass and its properties. Determination of compaction and extrusion energy data can provide a better understanding of the pelleting process and can aid in designing a new pellet mill with the least energy consumption.

The process of forming the biomass into pellets depends upon the physical properties of ground particles and the process variables: pressure and temperature. The compaction process can be better explained, if the compaction mechanism of the material is known. The compaction mechanism of different powder materials will be different from each other. It is also important to understand the compaction mechanism of biomass particles to design energy efficient compaction equipment and to study the effect of various process variables on pellet density to enhance the quality of the product.

In order to further understand the compaction mechanism of powder materials, a number of models have been proposed (Walker, 1923; Heckel, 1961; Cooper and Eaton, 1962; Kawakita and Lüdde, 1971). Many of the compaction models applied to pharmaceutical and biomass materials have been discussed and reviewed in detail by Denny (2002) and Mani et al. (2003). Among the different compaction models, the Heckel and Cooper-Eaton models are still in use to study the compaction mechanism of pharmaceutical and cellulosic materials. Kawakita- Lüdde model was proposed for soft and fluffy materials (Kawakita and Lüdde, 1971).

The main focus of this study is to understand the compaction mechanism of biomass grinds under different applied pressures, particle sizes and moisture content during pelleting or cubing processes; and to determine the energy required for compacting and extruding biomass using a laboratory densification unit.

4.2 Compaction Mechanisms

Forces contributed to the formation of briquettes and pellets were first explained by Rumpf (1962). Although mechanical forces in the processes of tumbling, kneading, agitation, extruding, rolling and compression are needed to bring individual particles in contact with one another, the basic physical forces are also responsible for the inherent

strength of other types of agglomerated particles (Sastry and Fuerstenau, 1973). According to Rumpf (1962), the possible mechanisms can be divided into five major groups:

1) attraction forces between solid particles;

2) interfacial forces and capillary pressure in movable liquid surfaces;

3) adhesion and cohesion forces at not freely movable binder bridges;

4) solid bridges; and

5) mechanical interlocking or form-closed bonds.

The compaction mechanism of different particulate materials will be different from each other. Figure 4.2 shows the schematic representation of typical compression process. In general, during the first stage of compression, particles that are preheated through dry blending or wet granulation, rearrange themselves to form a closely packed mass (Figure 4.2). During this phase, the original particles retain most of their properties, although energy is dissipated due to interparticle and particle-to-wall friction. At high pressures, the particles are forced against each other even more and undergo elastic and plastic deformation, thereby increasing interparticle contact. Because the particles approach each other closely enough, short range bonding forces like van der Waal's forces, electrostatic forces and sorption layers become effective (Rumpf 1962; Sastry and Fuerstenau 1973; Pietsch 1997). Under stress, brittle particles may fracture leading to mechanical interlocking. Mechanical interlocking is the only bonding mechanism that does not involve atomic forces and is expressed to contribute very little to the overall strength of the pellet (Gray, 1968). At still higher pressures, reduction in volume continues until the density of the pellet approaches the true densities of the component ingredients. If the melting points of the ingredients in a powder mix that form a eutectic mixture is favorable, the heat generated at a point of contact can lead to a local melting of materials. Once cooled, the molten material forms very strong solid bridges (Ghebre-Sellassie, 1989).
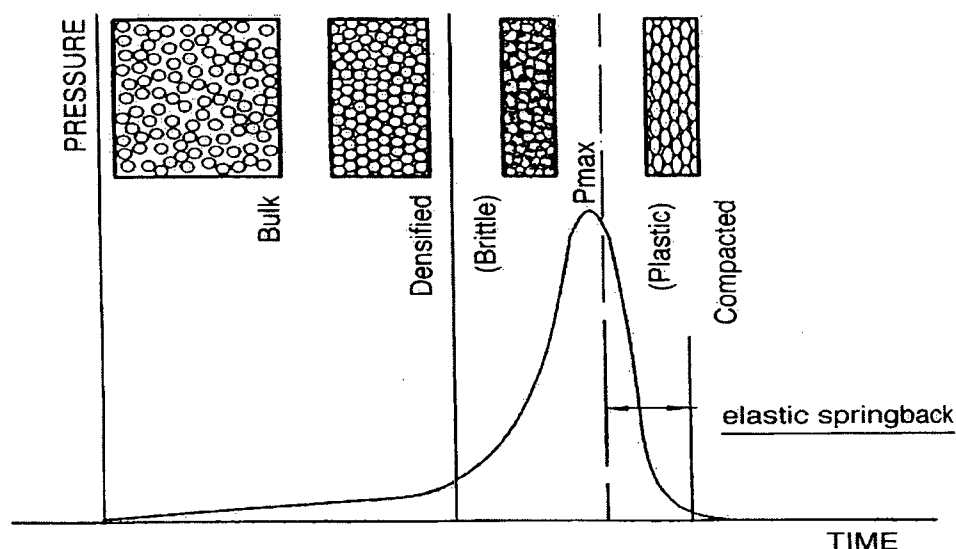
Figure 4.2 A typical compaction process.

Biomass contains components namely cellulose, hemicellulose, protein, lignin, crude fiber and ash. Among these chemical components, lignin has a low melting point of about 140°C. When biomass is heated, lignin becomes soft and sometimes melts and exhibits thermosetting properties (van Dam et al., 2004). Similar compaction mechanism was identified in the alfalfa pelleting process (Tabil and Sokhansanj, 1996). When alfalfa is compacted in circular die pellet mill, the temperature of the compacted material reaches more than 90°C due to preconditioning of the material and heat generated due to friction between a die and the material (Tabil, 1996). During compression of pharmaceutical powders, a series of compression mechanisms has been suggested to be involved in the compression process, i.e. particle rearrangement, deformation, densification, fragmentation and attrition (Alderborn and Wikberg, 1996). In two recent studies (Johansson et al., 1995; Johansson and Alderborn, 1996) on pharmaceutical tablet production, the compression behavior of pelletized microcrystalline cellulose has been investigated. The relevant compression mechanism was due to permanent deformation (change in the shape of the individual particles) and densification (contraction or porosity reduction of the individual compacts).

4. 3 Compaction Models

The compaction models represent the compression behavior of various particulate materials and predict the pellet/compact density. A number of empirical equations have been developed to relate the compaction behavior of the biomass, which are generally in the form of exponential and power law relationships (Mewes, 1959a, b). Heckel (1961) proposed a model to express the compaction behavior of compressed powder. The equation (Eq. 4.1) expresses the density of powdered materials in terms of packing fractions as a function of applied pressure:

$$\ln \frac{1}{1-\rho_f} = m_0 P + b_0 \tag{4.1}$$

$$\rho_f = \frac{\rho}{\rho_1 X_1 + \rho_2 X_2} \tag{4.2}$$

where, ρ_1 and ρ_2 are the particle density of components of the mixture (kg m^{-3}); ρ_f is the packing fraction or relative density of the material after particle rearrangement; ρ is the bulk density of compacted powder mixture (kg m^{-3}); m_0 and b_0 are the Heckel model constants; P is the applied pressure (MPa); and, X_1 and X_2 are the mass fraction of components of the mixture.

Shivanand and Sprockel (1992) showed that constant b_0 is related to the relative density at particle rearrangement:

$$b_0 = \ln \frac{1}{1-\rho_f} \tag{4.3}$$

A high ρ_f value indicates that there will be a high volume reduction of the sample due to particle rearrangement. Constant m_0 has been shown to be equal to the reciprocal of the mean yield pressure required to induce plastic deformation. A larger value for m_0 (low yield pressure) indicates the onset of plastic deformation at relatively low pressure; an indicator that the material is more compressible.

Jones (1960) used Eq. 4.4 to represent the compression model for metal powders:

$$\ln \rho = m_1 \ln P + b_1 \tag{4.4}$$

where, m_1 and b_1 are the Jones model constants.

Walker (1923) used Eq. 4.5 to characterize the compaction of non-metallic powders and the particles of sulfur, ammonium, sodium chloride, and trinitrotoluene (TNT).

$$V_R = m_2 \ln P + b_2 \tag{4.5}$$

$$V_R = \frac{V}{V_S} \tag{4.6}$$

where, V_R is the packed volume ratio, defined in equation (4.6); V_S is the void-free solid material volume (m^3); V is the volume of compact at pressure P (m^3); and, m_2 and b_2 are the Walker's model constants. Cooper and Eaton (1962) classified two broad processes that are involved in compaction, based on the assumption that compaction proceeds through particle rearrangement and deformation. The first process is the filling of voids of the same order as the size of the original particles, which may require elastic deformation or even slight fracturing or plastic flow of particles. The second process involves the filling of voids that are substantially smaller than the original particles. The process can be accomplished by plastic flow or fragmentation, in which the former is more efficient because the material is always forced into the voids. Cooper and Eaton (1962) proposed Eq. 4.7 to describe compaction behavior of ceramic powders:

$$\frac{V_0 - V}{V_0 - V_S} = a_1 e^{-\frac{k_1}{P}} + a_2 e^{-\frac{k_2}{P}} \tag{4.7}$$

where, V_0 is the volume of compact at zero pressure (m^3); a_1, a_2, k_1 and k_2 are the experimentally determined Cooper-Eaton model constants.

Kawakita and Ludde (1971) published the following piston compression equation from the observed relationship between pressure and volume:

$$\frac{P}{C} = \frac{1}{ab} + \frac{P}{a} \tag{4.8}$$

$$C = \frac{V_0 - V}{V_0} \tag{4.9}$$

where, a and b are the constants related to characteristic of the powder in Kawakita model; and, C is the degree of volume reduction or engineering strain, as defined in equation (4.9).

The linear relationship between P/C and P allows the constants to be evaluated graphically. This compression equation holds for soft and fluffy powders (Kawakita and Ludde 1971; Denny 2002), but particular attention must be paid on the measurement of the initial volume of the powder. Any deviations from this expression are sometimes due to fluctuations in the measured value of V_0. The constant a equals to the value of C at infinitely (C_∞) large pressure P.

$$C_\infty = \frac{V_0 - V_\infty}{V_0} = a \qquad (4.10)$$

Constant b is related to the resisting forces in the case of piston compression and V_∞ is the net volume of the powder (m^3).

4.4 Specific Energy Requirement

Energy requirement for densification of biomass depends primarily on the pressure and the moisture content. It also depends on the physical properties of the material and the method of compaction. Most of the densification process involves both compression and pushing/extrusion work. Although compression work is independent of the dimension of pressing channel, the pushing or extrusion work demands more energy due to friction and also smaller cross section area of the pressing channel. Mewes (1959a) studied the consumption of energy to overcome friction during compression for straw and hay and showed that 37 to 40% of the energy was required to compress the materials. So the rest of the energy was required to overcome friction. The energy consumption to compress the materials was around 0.9 MJ/t for pelleting meadow grass at 16% (wb) moisture content. But the pushing/extrusion work consumed about 1.35 MJ/t to attain the same compact density of 500 kg/m^3 (Figure 4.3). On the other hand, Bellinger and McColly (1961) reported that pushing energy for circular dies was up to 2 MJ/t for alfalfa and it was about 10 to 15% of the forming energy.
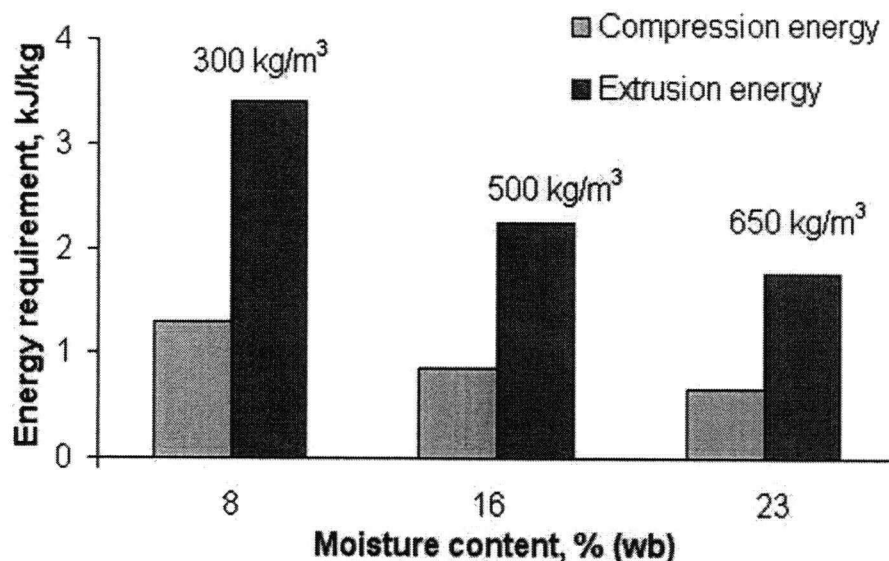
Figure 4.3 Energy requirements for densification of biomass.

Mohsenin and Zaske (1975) studied the energy requirement to compress alfalfa hay at different moisture contents. They reported that with increased moisture content, less energy was required to achieve a certain density. For wood-based (bark) materials, the energy required for a certain density was less for the moist material compared to the same material at equilibrium moisture content of 8%. Reed et al. (1980) reported that the work and pressure required for compaction or extrusion can be reduced by a factor of about two by preheating the raw material. Abd-Elrahim et al. (1981) reported a value of 7.2 MJ/t for compression of cotton stalks in circular dies. Work by O'Dogherty and Wheeler (1984) on barley straw compression in circular die resulted in a range of specific energy from 5 to 25 MJ/t depending on wafer density. Faborode and O'Callaghan, (1987) studied the energy requirement for compression of fibrous agricultural materials. They found that the chopped barley straw at 8.3% (wb) moisture content consumed 28 to 31 MJ/t of energy, while unchopped material consumed 18 to 27 MJ/t.

Table 4.1 Summary of specific energy consumption data for different biomass species.

Materials	Type of densification unit	Specific energy consumption (kWh/t)	Sources
Sawdust	Pellet mill	36.8	Reed & Bryant (1978)
MSW	Pellet mill	16.4	Reed & Bryant (1978)
Bark + wood	Pellet mill	30-45	Miles & Miles (1980)
Straws + binders	Pellet mill	37-64	Miles & Miles (1980)
Straws	Pellet mill	22-55	Neale (1986)
Grass	Pellet mill	33-61	Shepperson & Marchant (1978)
Switchgrass	Pellet mill	74.5	Jannasch et al (2002)
Alfalfa	Pellet mill	30	Tabil & Sokhansanj (1996)
Straws + binders	Cubing machine	75	Miles & Miles (1980)
Grass	Cubing machine	28-36	Balk (1964)
Cotton trash	Cubing machine	60	Miles & Miles (1980)
Hay	Cubing machine	37	Miles & Miles (1980)
Sawdust	Piston press	37.4	Reed et al (1980)
Straws	Screw press	150-220	Carre et al (1987)
Grass	Piston press	77	Shepperson & Marchant (1978)
Straws + binder	Ram extruder	60-95	Miles & Miles (1980)

Aqa and Bhattacharya (1992) studied the effect of varying the die temperature and the raw material preheating temperature on the energy consumption for sawdust densification using a heated die screw press. They found that the energy inputs to the

briquetting machine motor, die heaters and the overall system were reduced by 54, 30.6 and 40.2%, respectively in case of sawdust preheated to 115°C. They also found that operating the briquetting machine at higher throughput further reduces the electrical energy requirement per kg of sawdust. Table 4.1 summarizes the specific energy consumption of various densification machines for different feed materials. It can be seen that preparation of briquettes using a screw press or a piston press is more energy consuming than pelleting process. However, the pelleting process sometimes requires binding agents or some pre-treatments, for example fine grinding and steam conditioning for better product quality. Pellets are also often preferred due to its uniform physical properties and easy feeding and handling properties.

4.5 Materials and Methods

4.5.1 Materials

Materials received for the grinding study (see Chapter 3; section 3.2.1) were used for the evaluation of compaction mechanisms and compaction models. The average chemical composition of each biomass samples is given in Table 4.2. The protein content, crude fat, lignin, acid detergent fiber (ADF) and neutral detergent fiber (NDF) were determined using the AOAC methods (AOAC, 1990). The cellulose and hemicellulose content of biomass were in directly calculated from ADF, NDF and lignin values. ADF value refers to the cellulose and lignin content of the biomass, whereas NDF value referes to the cellulose, hemicellulose and lignin content of the biomass. In order to determine the compression and extrusion energy, corn stover was used. A portion of the chop at 5% (wb) moisture content was set aside for testing. Another portion of the chop was further conditioned by spraying a predetermined amount of distilled water over the samples, thoroughly mixed and kept for 48 h at 5°C to obtain chops with moisture content of 10 and 15% (wb).

Table 4.2 Average compositions of selected biomass.

Composition (% DM)	Wheat straw	Barley straw	Corn stover	Switchgrass
Protein	5.70	6.60	8.70	1.59
Crude fat	1.61	1.33	1.33	1.87
Lignin	7.61	6.81	3.12	7.43
Cellulose	42.51	42.42	31.32	44.34
Hemicellulose	22.96	27.81	21.80	30.00

4.5.2 Single pelleter unit

Figure 4.4 shows a schematic diagram of the single pelleter used to study the compression behavior of biomass. The pelleter was a plunger and cylinder assembly attached to the Instron Model 1011 testing machine (Instron Corp., Canton, MA) as shown in Figure 4.5. The cylinder had an internal diameter of 6.4 mm and a length of 135.5 mm. The cylinder was wrapped with a heating element covered by insulation material. Two type-T thermocouples were placed close to the inside of the cylinder wall at each of the cylinder ends. The thermocouple close to the base was connected to a temperature controller. The cylinder was installed on a stainless steel base. This setup has been used to establish compression characteristics of biomass grinds.
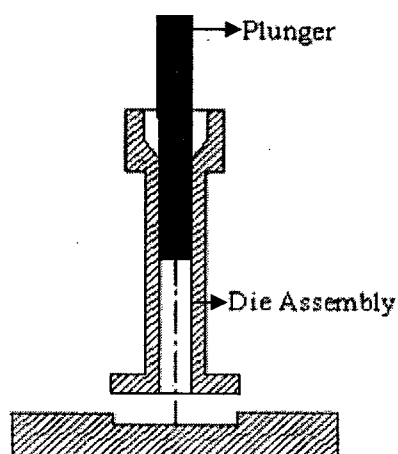
Figure 4.4 Single pelleter unit.
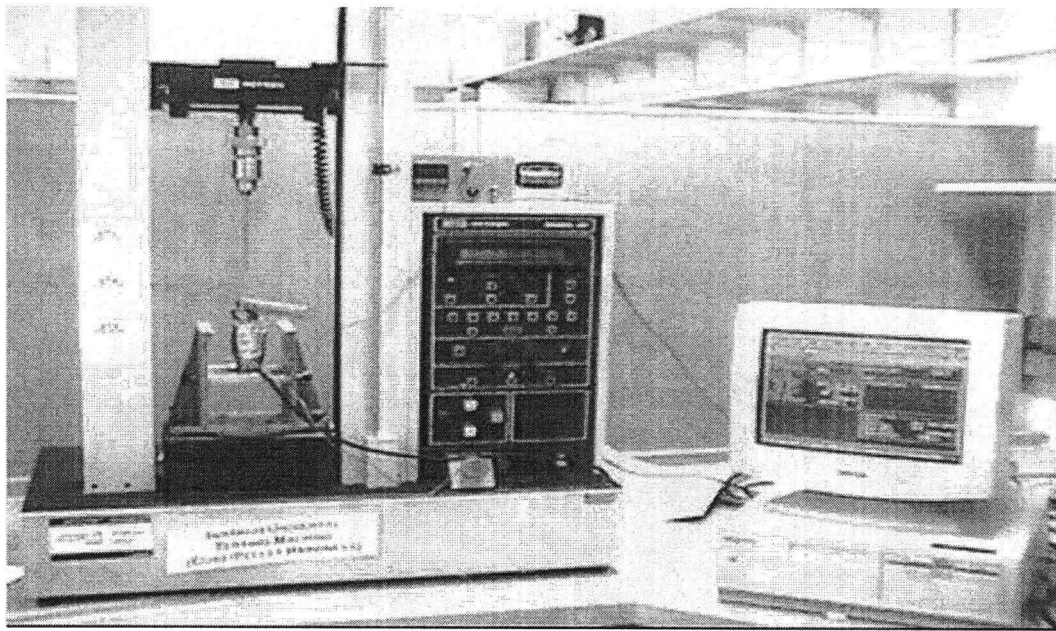
Figure 4.5 Single pellet unit setup in Instron model 1011.

4.5.3 Compression test

The experiments consisted of a complete block design consisting of four biomass grinds (wheat straw, barley straw, corn stover, and switchgrass), three levels of hammer mill screen sizes (3.2, 1.6 and 0.8 mm), and two moisture levels (12% and 15%). A known mass of grind samples (0.2-0.4 g) was compacted in the single pelleter. Prior to each test, the cylinder was heated to 100°C to have a thermal environment similar to that in commercial pelleting of alfalfa. The cross head of the Instron was fitted with a load cell (maximum capacity 5000 N). The preset loads were 1000, 2000, 3000, 4000 and 4400 N. The crosshead speed was 50 mm/min. In the case of corn stover grind, a preset load of 500 N was also used.

To conduct a force deformation test, the pre-heated cylinder was filled manually with the grind sample. The material was compressed up to the specified preset load and held for 60 s before the plunger was withdrawn. The force-deformation data during compression and the force-time data during relaxation (60 s under a constant load) were logged by the computer. The compacted biomass was removed from the cylinder by gentle tapping using the plunger. The mass, length and diameter of the compacted

62

biomass were measured. Pressure-density data from the compression test for each biomass grind are fitted with the different compaction models given in Eq. 4.1 -4.10. Model parameters were estimated using MS Excel software and SAS software packages. Model parameters for Cooper Eaton model were determined using PROC NLIN program in SAS software package (SAS, 1999).

4.5.4 Compaction and extrusion test

A hydraulic press (briquetting machine) was used to compress and extrude corn stover. The press was constructed by a local manufacturing company (Figure 4.6). The press consists of an upper and lower hydraulic driven ram moving inside an electrically heated die. There are pressure regulation valves and pressure gauges for adjusting both the upper and lower ram pressures in the die. The die size is about 30 mm and the length of the briquette may be changed depending on the mass of the feed material. Two pressure transducers, one measuring the top piston pressure and the other measuring the bottom piston pressure, were used. A displacement transducer was set up to measure the top piston displacement.

A known amount (about 15 g) of corn stover was allowed to flow freely from a tube and fills the cylindrical die. The material was compressed to a pre-set pressure and kept under pressure for 60 s. The compacted material was pushed out of the bottom of the die using the top piston and letting the bottom piston move freely. The pressure exerted to the compacted material during pushing was recorded. This pressure was considered as a frictional pressure. Heating of the die surface resulted in unstable and cracked briquettes surfaces. So, in all the experiments, the die was not heated. During the compression process, the compression pressure, back pressure, and displacement of the upper ram were measured and logged in to the computer. These data were used for the analysis of energy requirement. The levels for moisture content (5, 10, & 15%), and pressure (5, 10, 15 MPa) were selected after some tests and factorial experimental design was used to conduct compaction tests. Each test was repeated twenty times.
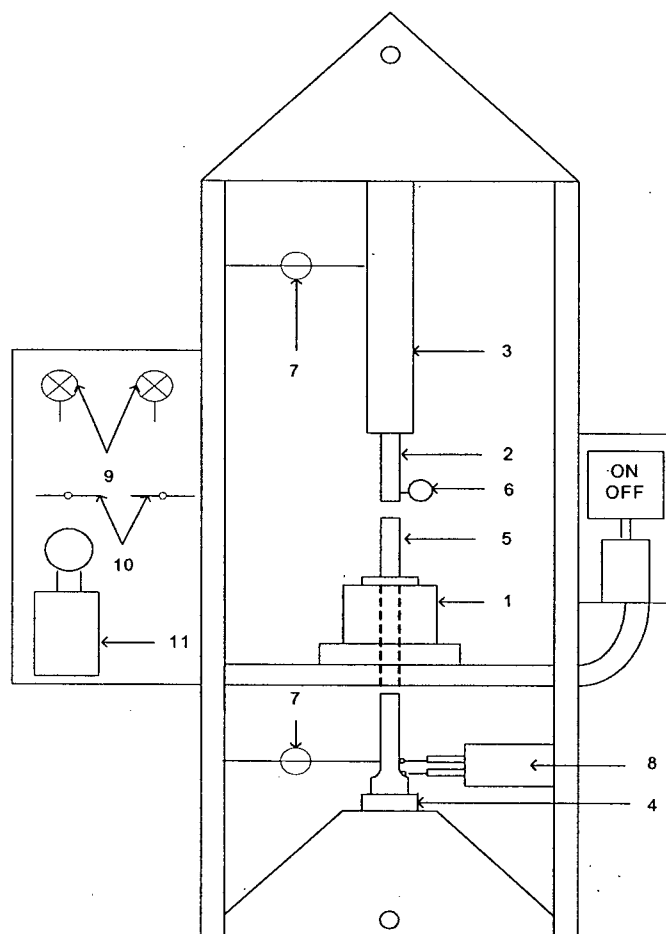
1. Cylindrical die, 2. Plunger, 3. Upper cylindrical ram, 4. Lower cylindrical ram, 5. Feeding column, 6. Displacement transducer, 7. Pressure sensors, 8.Microswitches which activate the directional control valve, 9 Pressure gages, 10. Pressure control valves and 11. Directional control valve for both rams.

Figure 4.6 Schematic diagram of a briquetting machine.

4.5.5 Specific energy consumption

Specific energy required for producing briquette was determined from the pressure - displacement data. The area under the pressure-displacement curve was divided into two sections: compression and extrusion/frictional portions. The area under each section was calculated using trapezoidal formula to report compression and frictional energy data in MJ/t. The extrusion energy was calculated up to the total length of the briquette pushed out of the die. The total energy required to produce the briquette

is the energy required to compress the briquette plus the energy required to extrude the briquette from the die.

4.6 Results and Discussions

4.6.1 Compression test

Figure 4.7 shows a typical force-time diagram of compression and relaxation of biomass grinds at 12% moisture content when the load was set at 4400 N. The actual load achieved during compression at 4400 N was slightly higher than the preset load. This was due to the rapid movement of the crosshead of the Instron testing machine. As a result, the plunger, which compresses the sample, could not be stopped instantaneously and the maximum load exerted on the plunger exceeded the preset load. From Figure 4.7, it can be seen that the compression curve slowly increased during the initial stages of loading. It appears that during this period, particles were displacing while air was being expelled from the system. This mechanism is called particle rearrangement, which occurs at low pressures. This initial stage was short for barley straw but was long for corn stover, switchgrass and wheat straw. During particle rearrangement, the slope of the compression curve was constant and as compressive force progressed, the slope increased indicating densification by elastic, plastic deformation, and perhaps interlocking of particles.
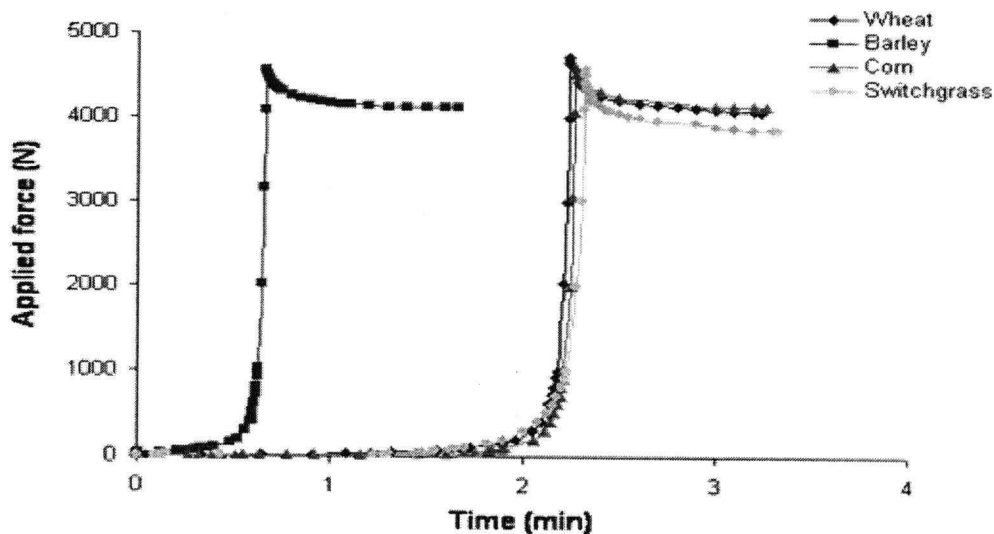
Figure 4.7 Typical compression curve of biomass grinds.

Table 4.3 shows a typical pressure and final pellet density relationships for each biomass at different screen sizes. Within the selected pressure range, corn stover grinds reached a maximum density. Any significant increase in pressure had no effect on pellet density. It can be said that corn stover required less pressure to densify than other biomass grinds. Due to the limitation of load cell mounted in the Instron testing machine, the maximum pressure was limited to 137 MPa. For other biomass grinds, a significant increase in applied pressure increased the pellet density.

4.6.2 Fit of compression models to the data

The Heckel model postulated that compression of powder is analogous to a first order chemical reaction. The Heckel model was often used to explain the compression behavior of many pharmaceuticals (Garekani et al., 2000), food powders (Ollet et al., 1993) and alfalfa grind (Tabil and Sokhansanj, 1996). However, it did not fit well with the compression data of biomass grinds. The model also failed to explain the pressure-volume relationship of many powders and agglomerates (Adams and McKeown, 1996). The Cooper-Eaton model fitted fairly well for all four biomass grinds at 12% (wb) moisture content. The Jones and Walker models did not fit well with compression data of all four biomass species. Biomass particles are generally fluffy, have porous structure and are very brittle. The Kawakita model (Figure 4.8) fitted very well with the compression data of biomass grinds. The model parameters a and b were related to initial porosity of particle bed and yield strength of compact formed, respectively. The parameter 1/b is thought to be related to the failure stress of compacts formed from individual particles (Adams and McKeown, 1996).

Table 4.3 Typical pellet density and pressure relationships for four biomass grinds at moisture content of 12% (wb).

Applied pressure (MPa)	Screen size (mm)	Compact density of biomass pellets (kg/m^3)			
		Wheat	Barley	Corn stover	Switchgrass
31.08	3.2	748±25[*]	733±13	950±12	618±13
62.17		884±13	814±11	1090±15	805±18
93.25		956±18	873±16	1108±20	887±25
124.34		991±14	862±28	1126±14	945±40
136.77		1025±20	868±15	1140±32	1006±20
31.08	1.6	778±20	759±26	1095±16	754±17
62.17		889±23	849±17	1167±13	882±13
93.25		937±14	967±09	1163±13	936±16
124.34		980±09	988±31	1174±10	948±11
136.77		1030±28	1008±09	1171±08	949±07
31.08	0.8	822±08	681±19	1067±31	727±20
62.17		925±04	796±22	1147±13	870±34
93.25		962±08	943±29	1172±24	976±09
124.34		966±17	981±13	1177±14	993±10
136.77		1017±14	1017±10	1179±14	1016±17

[*]Standard deviations for n = 5.
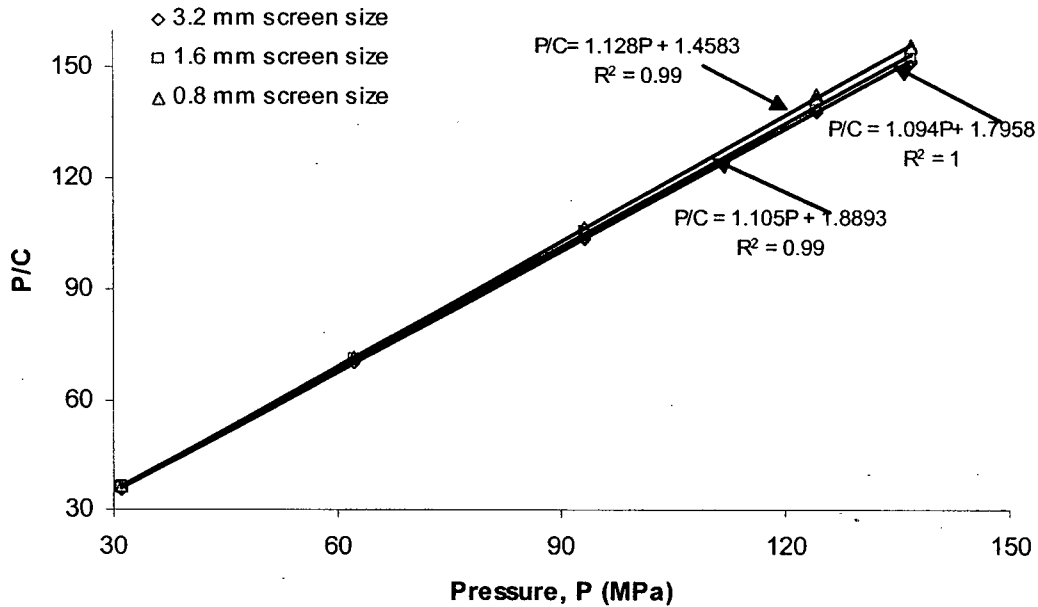
Figure 4.8 Typical Kawakita plot for wheat straw grind at 12% moisture content.

4.6.3 Physical significance of parameters

The parameters of the Kawakita and Cooper-Eaton models are presented in Table 4.4. Figure 4.9 shows the typical Cooper-Eaton plot for all biomass grinds with 3.2 mm screen size at moisture content of 12% (wb). The intercept a_1 of the Cooper-Eaton model is actually the relative density after particle rearrangement. The second intercept a_2 is the relative density after deformation. In general, all biomass grinds exhibited slightly lower a_1 values than a_2 values, indicating that these particles are densified more by elastic and plastic deformation than by particle rearrangement. The compaction of biomass grinds occurs partly by particle rearrangement and partly by particle deformation. The sum of the first and second intercept ($a_1 + a_2$) yielded the theoretical density at infinite pressure, which ideally should be unity. The theoretical density was more than one for all biomass grinds from 3.2 mm screen size at 12% moisture content, which was similarly observed by Shivanand and Sprockel (1992) in cellulose acetate and cellulose acetate propionate and by Tabil and Sokhansanj (1996) in alfalfa grinds. For all other biomass grinds, the theoretical density was less than one. The same a_1 and a_2 values indicated that a portion of the particles (50%) underwent particle rearrangement and the other particles (50%) underwent particle deformation.
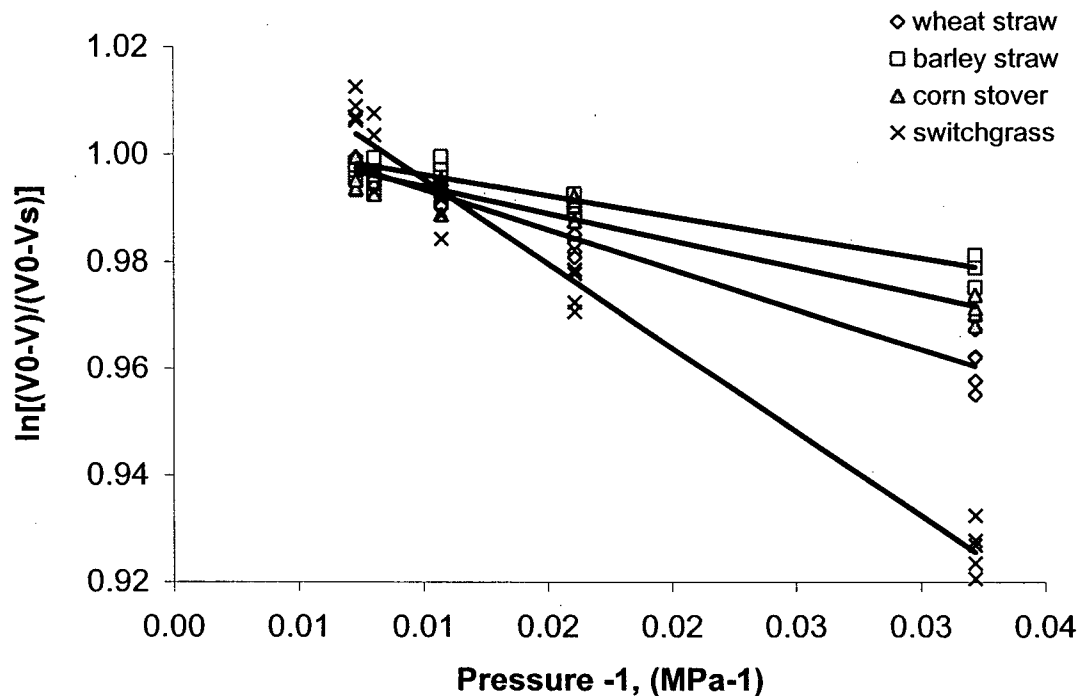
Figure 4.9 Typical Cooper-Eaton plot for all biomass grinds with 3.2 mm screen size at a moisture content of 12% (wb).

According to Shivanand and Sprockel (1992), k_1 in the Cooper-Eaton model represents the pressure required to induce densification by particle rearrangement (P_r), whereas k_2 represents the pressure required to induce densification through deformation (P_d). For both wheat and barley straw grinds, the P_r values were slightly lower than the P_d values indicating that the straw grinds required slightly less pressure for particle rearrangement than particle deformation. Overall, both wheat and barley straw grinds had similar densification characteristics. Observations on the parameters, P_r and P_d for corn stover grind indicated that all particles required equal amount of pressure for both particle rearrangement and particle deformation. Basically, the total applied pressure was distributed partly for particle rearrangement and partly for particle deformation. In the case of switchgrass grind densification, the high P_r value and low P_d value indicated that high pressure was required for particle rearrangement than particle deformation. So, it can be concluded that switchgrass grind was more difficult to densify by particle rearrangement than by particle deformation. This may be due to fibrous nature of switchgrass compared to other biomass grinds (Table 4.2). When comparing values of P_r

69

and P_d for the biomass grinds, higher values were observed for switchgrass grinds and low values were observed for corn stover grinds. So, switchgrass grind was more difficult to densify among the biomass grinds tested. Whereas, corn stover was the easiest to densify among the four biomass grinds studied.

Table 4.4 Compression parameters of biomass grinds.

Model parameters	Hammer mill screen size (mm)	Moisture content (wb)							
		Wheat straw		Barley straw		Corn stover		Switchgrass	
		12%	15%	12%	15%	12%	15%	12%	15%
P_r (MPa)	3.2	2.0	1.7	0.8	1.0	1.2	0.7	3.3	4.8
	1.6	0.8	1.7	1.3	0.6	0.8	0.5	2.3	4.8
	0.8	0.4	0.6	3.1	1.9	0.9	0.6	5.5	5.1
P_d (MPa)	3.2	1.1	1.0	0.8	1.0	1.2	0.7	3.3	2.0
	1.6	2.0	1.7	1.8	2.0	0.8	0.5	2.0	2.0
	0.8	2.0	0.6	2.0	1.9	0.9	0.6	2.0	2.0
(a_1+a_2)	3.2	1.01	1.00	1.00	0.99	1.01	0.99	1.03	1.03
	1.6	0.99	0.98	0.99	0.97	0.99	0.98	0.99	0.98
	0.8	0.97	0.95	0.99	0.98	0.98	0.97	1.00	0.97
a	3.2	0.91	0.91	0.91	0.90	0.89	0.88	0.91	0.91
	1.6	0.91	0.89	0.91	0.89	0.87	0.86	0.85	0.85
	0.8	0.89	0.86	0.91	0.89	0.87	0.86	0.85	0.82
a^*	3.2	0.91	--	0.91	--	0.89	--	0.88	--
	1.6	0.92	--	0.91	--	0.88	--	0.86	--
	0.8	0.91	--	0.91	--	0.89	--	0.85	--
1/b (MPa)	3.2	1.64	1.60	0.71	1.07	1.09	0.63	3.65	3.92
	1.6	1.71	1.15	1.78	1.68	0.59	0.44	2.04	4.03
	0.8	1.29	1.32	3.05	1.70	0.75	0.60	3.97	4.03

a^* indicates theoretical initial porosity of biomass grinds.

The Kawakita parameter, a can be related to the initial porosity (a^*) of biomass grinds. When comparing initial porosity with parameter a, both values were almost the same for all biomass grinds. The parameter 1/b indicates the yield strength or failure

stress of the compact. A higher 1/b value indicates that the compact has high yield strength. It can be observed from Table 4.4 that compacts from switchgrass grind had higher yield strength than compacts from other biomass grinds. Low 1/b value was observed for compacts from corn stover grinds. Almost the same 1/b value was observed for compacts of both wheat and barley straw grinds. It can be concluded that compact from corn stover grind may have less failure stress, whereas compacts made from switchgrass will be harder to break than other compact made from cereal straws and corn stover.

4.6.4 Compaction and extrusion test results

Corn stover used in this study had a chop size of 5.6 mm with a standard deviation of 3.12 mm. The bulk density of the corn stover was about 42 kg/m^3. The loose corn stover was compacted to a density range of 600 - 950 kg/m^3 depending on the moisture content and pressure. The average briquette dimension was about 32 mm diameter and 20-25 mm long. Figure 4.10 shows the relationship between briquette density and pressure at different moisture contents. Briquette density significantly increased as the pressure was increased.

The moisture content of corn stover plays a major role in determining density and strength of the densified masses. An increase in corn stover moisture content considerably decreased the briquette density even at high applied pressures. The maximum briquette density of about 950 kg/m^3 was observed in the moisture range of 5 - 10%. At high moisture, more surface cracks and axial expansions were observed on the briquettes. A similar result was observed for wheat straw as the briquette tends to expand at higher pressure and moisture levels (Smith et al., 1977). Gustafson and Kjelgaard (1963) studied the compaction of hay for a wide range of moisture (28 to 44%) and found that the density of the product decreased as moisture content increased. Wamukonya and Jenkins (1996) produced a relatively high quality briquette from agricultural residues and wood wastes with an optimum moisture content of 12 to 20% by using a hydraulic press. In contrast, Al-Widyan et al. (2002) reported that the briquette density increased with an increase in moisture content for olive cake. So, optimal moisture content exists for each

71

feedstock to produce high briquette density and strength. Corn stover can be compacted into high density briquettes at low feed moisture (about 10%). Grover and Mishra (1996) also recommended low feed moisture content (8 and 10%) for biomass materials to produce strong and crack-free briquettes.
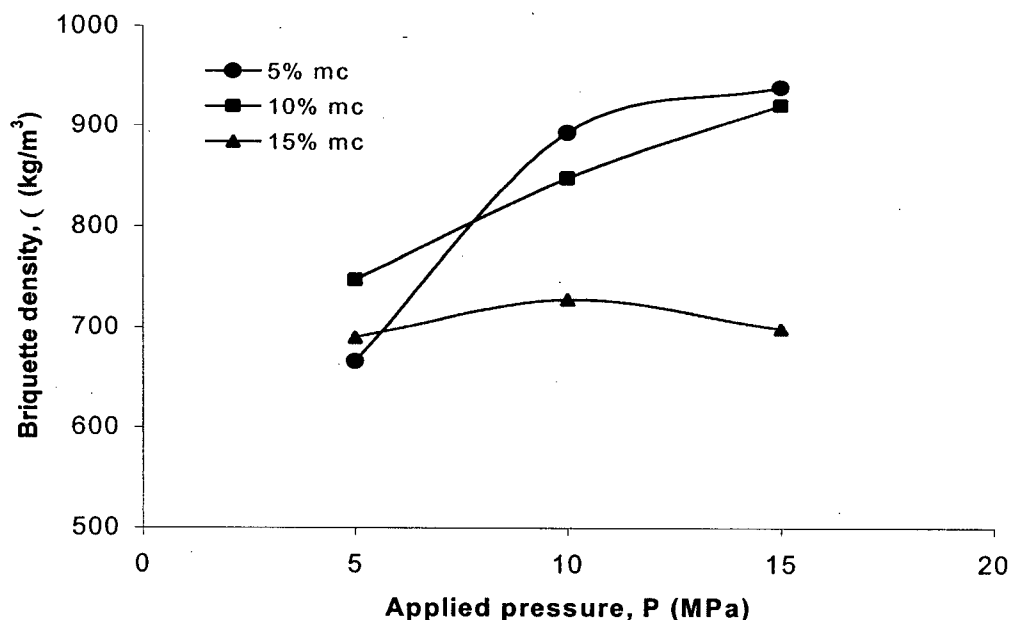
Figure 4.10 Relationship between corn stover briquette density and pressure at different moisture content.

The effect of moisture content and pressure on briquette density was analyzed by Duncan's multiple range test procedure using SAS statistical software package (SAS, 1999). Table 4.5 shows the analysis of variance (ANOVA) test result for briquette density data. The result showed that the effect of pressure and moisture content on briquette density was highly significant at 95% confidence level. The interaction effect of moisture content and pressure on briquette density data was also statistically significant. However, there were no significant difference between the briquette densities produced at 5 and 10% moisture content.

Table 4.5 The ANOVA test results for briquette density data.

Source	DF	Sum of Squares	Mean Sum of Squares	F value α=0.05	Probability
Pressure, P	2	776515	388258	533	<0.0001
Moisture, M	2	679378	339688	466	<0.0001
Interaction, (P x M)	4	399287	99822	137	<0.0001
Error	171	124582	729		

4.6.5. Specific energy requirement

The specific energy required compacting corn stover into briquettes at different applied pressures and moisture contents of stover as shown in Table 4.6. The total specific energy required for producing a corn stover briquette is the sum of the energy required for compressing the loose material into briquette and the energy required for extruding it from the die. Figure 4.11 shows the different components of specific energy for corn stover at 5% moisture content. It is observed from Figure 4.11 that both compression and extrusion energies increased as the pressure increased. Extrusion (frictional) energy is the energy required for the material to overcome the skin friction. This energy should be reduced or eliminated to mitigate the overall energy requirement for the briquetting process.

The specific energy consumption of corn stover was in the range of 12 - 30 MJ/t depending on the briquette density. The compression energy for corn stover was comparable with the compression energy of cotton stalks and barley straw (Abd-Elrahim et al., 1981; O'Dogherty and Wheeler, 1984). As anticipated, the corn stover consumed less energy to compress than any other agricultural materials (Mani et al., 2002). However, the total specific energy was high due to the high extrusion energy. At low pressure (5 MPa), the extrusion energy was less than the compression energy at all three moisture levels, whereas at high pressure levels (10 and 15 MPa), the extrusion energy was almost equal to the compression energy. The higher extrusion energy was due to the increase in normal pressure between the die and the briquette. Hann and Harrison (1976) reported higher frictional energy at the higher compression pressures. The frictional

energy can be reduced by preheating the feed or die surfaces, maintaining smooth die surfaces and shortening the extrusion time (Reed et al., 1980). Preheating of die surface would considerably reduce the frictional energy. However, care should be taken to maintain uniform distribution of temperature between the die and briquette to avoid the surface cracking and breakage of briquettes during processing and storage.

Table 4.6 Specific energy requirement for compacting corn stover into briquettes.

Pressure, P (MPa)	Moisture content, M (% wb)	Compression energy, E_c (MJ/t)	Extrusion energy, E_e (MJ/t)	Total energy, $E= E_c + E_e$ (MJ/t)
5	5	8.41(0.17)*	4.23(0.17)*	12.64(0.24)*
	10	8.08(0.42)	3.41(0.11)	11.49(0.45).
	15	7.31(0.35)	3.88(0.40)	11.18(0.60)
10	5	11.61(0.73)	8.24(0.18)	19.85(0.84)
	10	10.38(0.48)	9.29(0.54)	19.67(1.01)
	15	11.80(1.34)	11.68(1.14)	23.47(2.11)
15	5	16.08(0.48)	13.22(0.68)	29.30(0.71)
	10	14.01(1.52)	14.92(0.28)	28.93(1.44)
	15	15.80(1.11)	15.25(1.11)	31.05(2.01)

*Numbers in the parenthesis are standard deviations for n = 5.
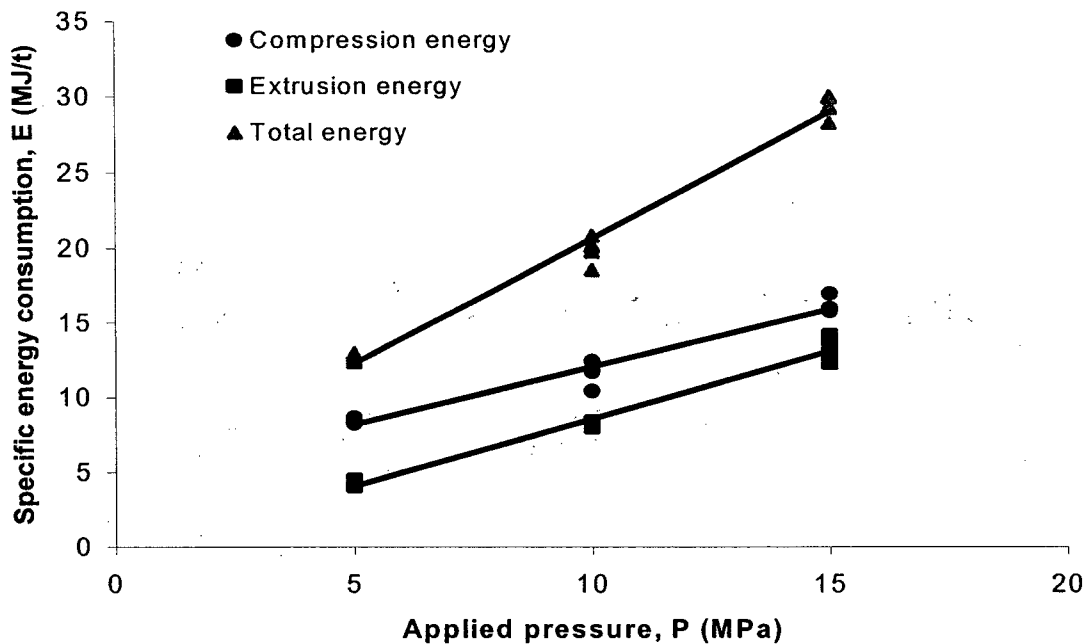
Figure 4.11 Relationship between specific energy of corn stover and pressure at 5% moisture content.

Analysis of variance showed that applied pressure, moisture content and interaction term had significant effect (P> 0.05) on the total energy consumption (Table 4.7). The magnitude of these variable effects was investigated from the linear model. From equation (4.11), it can be seen that applied pressure had the highest effect on the total energy consumption followed by moisture content and the interaction term. The negative effect of moisture content on the total energy consumption shows that an increase in moisture content decreases the total energy consumption. However, the magnitude of the moisture effect is considerably less than the magnitude of the applied pressure. Although there was a positive effect of interaction term (P x M) on the total energy consumption, the magnitude of the term is very less compared to other main effects. A linear relationship developed to predict the total specific energy consumption for corn stover was:

$$E = 4.76 + 1.48P - 0.19M + 0.032PM \qquad\qquad R^2 = 0.96 \qquad (4.11)$$

where, E is the total specific energy required producing briquettes in MJ/t; P is the pressure in MPa and M is the corn stover moisture content in percent wet basis.

Table 4.7 The ANOVA test results for the total energy consumption data.

Source	DF	Sum of Squares	Mean Sum of Squares	F value $\alpha=0.05$	Probability
Pressure, P	2	2426	1213	58	<0.0001
Moisture, M	2	28	14	11	0.0006
Interaction, (P x M)	4	37	9	11	0.0006
Error	36	54	1.5		

5.7 Summary

Among the five compaction models, the Kawakita-Lüdde and Cooper-Eaton models fitted well with the compression data of all biomass grinds. The Cooper-Eaton model parameters for biomass grinds showed that the prominent compaction mechanisms for biomass grinds are by particle rearrangement and elastic and plastic deformation. However, the mechanism of mechanical interlocking and ingredient melting phenomenon during compression of biomass must be studied for the comprehensive understanding of the compaction mechanism. The Kawakita-Lüdde parameter a, was related to the initial porosity of biomass grinds studied. From the parameter 1/b, the yield strength of compacts made from switchgrass was predicted higher than compacts from straws and corn stover. The compacts from corn stover grind had low yield strength value (1/b).

In the compaction study, the corn stover was densified up to a density range of 650 to 950 kg/m^3. The specific energy required to compress and extrude corn stover was in the range of 12 to 30 MJ/t. The extrusion (frictional) energy required to overcome the skin friction was about 60% of the total energy consumption at high pressure (15 MPa) and it should be reduced or eliminated to minimize the energy consumption. Therefore, future research should be focussed on designing a new densification unit with least energy demand.

CHAPTER 5

ENVIRONMENTAL SYSTEMS ANALYSIS

5.1 Introduction

The transformation of loose biomass into pellets requires power and heat energy and also generates emissions. As stated previously, drying of biomass using natural gas would result in high energy cost. In order to replace natural gas, other alternative fuels: coal, sawdust and pellets may be used in the drying process. In order to select the best fuel option, energy consumption, environmental impacts, cost and fuel quality must be considered. Biomass and coal are cheaper fuels compared to natural gas. However, the use of these alternative fuels would emit potential toxic pollutants namely, dioxin, furans, benzene, volatile organic compounds, trace metals. In the context of cleaner production, it is essential to quantify all potential emissions for each fuel used. The cost of production of biomass pellets depends on the total energy consumption, fuel cost and operating cost determined by the hours of operation and plant capacity. In order to achieve this goal, the environmental systems assessment technique is used to quantify energy, emissions and cost of the entire densification process. The assessment technique comprehensively evaluates the environmental impacts of producing pellets. The analysis can compare alternative choices, identify points for environmental enhancement, and provide support information for decision makers, who can have opportunities to improve the existing systems (Sonnemann et al., 2004).

Environmental systems assessment (ESA) technique is a decision making tool, which can be used to quantify the emission inventories and evaluate potential impacts of the entire system. The methodological framework of ESA is similar to the life cycle assessment (LCA) approach, but is streamlined within the confined system. It evaluates the calculation of total input and output streams of materials and energy from and to the system and quantifies the emissions in each step of the processes for the assessment of environmental impacts in a holistic manner. The methodological framework of this analysis is similar to the so-called simplified or streamlined LCA (SLCA) (Curran, 1996; Todd and Curran, 1999). The main intent of SLCA is to preserve the concept of LCA and

produce credible results, while at the same time to meet the economic, scientific and logistical constraints that are present in the analysis (Graedel et al., 1995).

The methodology of environmental assessment comprises of four stages: goal and scope definition, inventory analysis, impact assessment and interpretation (Figure 5.1.). The goal should state the intended application, the reasons for carrying out the study and the intended audience. The scope of ESA study is an iterative process that results in the definition of the functional unit, the establishment of system boundaries and data quality requirements. Inventory assessment is the process involving the compilation and quantification of inputs and outputs for a given product system throughout its system boundary. The goal and scope of the ESA provide the initial plan for the study and the inventory assessment concerns with the data collection and calculation procedures.
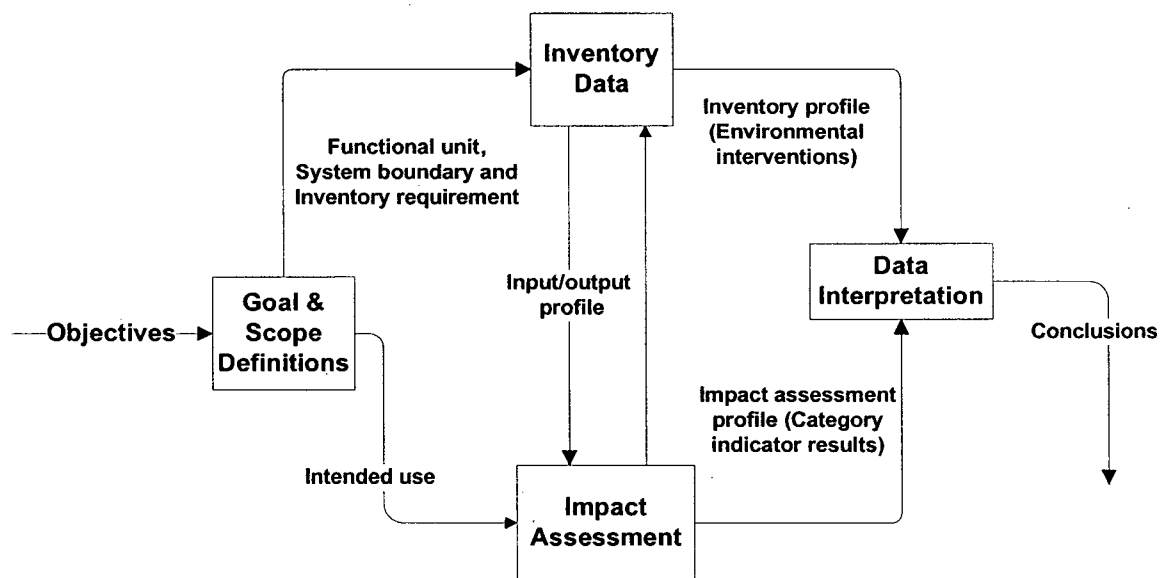
Figure 5.1 Methodological framework of environmental systems analysis.

The third stage of ESA study is to examine the impact assessment of the system from an environmental perspective, using impact categories and category indicators connected with the inventory results. The impact assessment connects the physical interventions included in the inventory assessment with recognized environmental impact categories (called classification). It continues to calculate the relative contribution of these physical interventions to the environmental impacts of concern (called characterization). The category indicator provides a link between a physical input or output to the natural environment and the estimates incremental increase in the

environmental impact (Fava et al., 1991; Consoli et al., 1993). Finally, the environmental impacts are interpreted and compared with alternatives to enhance the environmental performance of the system. Comparison and selection of alternatives may be performed based on the criteria set for each alternative. If a system deals with more than one number of criteria, it is difficult to compare and select the best alternative. For example, selection of the best alternative fuel for biomass densification system depends on the fuel quality, cost of the fuel, environmental impacts and energy consumption. Since many criteria are involved in selecting the best alternative, a multi-criteria decision making tool may be used. There are many multi-criteria decision making tools reported in the literature for outranking different alternatives (Albadvi, 2004; Pohekar and Ramachandran, 2004). Among them, Preference Ranking Organization METHod for Enrichment and Evaluation (PROMETHEE) is one method used in the development of decision making analysis (Brans et al., 1986; Al-Rashdan et al., 1999; Haralambopoulos and Polatidis, 2003). PROMETHEE is simple method for both quantitative and qualitative analysis of different alternatives. It performs a pair-wise comparison of alternatives in order to rank them with respect to a number of criteria. Aquino and Tan (2004) used the streamlined life cycle assessment tool to compare different packaging materials of industrial system and outranked the materials using PROMETHEE. The PROMETHEE is also extensively used in energy planning (Goumas and Lygerou, 2000), impact analysis of energy alternatives (Siskos and Hubert, 1983), building products design (Teno and Marseschal, 1998) and many other fields. In the present study, the PROMETHEE ranking method is used to select the best alternative fuel for the biomass densification process.

The environmental impact assessment tool has been used in many fields including agriculture, biomass and bioenergy production sectors. Rodrigues et al. (2003) reviewed and reported a strategic implementation of environmental impact assessment for the Brazilian agricultural system. Forsberg (2000) analyzed the bioenergy transport chain system in the form of biomass bales, pellets, tree sections for biofuel and electricity transport using life cycle inventory method. He concluded that biomass for energy can be transported for long distances without losing its environmental benefits. Environmental impacts and benefits of willow crop production system were analyzed by Heller et al. (2003) and it was reported that biomass crops are sustainable from an energy balance

perspective and contribute additional environmental benefits. Environmental impact assessment of various crop and animal feed production systems have been studied by many researchers to evaluate the environmental burdens using the concept of life cycle assessment method (Lewandowski and Heinz, 2003; Brentrup et al., 2004a,b; Skodras et al., 2004; van der Werf et al., 2005; Basset-Mens and van der Werf, 2005).

The main objectives of this study are: a) to conduct a systems analysis of the biomass densification process with alternative fuel sources; and b) to select the best alternative system based on the energy use, environmental impacts, economics and fuel quality for cleaner and economic production of biomass pellets.

5.2 Methodology

Systems analysis of biomass densification process was conducted using the environmental systems assessment approach along with energy and cost analysis. This section provides the description of the methodology used to calculate energy, emissions and cost of pellet production. The Multi criteria ranking method - PROMETHEE was also discussed to rank the alternative fuels for the biomass densification process.

5.2.1 Goal definition

The goal of this analysis is to identify and quantify the energy and emissions from the biomass densification process while using alternative fuels namely, pellets, wet biomass, dry biomass, coal and natural gas in the pellet production system and assess the environmental impacts on the pellet production process. The different alternative fuel systems are compared based on their environmental impacts and energy use. The economics of each fuel system are incorporated into the system during selection and outranking of the best alternative system. The functional unit used in the emission analysis is kg/t of pellet produced. The energy required for producing pellet is represented in MJ/t of pellet produced.

5.2.2 Scope of the study

The scope of this study is to perform a gate-to-gate analysis of biomass densification process based on the energy models developed in the previous chapters. The flue gas emissions from the dryer due to the direct combustion of different fuels are calculated based on the mass balance and emission factor methods. Electricity consumption of each unit operation in the process is estimated and converted into emission units. Emissions associated with electricity production are based on the local mix, i.e. 90% from hydropower and 10% from natural gas power plants in British Columbia. The emissions generated to produce electricity from hydro and natural gas power plants are included in this study. Emissions generated to produce coal, natural gas, diesel and wood pellets are also included based on the life cycle analysis of each fuel. Diesel fuel is consumed in the system to operate fork lifts, front end loader and dump trucks. In this study, the emission values for power and fuel sources are calculated on the basis of life cycle analysis, whereas the pellet production process is performed on the gate-to-gate basis.

5.2.3 System boundary

The system boundary for the present study is shown in Figure 5.2. The description of the densification process is given in Chapter 1. The wood pellet production plant located in Princeton, BC, was considered as a representative process system in this analysis. The equipment type, size and power data were taken from the plant for energy, emissions and economic analyses. In this system, wet sawdust at 40% moisture content was used as an input material. The sawdust is dried in the rotary dryer by the use of various alternative fuels. The dried material is collected by the cyclone separator and ground using a hammer mill. The ground sawdust is pelleted and cooled to room temperature before screening and packing. In this system, heat is supplied from combustion of different alternative fuels for the drying process, whereas electricity is used for operating equipment that are hammer mill, pellet mill, air supply fans, conveyers, feeders, cooling fan and packaging machinery.
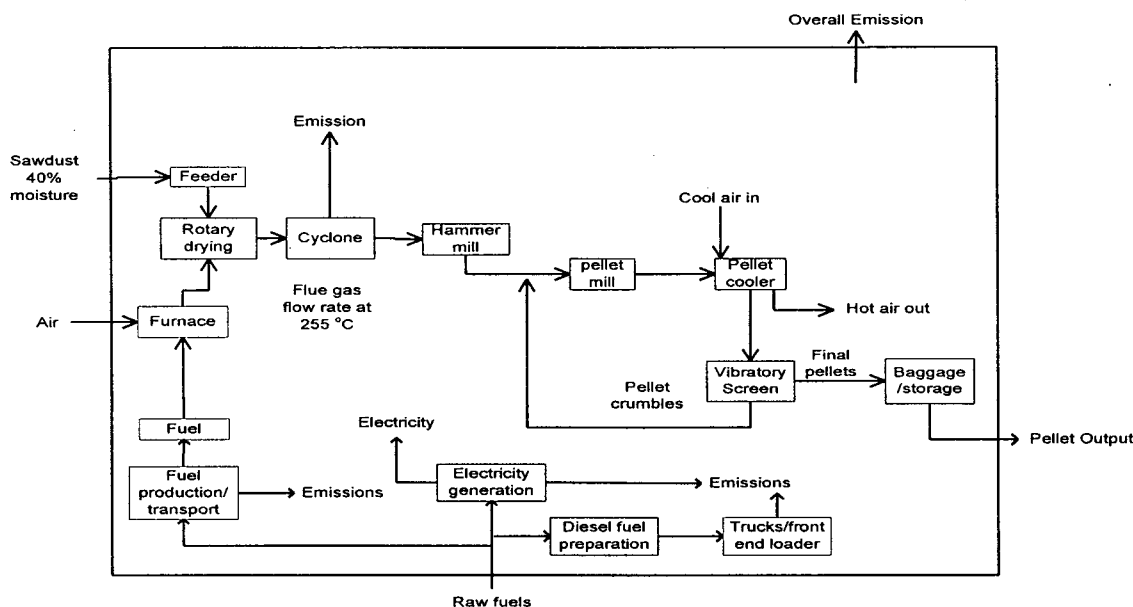
Figure 5.2 Process flow diagram of biomass densification plant and system boundary.

In the drying process, a single pass rotary dryer was used to dry sawdust. All the solid fuels were burned using a cyclonic burner and the flue gas generated were diluted to supply a required dryer temperature. The dryer inlet gas temperature is about 255°C. The burner system is modified if natural gas is used as a fuel. The alternative fuels used in the systems are wet sawdust, dry sawdust, wood pellets and bituminous coal. Except coal, all other alternative fuels were supplied within the system. However, in the environmental impact study, each fuel category was considered separately for impact assessment and system outranking. Size reduction of sawdust was performed using a hammer mill, which is operated by an electric motor. Similarly, the pellet mill, cooler fan, packing machine, screw conveyors, screw feeder and other accessories were operated using electric motors. The feeding of sawdust to the dryer was done by a front end loader. The raw material (sawdust) was supplied to the plant by a heavy-duty truck unit. The sawdust was collected from the sawmill plant, located closer to the pelleting plant and the sawdust is transported by dump trucks. The pellet plant has a sawdust buffer storage facility to feed the plant for up to three weeks.

5.2.4 Energy requirement calculations

Energy required for each unit operation is estimated based on the models developed in the previous chapters. The heat required by the dryer and the fuel required by the burner were estimated from the integrated single pass rotary dryer model. The hammer mill and pellet mill energy consumption was estimated based on the commercial mill data. Other accessories namely conveyors, feeders, fan power, dryer driving unit, burner air supply fan motor power was taken from the Princeton wood pellet plant. Table 5.1 shows different equipment used in the densification plant and the motor power. The energy required for the entire densification plant was estimated as both electric energy and heat energy and represented in kWh/t of pellet produced. Energy consumed by the trucks, front end loader and fork lifts were estimated in terms of diesel fuel consumption rate. Diesel fuel consumption rate of the machinery was estimated by ASAE Standard EP496.2 (ASAE, 2003):

$$Q_{avg} = (0.73)(0.305)P_m \qquad (5.1)$$

where Q_{avg} is the average fuel consumption in L/h and P_m is machinery power (kW).

Table 5.1 List of equipment used in the densification plant.

Equipment	Power (Hp)
Moving bed feeder motor	2
Hammer mill	200
Dryer drive unit	30
Dryer downstream fan	150
Air supply fan (burner)	20
Pellet mill	300
Cooler motor	20
Air supply fan (cooler)	30
Packing unit	10
Front end loader	70
Fork lifter	50
Dump truck	200
Conveyors and Elevators	70

5.2.5 Emission inventories

Emissions for the entire densification plant were calculated based on the energy and fuel use in the system. Electric energy data were used to calculate the emissions associated with electricity generation. Life cycle emission factors for producing electricity from various fuel sources are given in Appendix IV. Heat energy data were used to calculate emissions associated with the fuel's production and during fuel combustion process. Emissions from dump trucks, front end loader and fork lifts were also estimated based on the production and combustion of diesel fuel.

In the wood pellet densification system, major air pollutants were particulates, CO_2, CO, NO_x, SO_x, CH_4, TOC and VOC. The emissions generated during combustion of various fuel sources were considered from the burner model. Other minor pollutants for a particular fuel were calculated from the emission factors obtained from U.S. Environmental Protection Agency (EPA, 1995). Emissions generated due to the production of electricity from different sources were obtained from Koch (2000). In BC, 90% of the electricity is produced from hydro power plants and the remainder from natural gas power plants. Emissions from diesel fuelled-trucks, and other vehicles were obtained from EPA (1995) and Sheehan et al. (1998). Emissions during the production of coal and natural gas were obtained from Spath et al. (1999) and Spath and Mann (2001), respectively.

Wet sawdust and wood shavings are the waste products from sawmills. They have no monetary value. If the life cycle analysis of sawmill study allocates the total emissions based on the monetary value, all the emissions may be allocated to sawmill main product-lumbers. In this study, the emissions generated to produce wet sawdust and wood shavings are taken as zero. In the context of life cycle analysis, sawdust and wood pellets are considered as CO_2 neutral fuels. So, carbon dioxide emission during the combustion of sawdust and wood pellets is zero. However, other pollutants generated during biomass combustion were calculated from the emission factors. Recent study on wood chips and wood pellet combustion showed that under certain conditions, there would be a potential formation of some carcinogenic compounds, for example, benzene and some polycyclic aromatic hydrocarbons (PAHs). During the combustion of salt laden hog fuels, generation of dioxins and furans was found in the combustion flue gases (Bhargava et al.,

2002; Kjallstrand and Olsson, 2004; Olsson and Kjallstrand, 2004; Kakareka et al., 2005; Preto et al., 2005). Combustion of softwood pellet emits between 0.003 and 3.4 ppm of benzene and less than 0.01 ppm of Phenanthrene. Olsson et al (2003) stated that the concentration of benzene emissions from wood pellet combustion is lower than benzene concentrations in rooms with tobacco smokers and inside a private car in urban traffic (Barrefors and Petersson, 1993). Kakareka et al. (2005) have reported about 16 PAHs in fly ash and soot from the combustion of dry birch and pine firewoods. However, PAH emissions significantly depend on the type of fuel and furnace design. Since, most of the emitted PAHs were detected in fly ash and soot, they can be trapped or removed by bag houses and electro static precipitators (ESPs). Luthe et al. (1997, 1998) have found that more than 99% of the dioxins generated during combustion of hog fuels were collected by ESPs and multicyclones. Dioxin and furan emissions in the flue gas are below the emission regulations (Preto et al., 2005). So, emissions of dioxin and furans are not included in the emission inventory and impact assessment calculations. The emission of terpenes during drying of sawdust was reported to be as high as 80% of the initial terpene content. In this study, an emission factor of 1.85 kg terpene/dry tonne of sawdust is used (Stahl et al., 2004; Granstrom, 2003).

5.2.6 Impact assessment

The environmental impact assessment can be local, regional and global environmental issues. Global warming and stratospheric ozone depletion are problems with potential global implications for a large proportion of the earth's population. Smog formation and acid rain formation deposition are regional problems that can affect areas in size ranging from large urban basins up to a significant fraction of a continent. A health impact on human is due to the emission of toxic pollutants in the air.

Global warming potential: is the time integrated climate forcing from the release of 1 kg of a greenhouse gas relative to that from 1 kg of carbon dioxide

$$GWP_i = \frac{\int_0^n I_i C_i dt}{\int_0^{120} I_{CO_2} C_{CO_2} dt} \approx \frac{I_i \tau_i}{120 I_{CO_2}} \tag{5.2}$$

where, τ_i is the life time of the compound i in years, I_i is the infrared absorption band intensity of compound i and I_{CO2} is the infrared absorption banc intensity of carbon dioxide. For carbon dioxide, the lifetime is 120 years. The global warming index for any process is the sum of the emission weighed GWPs for each pollutant. Global warming potentials (GWPs) provide a means of comparing the effect of different greenhouse gases with that of CO_2 (Lashof and Ahuja, 1990; IPCC, 1994; and Rosa and Schaeffer, 1995). The global warming potential for different pollutants is given in Appendix V.

Acid rain potential: The potential for acidification by any compound is related to the number of moles of H^+ created per number of moles of the compound emitted. The precursor for acid rain, sulfur dioxide (SO_2) has been taken as a benchmark compound and the acid rain potential (ARP) of any emitted acid forming chemical is expressed relative to it (Heijungs et al., 1992).

$$ARP_i = \frac{(a/MW)_i}{(a/MW)_{SO_2}} \tag{5.3}$$

where, a is the number of H^+ ion emitted, MW_i is the molecular weight of the compound, i and MW_{SO2} is the molecular weight of sulphur dioxide.

Smog formation potential: Ozone formation in the lower atmosphere is due to the photo-dissociation of NO_2. The volatile organic compounds (VOCs) will form radicals, which can convert NO to NO_2 without causing O_3 destruction. The increase in the $[NO_2]/[NO]$ ratio will further increase the photolysis rate of NO_2. The tendency of individual VOCs to influence O_3 levels depends in part upon its reaction rate for the oxidation of the compound by the hydroxyl radical (OH^-), which is a measure of the tendency of the chemical to participate in photochemical reactions.

Incremental reactivity (IR) has been proposed as a method for evaluating smog formation potential for individual organic compounds. It is defined as the change in moles of ozone formed as a result of emission into an air shed of one mole (on a carbon atom basis) of the VOC. VOC incremental reactivities are generally higher at higher NO_x level. Lists of incremental smog formation reactivities for many VOCs have been compiled (Carter, 1994). Although several reactivity scales are possible, the most relevant for comparing VOCs is the maximum incremental reactivity (MIR), which occurs under high NO_x conditions when the highest ozone formation occurs (Carter,

1994). The smog formation potential (SFP) is based upon the maximum incremental reactivity (Carter, 1994):

$$SFP_i = \frac{MIR_i}{MIR_{org}}$$
(5.4)

where, MIR_i is the maximum incremental reactivity of compound, i and MIR_{org} is the average value for reactive organic gases or benchmark compound. Ethylene (C_2H_4) has also been widely used as the benchmark compound. The total smog formation potential is the sum of the MIRs multiplied by emission rates for each smog-forming chemical in the process.

Human toxicity impact: Human toxicity impact on air can be calculated by knowing the toxicity potential of each pollutant emitted to air. The human toxicity potential for some common pollutants and metal compounds is given in Appendix V.

After calculating all the emissions for the entire plant, the emission rates of pollutants were assessed based on the above impact categories. The above indicated emission impact indices can be calculated by knowing their impact potential factors. Impact categories and impacted areas of four selected potentials are given in Table 5.2.

Table 5.2 Impacts associated with emission categories.

Categories	Pollutants	Major impact category H = health impact E = Enviro. impact	Area impacted L= Local R= Regional G = Global
Greenhouse gas potential	CO_2, CH_4, CO, NO_x	H, E	R, G
Acid rain formation	SO_x, NO_x and more	H, E	L, R
Smog formation	NO_x and VOCs	H, E	L, R
Human toxicity	PM, VOCs, and more	H, E	L

5.2.7 Cost analysis

Cost analysis of a wood pellet densification plant was conducted to calculate the processing cost of wood pellet using various fuel sources. The total annual cost of any processing operation includes fixed (capital) cost and operating cost. The capital cost of the drying equipment is considered based on the total heat transfer area, and the flow rate of the fuel if the furnace is used for heat supply. All capital cost components follow the economy of scale, i.e. expansion of the unit size with respect to its characteristics dimensions will reduce the capital cost, non-proportional to the actual size of expansion (Kiranoudis et al., 1997; Krokida et al., 2002).

The total capital cost ($/y) can be given as:

$$C_c = eC_{eq} \qquad (5.5)$$

The capital recovery factor is given by the following equation:

$$e = \frac{i(1+i)^{N_t}}{(1+i)^{N_t} - 1} \qquad (5.6)$$

The equipment cost was found from the general relationship.

$$C_{eq}^{'} = \alpha_{eq} P^{n_{eq}} \qquad (5.7)$$

However, specific relationships were used for different equipment. The total cost, C_T can be calculated as:

$$C_T = C_c + C_{op} \qquad (5.8)$$

The process cost, C_P ($/kg) for any product can be estimated from the following equation

$$C_p = \frac{C_T}{t_{op} G_P} \qquad (5.9)$$

where C_T is the total annual cost ($/y), G_P is the production rate of the product (kg/h) and t_{op} is the operation hours per year (h/y).

Equipment price relationships quoted below are based on the 1985 US dollar value. These values are corrected to 2004 US dollar values by taking into account for consumer price index inflation factors (1.76) published by National Aeronautics and Space Administration (NASA) cost estimating website (http://www1.jsc.nasa.gov/bu2/inflateCPI.html). Specific cost relationship between equipment and characteristic parameter was obtained from Walas (1990).

88

Screw conveyor (k$ = $1000):

$$C_{eq} = 0.4L^{0.78} \qquad\qquad 7 < L < 100\,\text{ft} \qquad\qquad (5.10)$$

Bucket elevator (k$):

$$C_{eq} = 4.22L^{0.63} \qquad\qquad 10 < L < 100\,\text{ft} \qquad\qquad (5.11)$$

Centrifugal fans (k$):

$$C_{eq} = 2.2\exp\left[0.04 + 0.1821 * \ln Q + 0.0786 * (\ln Q)^2\right] \qquad 2 < Q < 900\,000\,\text{SCFM}$$

$$(5.12)$$

Rotary dryer(k$):

$$C_{eq} = 1.12\exp\left[4.9504 - 0.5827\ln A + 0.0925(\ln A)^2\right] \qquad 200 < A < 3000\,\text{ft}^2$$

$$(5.13)$$

Motors ($):

$$C_{eq} = 1.2\exp\left(5.1532 + 0.28931\ln \text{HP} + 0.14357(\ln \text{HP})^2\right) \quad 1 < \text{HP} < 7.5$$
$$= 1.2\exp\left(5.3858 + 0.31004\ln \text{HP} + 0.07406(\ln \text{HP})^2\right) \quad 7.5 < \text{HP} < 350$$

$$(5.14)$$

Variable speed drive coupling ($):

$$C_{eq} = \dfrac{12000}{1.562 + \dfrac{7.877}{\text{HP}}} \qquad\qquad \text{HP} < 75 \qquad (5.15)$$

Multicyclone (k$):

$$C_{eq} = 1.56Q^{0.68} \qquad\qquad 9 < Q < 180000\,\text{SCFM}$$

$$(5.16)$$

Equipment cost and capacity relationship (Ulrich, 1984) were used for pellet coolers, screen shakers, bagging unit.

$$C_{eq1} = C_{eq2}\left(\dfrac{C_1}{C_2}\right)^{ex} \qquad\qquad (5.17)$$

C_1 and C_2 are the capacity of equipment 1 and 2 and ex is the exponent.

The purchase and installation cost of various equipment were taken from Perry and Green (1999) and Walas (1990). The capital cost of hammer mill and pellet mill were received from the industrial experts.

5.2.8 Different scenarios of biomass densification system

In order to perform a systems analysis of the biomass densification process and select the best alternative fuel, the following five scenarios were considered:

1. A densification system using wood pellet as a fuel;
2. A densification system using wet sawdust as a fuel;
3. A densification system using dry sawdust as a fuel;
4. A densification system using coal as a fuel;
5. A densification system using natural gas as a fuel;

Figures 5.3 shows the system layout for all the scenarios considered in this analysis. Scenarios 1-5 plant layout produces about 5 t/h pellets, In addition to the above scenarios, two additional case studies (Scenario 6 & 7) were also included and compared with the above systems. Scenario 6 is the special case of the densification process (Figure 5.4), where the drying operation is eliminated due to the low moisture content of the feed material (wood shavings). Scenario 7 is similar to the plant located in Princeton with the pellet production rate of 11.5 t/h (Figure 5.5).
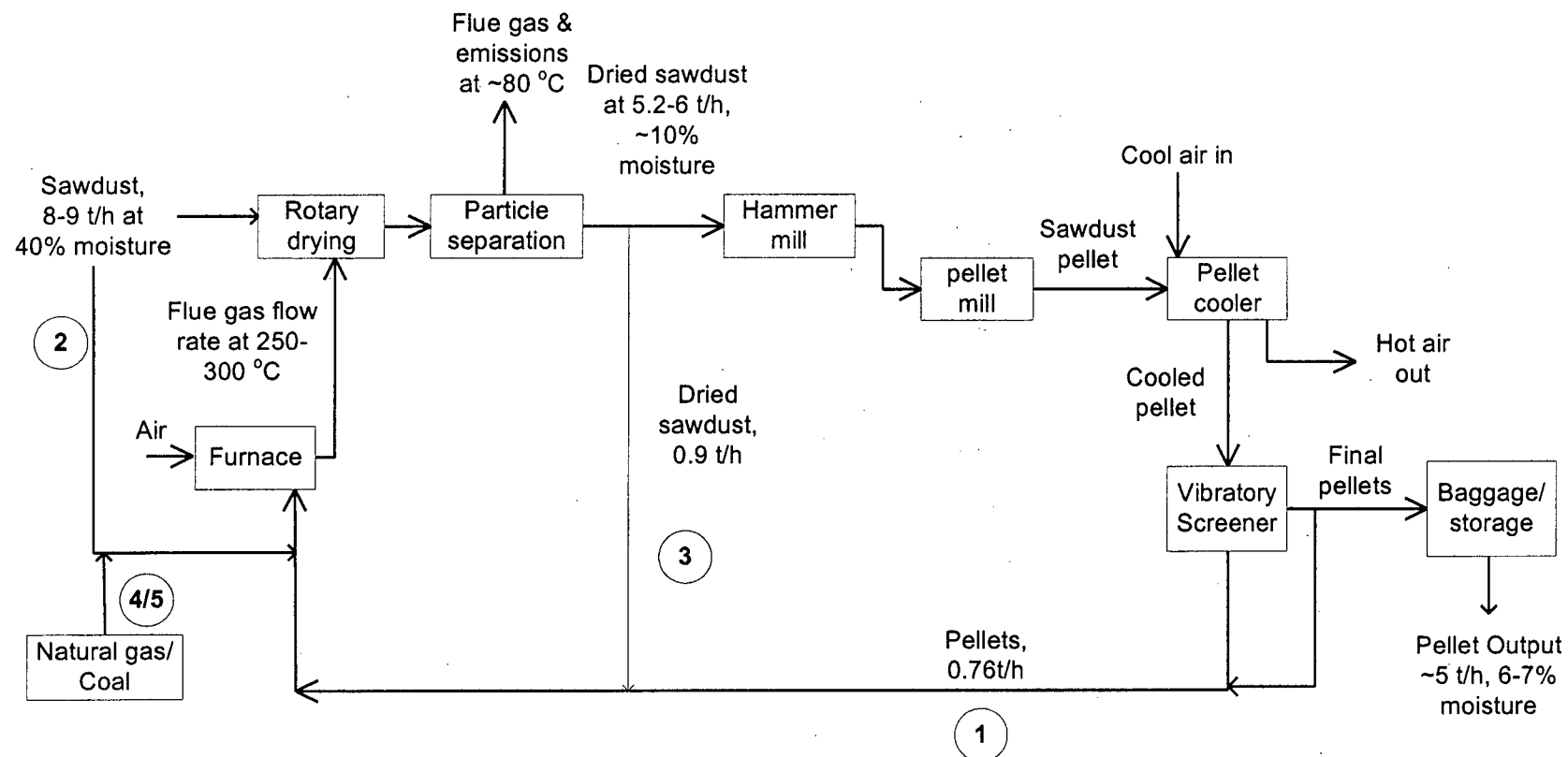
Figure 5.3 Process flow diagram of biomass densification plant for scenarios 1-5.
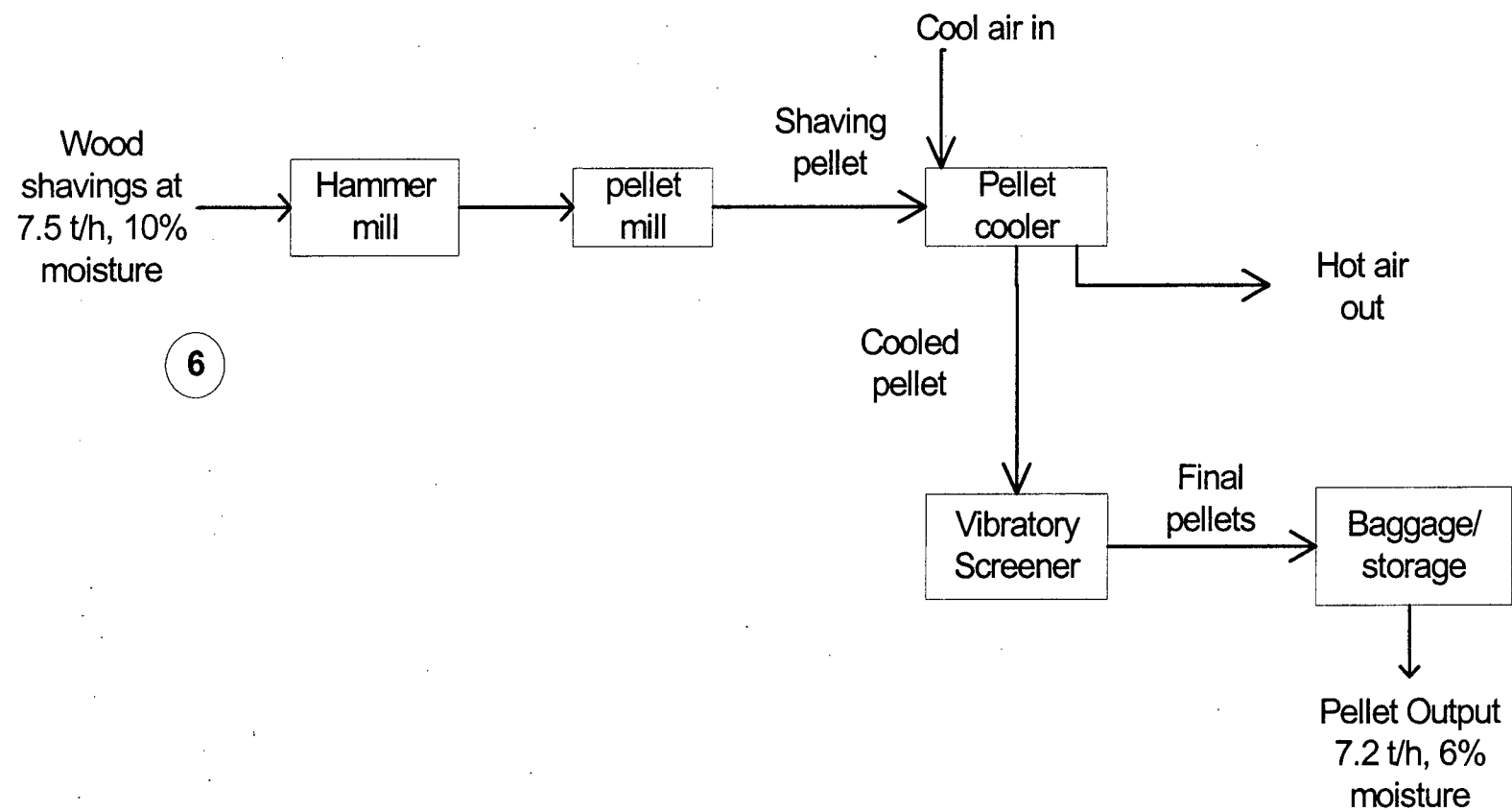
Figure 5.4 Process flow diagram of biomass densification plant for scenario-6.
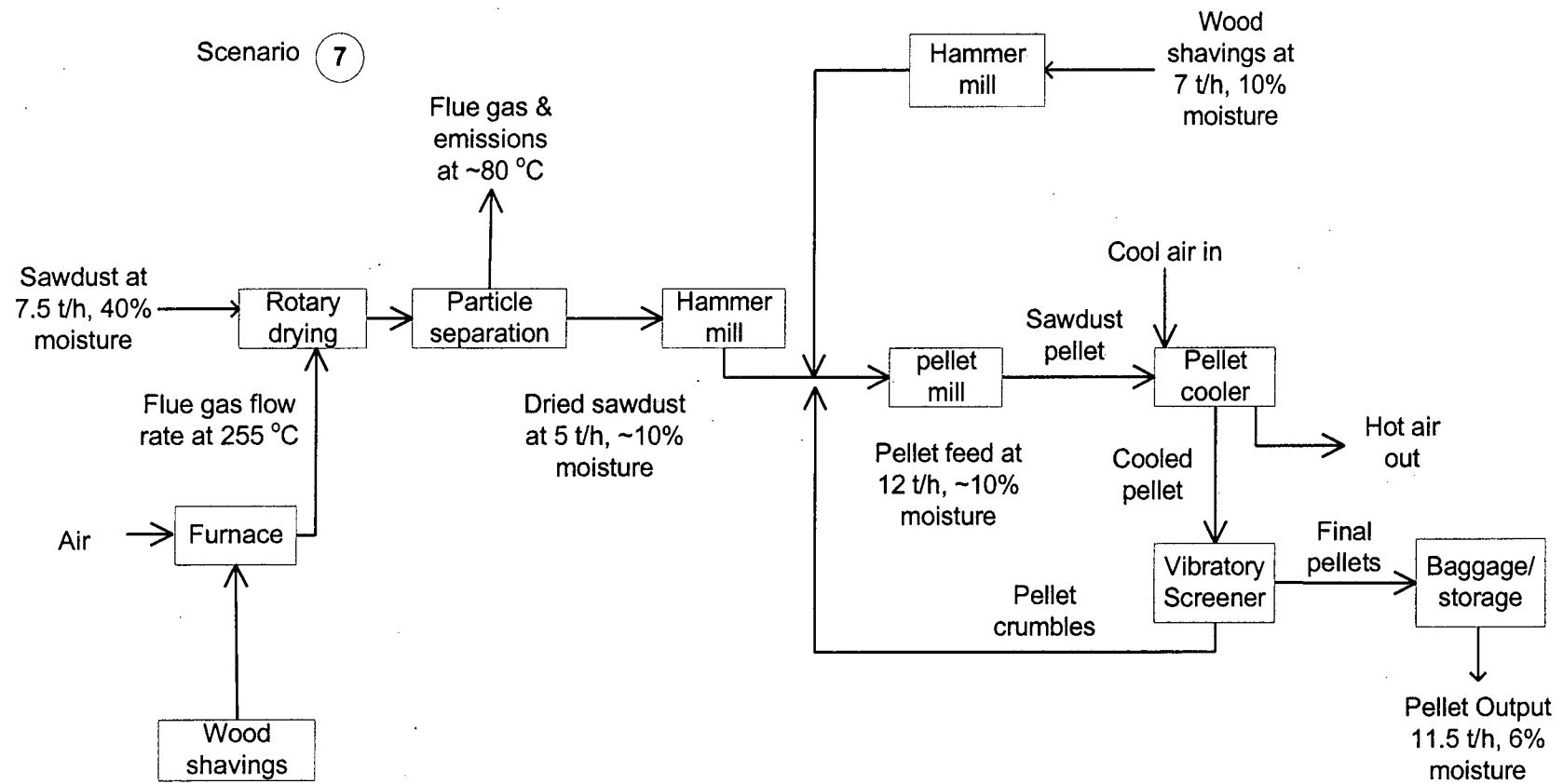
Figure 5.5 Process flow diagram of biomass densification plant for scenario-7.

5.2.9 Ranking of fuels using a multi-criteria decision making tool

Evaluation of energy, environmental impacts and economics of different scenarios, they were ranked based on four main criteria, i.e. energy use, environmental impacts, cost of production and quality of fuel source. Ranking of these scenarios were performed using Preference Ranking Organization METHod for Enrichment and Evaluations (PROMETHEE). PROMETHEE is a method of ranking a set of alternatives based on a number of criteria. The following are the procedures used in the PROMETHEE outranking method:

1. The scenarios to be compared are chosen with all the criteria values;

2. The differences among the criterion values for each scenario are calculated and used in the selection of preference criteria function;

3. For each criterion, the criterion function is selected by the decision maker and the threshold values - preference threshold and indifference threshold are defined for each function;

4. The preference index is calculated for each criterion of the scenario. The weighting factor for each criterion in the scenario is selected based on the decision maker's choice of preference. It is solely the responsibility of the decision maker to select or choose the weighting factors for each criterion;

5. Finally, the outranking is performed based on the calculation of leaving flow, entering flow and net flow calculations. The description of these calculations and the outranking schemes are outlined below.

Alternatives are compared in pairs, based on each criterion, and the result is a preference of one over the other. The preference is represented by a numerical value, P_i. P_i is estimated using a preference function (a function that translates the difference between the values of a criterion for two alternatives into a degree of preference). Six different preference functions are defined in the Decision Lab manual (Visual Decision Inc., 2003). The A "V" shaped (linear) preference function is often used for comparing quantitative criteria (cost, energy, and emission). A level based preference function is used to compare qualitative criteria. A 5-point scale can be used to assign values to qualitative criteria (Very High – 5, to Very Low - 1). The description of these preference

94

functions is given in Appendix VI. A weight, w_i, is assigned to each criterion based on the relative importance of the criterion. If two alternatives a and b are considered, the multi-criteria preference index, $\beta(a, b)$ for alternative a over b is the weighted average of the preference $P_i (a, b)$.

$$\beta(a,b) = \frac{\sum_{i=1}^{k} w_i P_i(a,b)}{\sum_{i=1}^{k} w_i} \qquad (5.18)$$

where $i = 1, 2, \ldots k$; k is the number of criteria (in this study, $k = 4$).

$\beta (a, b)$ represents the preference of a over b when k criteria are simultaneously. If $\beta (a, b) = 0$, there is no difference between a and b. If $\beta (a, b) = 1$, there is a strict preference of a over b. The weighting of each criterion in the PROMETHEE method is usually determined by an experienced decision maker. There is no standard rule in the PROMETHEE method to decide on the weighting of each criterion.

In order to outrank alternatives, two methods are proposed based on the strength and weakness of the alternatives (Brans et al., 1986). The strength of an alternative is defined by leaving flow, $\varphi^+ (a)$. The weakness of an alternative is defined by entering flow, $\varphi^- (a)$. The multi-criteria preference index, $\beta (a, b)$ defined previously, is used to evaluate the leaving flow $\varphi^+ (a)$ and entering flow $\varphi^- (a)$.

$$\varphi^+(a) = \sum_{i=1}^{m} \beta(a,i) \qquad (5.19)$$

$$\varphi^-(a) = \sum_{i=1}^{m} \beta(i,a) \qquad (5.20)$$

$$\varphi(a) = \varphi^+(a) - \varphi^-(b) \qquad (5.21)$$

where, m is the set of alternatives. The PROMETHEE method ranks the alternatives based on two ranking schemes - PROMETHEE I and PROMETHEE II. In PROMETHEE I ranking method, the best alternative is selected based on the highest value of leaving flow, $\varphi^+ (a)$, and the lowest entering flow, $\varphi^- (a)$. The PROMETHEE I partial ranking may be incomplete in some cases. This means that some alternatives cannot be compared and cannot be included in a complete ranking. This occurs when the first alternative obtains high scores on particular criteria for which the second alternative

obtains low scores and the opposite occurs for other criteria. In PROMETHEE II ranking method, the selection is based on the net flow, φ (a), which is defined as the difference between the leaving flow and the entering flow as given in Eq. 5.21. PROMETHEE II provides a complete ranking of the alternatives from the best to the worst one. Table 5.3 shows the cases when an alternative is preferred over the other using these ranking methods. Further description of PROMETHEE method and its application to decision supporting framework can be found elsewhere (Brans and Vincke, 1985; Brans et al., 1986; Al-Rashdan et al., 1999; Haralambopoulos and Polatidis, 2003; Albadvi, 2004; Macharis et al., 2004; Pohekar and Ramachandran, 2004).

Table 5.3 Description of ranking methods and preference cases.

Ranking Method	Decision	Cases
PROMETHEE I	a outranks b	if φ^+ (a) $> \varphi^+$ (b) & φ^- (a) $< \varphi^-$ (b)
		or, φ^+ (a) $> \varphi^+$ (b) & φ^+ (a) $= \varphi^+$ (b)
		or, φ^+ (a) $< \varphi^+$ (b) & φ^- (a) $= \varphi^-$ (b)
	a is indifferent to b	if φ^+ (a) $= \varphi^+$ (b) & φ^- (a) $= \varphi^-$ (b)
	a and b are incomparable	otherwise
PROMETHEE II	a outranks b	if φ (a) $> \varphi$(b)
	a is indifferent to b	if φ (a) $= \varphi$ (b)

In the present analysis, four main criteria namely energy consumption, environmental impacts, economics and fuel quality were considered. Energy consumption, economics and environmental impacts values must be minimized and the fuel quality must be maximized to select the appropriate alternative. The energy consumption of each scenario is important in the ranking procedure as it varies with different fuel options. The energy consumption criterion is defined by "V" shaped linear criterion function with preference threshold, p. The preference threshold value for energy consumption was set as 50 MJ/t of pellet. This implies that if the difference between the energy values for two alternatives is 50 MJ/t, the alternative with the lower energy value (min) is strongly preferred over the other.

Environmental impact criterion is further sub-divided into four criteria namely greenhouse gas (climate change), acid rain formation, smog formation and human toxicity impacts. A "V" shaped linear criterion function was assigned for both environmental impact and cost criteria. Fuel quality is also an important criterion as it provides better combustion efficiency, less environmental emissions and the quality of the flue gas, if some food materials are to be dried. Fuel quality is also important in terms of its accessibility and easy transportation to the pelleting plant. Fuel quality is the qualitative criterion and the rating for the selected five fuel sources are wood pellet – high; wet sawdust –low; dry sawdust – average; coal –very low; and natural gas – very high. The rating for different fuels is based on the combustion quality, easy accessibility and handling, potential emissions and discussions with experienced users.

Table 5.4 Input assumptions for ranking densification alternatives

Criteria	Energy consumption (MJ/t)	Fuel quality	Pellet cost ($/t)	Environmental impacts			
				Climate change (kg of CO_2 eq./t)	Acid rain formation (kg of SO_2 eq./t)	Smog formation (kg of C_2H_4 eq./t)	Human toxicity (kg/t)
Min/Max	Min	Max.	Min	Min	Min	Min	Min
Weight	0.25	0.25	0.25	0.0625	0.0625	0.0625	0.0625
Preference function	V- shape	level	V – shape	V – shape	V- shape	V- shape	V- shape
Preference threshold	50	0.5*	3	20	0.2	0.5	0.2

* indifference threshold

The preference and indifference thresholds for each criterion were set based upon discussions with experienced scientists and stakeholders. However, these values could be changed, if the decision maker is not satisfied with the outranking results. The decision maker has more power to select the best alternative for this complex multi-criteria problem. It may be a drawback of this method, if an inexperienced decision maker conducts this analysis. Consistency of the ranking may not be obtained. The outranking of alternatives was performed using the Visual Decision Lab software (Visual Decision

Inc., Montreal, QC). The parameters used for each criterion to select the best alternative are given in Table 5.4. The PROMETHEE I, PROMETHEE II ranking schemes and the weighting factor stabilities were analyzed for the best selection of the alternative.

5.3 Results and Discussions

This section presents the results obtained from the energy, emissions and cost calculations for each scenario and discusses ranking of alternative fuels for the biomass densification process. Sensitivity analysis of the weighting factors for each criterion was also performed to analyze the stability of the ranking scheme.

5.3.1 Energy consumption of biomass densification systems

Table 5.5 shows the complete heat and mass balance for all the scenarios considered in this study. Figure 5.6 shows the breakdown energy consumption of producing wood pellets using different proposed fuel sources. It can be observed that the electrical energy and diesel energy data were constant in the first five scenarios. However, the heat energy consumption varies widely depending on the fuel used. The highest heat energy is consumed by scenario 2, which uses wet sawdust as a fuel with low combustion efficiency and thus requires high heat energy input. In the case of scenarios 1 and 3, the heat energy is high, because large amount of sawdust must be dried in order to meet the constant production rate. The densification plant itself supplies the fuels to the burner for scenarios 1 and 3. In the case of scenario 6, the total energy consumption is the least per tonne of pellet produced, as there is no drying operation in this process. Scenario 7 also has low energy consumption due to the combined effect of scenarios 6 and 1.

Table 5.5 Material and energy balances for different biomass densification scenarios.

	Scenario 1	Scenario 2	Scenario 3	Scenario 4	Scenario 5	Scenario 6	Scenario 7
Input							
Raw material (t/h)	9	7.8	9	7.8	7.8	7.5	7.5 + 7.0
Feed moisture (% (wb))	40	40	40	40	40	10	40+ 10
Fuel type	Wood pellet	Wet sawdust	Dry sawdust	Coal	Natural gas	no fuel	Shavings
Dryer inlet temp. (°C)	280	255	280	255	255		255
Fuel rate (kg/t)	152.6	264	179.6	97	44.6	0	70.09
Total electricity use (kWh/t)	119.53	112.17	119.53	112.17	112.17	54.50	93.90
Diesel use (l/h)	5.56	5.29	5.56	5.29	5.29	3.67	3.25
Energy (MJ/t pellet)							
Electrical energy	430.31	403.80	430.31	403.80	403.80	196.19	338.02
Fuel energy	2746.80	3168.00	3053.20	2813.00	2363.80	0.00	2032.52
Diesel energy	205.73	205.73	205.73	205.73	205.73	135.86	120.14
Total	3382.84	3777.53	3689.24	3422.53	2973.33	332.05	2490.69
Output							
Pellet production (t/h)	5	5	5	5	5	7.2	11.5
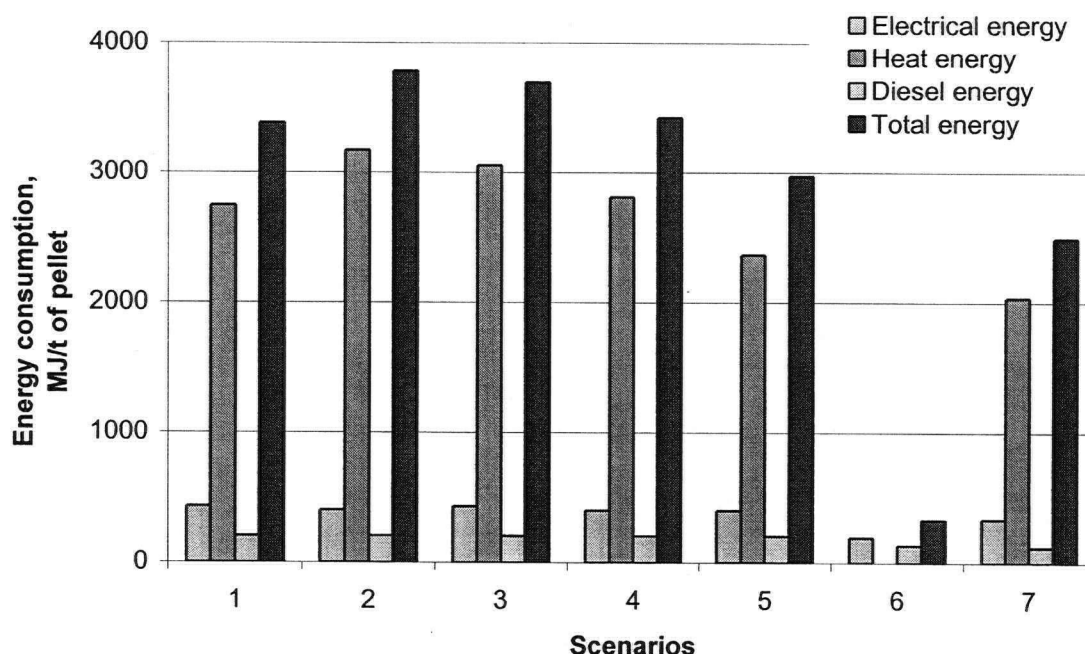
Figure 5.6 Energy consumption of different biomass densification systems.

5.3.2. Environmental emissions inventory

Emissions from different biomass densification systems are presented in Table 5.7. Carbon dioxide emissions from coal combustion (scenario 4) is the highest followed by natural gas combustion (scenario 5). Since the net CO_2 emission from combustion of biomass fuels is zero, less amount of CO_2 is generated, which is associated with the consumption of electric energy and diesel energy in the system. All terpene emission is accounted for emissions during the drying of sawdust. Stahl et al. (2004) reported that more than 80% of the terpenes available in the feed material are emitted during the drying process and the other 10% of terpenes are emitted during the pelleting process. During the drying process, most of the terpenes are emitted in the form of alpha-pinenes, beta-pinenes and carenes. Among these compounds, carene is the most toxic to humans due to its carcinogenic effect (Kurttio et al., 1990). However, emissions of these compounds are affected by many factors namely, wood species, dryer type and operating parameters. Combustion of wood pellets and wood powders also emits many polycyclic aromatic hydrocarbons (PAHs), dioxins and furans. Emission of these compounds

depends on the type of burner and quality of combustion. Apart from these emissions, wood pellets are environmentally friendly fuels due to the uptake of the major greenhouse gas-carbon dioxide by photosynthesis. Biofuels play a key role in supporting the non-dependence of fossil fuels and the mitigation of greenhouse gas emissions to the atmosphere.

Table 5.7 shows a breakdown of emissions from fuels, electricity and heat energy for scenario 1, which uses wood pellet as a fuel. Although wood pellet is considered as a CO_2 neutral fuel, air pollutants emitted during the wood pellet production cycle can't be neglected. In Table 5.7, wood pellet contributes about 13% of the total emissions generated from the wood pellet plant. The major emission contributions are from combustion of various fuels. Tables 5.8 and 5.9 show the breakdown emissions for scenario 4 (coal) and 5 (natural gas), respectively. Combustion of coal contributes more than 90% of emissions namely, CO_2, particulate matters, SO_x, HF and HCl. These emissions are very significant compared to other fuels: wood pellets and natural gas. Therefore, application of coal for the biomass drying process is not good due to a large amount of environmental emissions. It can be observed from Table 5.9 that more than 90% of benzene, VOCs and methane are generated during the production of natural gas. Emissions from the combustion of natural gas are very low compared to other solid fuels: coal and wood pellets. All emissions data were calculated from the uncontrolled emission factors except for the particulate matter emissions.

Table 5.6 Emission inventory for different biomass densification systems.

Air emission (kg/t of pellets)	Scenario 1	Scenario 2	Scenario 3	Scenario 4	Scenario 5	Scenario 6	Scenario 7
CO_2	3.39E+01	2.78E+01	2.94E+01	2.80E+02	1.93E+02	1.77E+01	2.66E+01
CO	1.78E-01	2.22E-01	1.72E-01	1.36E-01	2.39E-01	3.78E-02	4.00E-01
SO_x	1.51E-01	1.27E-01	1.32E-01	3.24E+00	2.09E-01	6.38E-02	1.12E-01
NO_x	4.53E-01	4.82E-01	4.17E-01	4.71E-01	5.14E-01	1.65E-01	3.71E-01
CH_4	6.43E-03	5.30E-03	5.58E-03	1.92E-01	9.24E-01	3.67E-03	5.45E-03
NH_3	0.00E+00	0.00E+00	0.00E+00	4.50E-02	3.81E-03	0.00E+00	0.00E+00
Terpene	1.04E+01	9.04E+00	7.83E+00	7.83E+00	7.83E+00	2.51E+00	7.53E+00
VOCs	5.79E-03	4.85E-03	4.94E-03	2.35E-02	2.20E-01	3.02E-03	4.54E-03
PM	1.80E+00	1.42E-02	1.46E-02	7.65E-01	2.26E-02	9.04E-03	1.74E+00
N_2O	2.15E-04	1.77E-04	1.87E-04	3.82E-04	3.01E-03	1.23E-04	7.63E-03
HCl	1.00E-04	8.27E-05	8.70E-05	5.29E-02	8.27E-05	5.72E-05	1.10E-02
HF	1.26E-05	1.04E-05	1.09E-05	6.61E-03	1.04E-05	7.16E-06	1.06E-05
Benzene	6.90E-04	5.52E-04	5.65E-04	3.09E-06	2.46E-05	7.66E-07	2.22E-04
Formaldehyde	1.80E-05	1.49E-05	1.56E-05	1.49E-05	1.49E-05	1.03E-05	1.53E-05

Table 5.7 Average air emission for scenario 1 (wood pellet as a fuel)

Air emission (kg/t)	% of total from producing diesel	% of total from diesel use	% of total from electricity Use	% of total from producing pellet fuel	% of total from flue gas drying	Total emission kg/t of pellet
CO_2	51.44	11.49	23.83	13.24	n.a	3.4E+01
CO	19.61	12.69	n.a	13.24	54.46	1.8E-01
SO_x	16.90	4.60	61.81	13.24	3.45	1.5E-01
NO_x	30.41	23.16	2.53	13.24	30.66	4.5E-01
CH_4	86.76	n.a	n.a	13.24	n.a	6.4E-03
Terpene	n.a	n.a	n.a	13.24	86.76	1.0E+01
VOCs	62.41	n.a	24.35	13.24	n.a	5.8E-03
PM	0.33	0.41	0.03	13.24	85.99	1.8E+00
N_2O	86.76	n.a	n.a	13.24	n.a	2.2E-04
HCl	86.76	n.a	n.a	13.24	n.a	1.0E-04
HF	86.76	n.a	n.a	13.24	n.a	1.3E-05
Benzene	0.47	n.a	n.a	13.24	86.29	6.9E-04
Formaldehyde	86.76	n.a	n.a	13.24	n.a	1.8E-05

n.a = data not available

Table 5.8 Average air emissions from the pellet plant (scenario 4 – Coal as a fuel)

Air emission (kg/t)	% of total from producing diesel	% of total from diesel use	% of total from electricity Use	% of total from producing coal	% of total from flue gas drying	System total kg/t of pellet
CO_2	5.92	1.32	2.70	0.70	89.36	2.8E+02
CO	24.44	15.82	n.a	1.38	58.35	1.4E-01
SO_x	0.75	0.20	2.70	0.45	95.90	3.2E+00
NO_x	27.79	21.16	2.28	2.06	46.72	4.7E-01
CH_4	2.76	n.a	n.a	95.87	1.37	1.9E-01
NH_3	n.a	n.a	n.a	44.68	55.32	4.5E-02
Terpene	n.a	n.a	n.a	n.a	100.00	7.8E+00
VOCs	14.61	n.a	5.63	70.40	9.36	2.4E-02
PM	0.73	0.93	0.07	0.34	97.92	7.6E-01
N_2O	46.47	n.a	n.a	53.53	n.a	3.8E-04
HCl	0.16	n.a	n.a	n.a	99.84	5.3E-02
HF	0.16	n.a	n.a	n.a	99.84	6.6E-03
Benzene	100.00	n.a	n.a	n.a	n.a	3.1E-06
Formaldehyde	100.00	n.a	n.a	n.a	n.a	1.5E-05

n.a = data not available

Table 5.9 Average air emissions from pellet plant (Scenario 5 – Natural gas as a fuel)

Air emission (kg/t)	% of total from producing diesel	% of total from diesel use	% of total from electricity Use	% of total from producing natural gas	% of total from flue gas drying	Total emission kg/t of pellet
CO_2	8.60	1.92	3.93	11.28	74.27	1.9E+02
CO	13.92	9.01	n.a	35.11	41.97	2.4E-01
SO_x	11.61	3.16	41.90	42.99	0.34	2.1E-01
NO_x	25.47	19.40	2.09	29.86	23.18	5.1E-01
CH_4	0.57	n.a	0.00	99.13	0.30	9.2E-01
NH_3	n.a	n.a	n.a	n.a	100.00	3.8E-03
Terpene	n.a	n.a	n.a	n.a	100.00	7.8E+00
VOCs	1.56	n.a	0.60	94.85	2.98	2.2E-01
PM	24.80	31.31	2.51	30.82	10.56	2.3E-02
N_2O	5.89	n.a	n.a	6.91	87.20	3.0E-03
HCl	100.00	n.a	n.a	n.a	n.a	8.3E-05
HF	100.00	n.a	n.a	n.a	n.a	1.0E-05
Benzene	12.59	n.a	n.a	87.41	n.a	2.5E-05
Formaldehyde	100.00	n.a	n.a	n.a	n.a	1.5E-05

n.a = data not available

5.3.3 Environmental impact assessment

All the air emissions were analyzed based on the four impact categories previously discussed and were assessed based on global, regional and local issues (Table 5.2). The impact categories for each scenario were used to rank different alternatives. Figure 5.7 shows the greenhouse gas emissions from the different wood pellet production scenarios. The global warming potential is used to express the contribution of gaseous emissions from arable production system to the environmental problem of climate change. The CO_2 equivalent for scenario 4 (coal) was the highest among all the scenarios followed by scenario 5 (natural gas). Figure 5.8 shows the acid rain formation, smog formation and human toxicity potentials of the different wood pellet production scenarios. In terms of smog formation potential, scenario 6 had the lowest environmental impact due to the elimination of the drying process. Terpene emissions during the drying process contribute to the highest value of smog formation potential for all the scenarios, except scenario 6. It can be concluded that scenario 4 has the highest environmental and health impacts among the scenarios considered in this analysis.
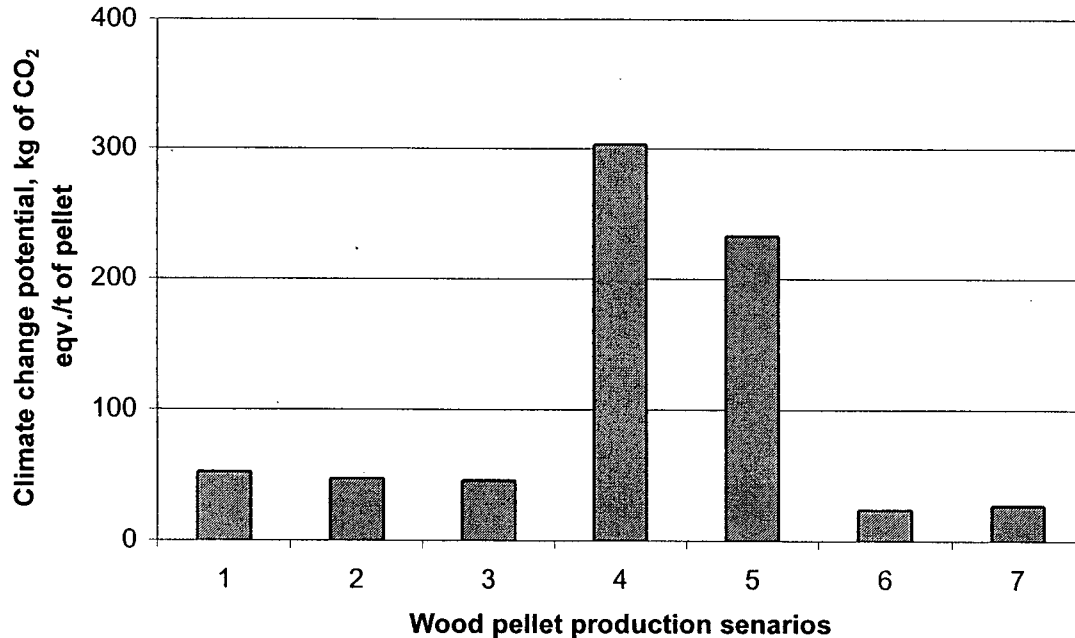
Figure 5.7 Comparison of wood pellet production scenario with climate change (greenhouse gas impact).
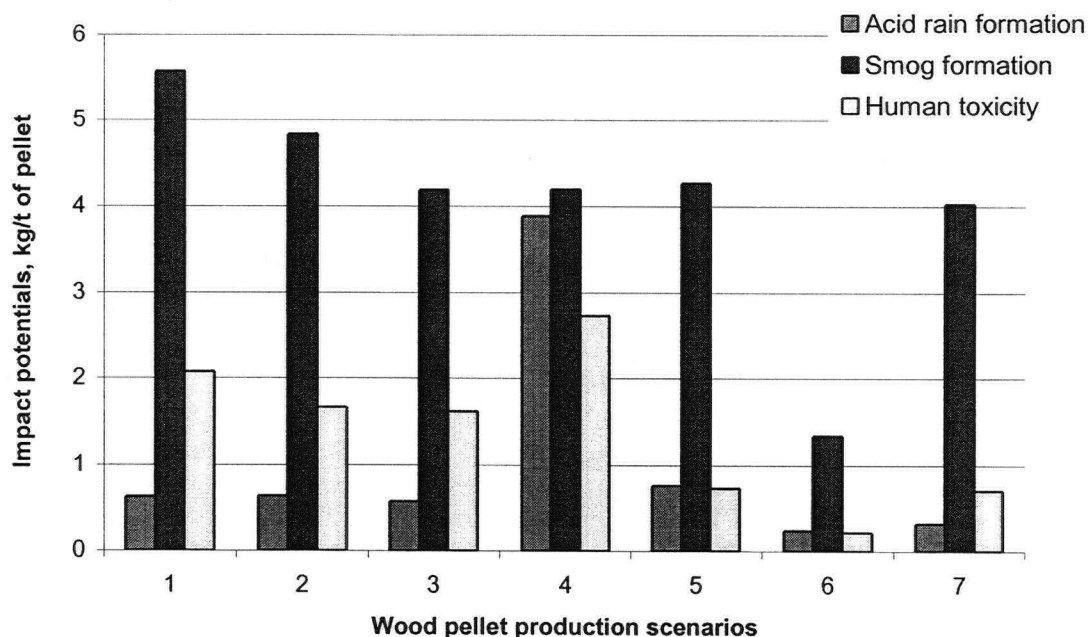
Figure 5.8 Comparison of pellet production scenarios with local and regional impact categories.

5.3.4 Cost analysis

Figure 5.9 shows the breakdown of the cost of producing wood pellets from different densification systems. The capital cost of the plant was almost constant for all the scenarios except scenario 6. For scenario 5, the capital cost was slightly less due to natural gas burner. All other scenarios (1-4) use the same solid fuel burner for fuel combustion. Pellet production cost depends on plant capacity and hours of operations, which account for the operating cost of the plant. Since the pellet production capacity was high for scenarios 6 and 7, the total cost of wood pellet was low compared to other scenarios. From the first five scenarios, the operating cost for scenario 5 (natural gas) is the highest (US$ 71/t) followed by scenario 1, which uses wood pellets as a fuel. This is mainly due to the high fuel cost. The pellet production cost may be reduced, if coal or sawdust is used as a fuel. Appendix VII presents a typical costing procedure and the parameters used in the cost analysis. A detailed cost calculation for scenario 7 was also given in Appendix VII.
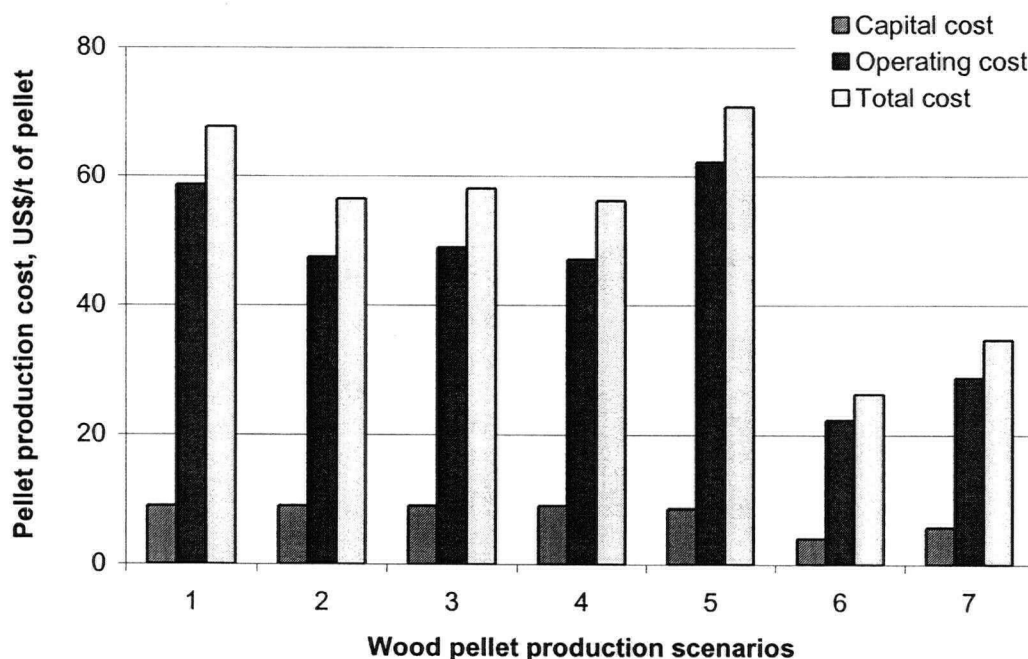
Figure 5.9 Pellet production cost for different scenarios.

5.3.5 Ranking of biomass densification systems

In order to rank the different alternative systems of biomass densification, the Decision Lab 2000 software was used. The ranking was performed based on the PROMETHEE method as previously described. The criteria used for the decision process were: 1) total energy consumption; 2) environmental and human impacts; 3) pellet production cost; and 4) fuel quality. In the initial decision making process, equal weighting factors were assigned with all the criteria. PROMETHEE I ranking provides the partial ranking of all the alternatives. On the other hand, PROMETHEE II provides a complete ranking of all selected scenarios without any comparable scheme. From Figure 5.10, it can be seen that wood pellet and dry sawdust are not comparable or can not be ranked. The inflow (φ^-) and outflow (φ^+) values for both wood pellet and dry sawdust were very close to each other. PROMETHEE II ranking scheme provides a complete ranking of the alternatives based on the net flow value (φ). Higher the fuel netflow value, better is the fuel ranking. Weighting is a critical factor in the decision making process. The outranking of alternatives is influenced by the weighting factors selected by the decision maker. Table 5.10 shows the stability of weighting factors used in the

108

outranking, when equal weighting factors are used for each criterion. Within the weighting values (min – max) allocated for each criterion, the ranking of alternatives would not change. For example, if the weight factor for the energy consumption value is changed up to 0.46, the outranking scale would be influenced a lot.
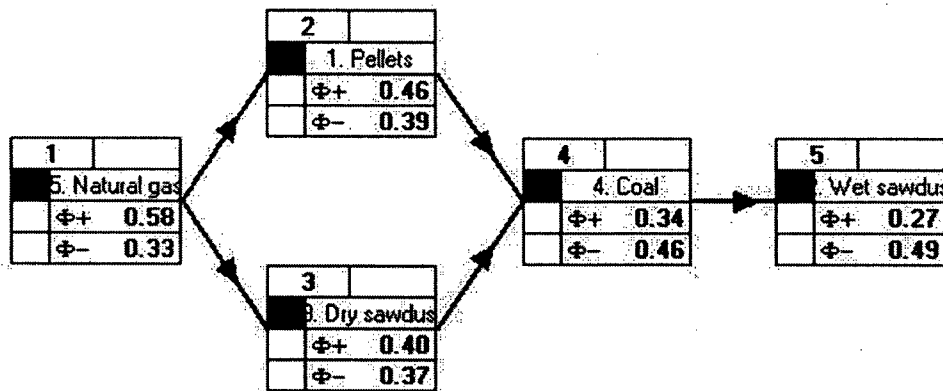
Figure 5.10 PROMETHEE I partial ranking scheme (equal weighting).
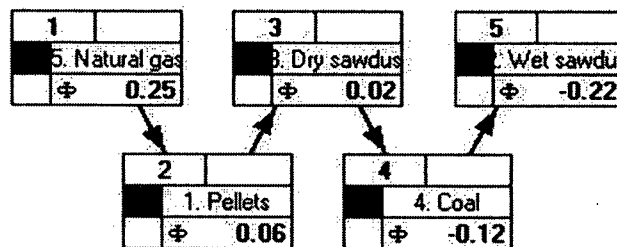
Figure 5.11 PROMETHEE II complete ranking scheme (equal weighting).

Table 5.10 Stability of weighting factors allocated for ranking.

Criteria	Weight factors	Min	Max
Energy consumption	0.25	0.205	0.499
Climate change	0.063	0	0.222
Acid rain formation	0.063	0	0.138
Smog formation	0.063	0	0.090
Human toxicity	0.063	0	0.115
Cost of production	0.25	0	0.309
Fuel quality	0.25	0.164	0.517

Based on equal weighting, wood pellet or dry sawdust may be the best alternative to natural gas followed by coal and wet sawdust. Wood wastes as a direct heating fuel for drying application may be used with caution, because if PAHs, dioxins and furans are found in combusted flue gases with high concentration, there may be a chance that these toxic compounds might contaminate with the material being dried. Similarly, the use of coal in the drying process is also critical due to sulfur emissions and other toxic metals namely mercury, cadmium, cyanide. In order to assess the effect of each criterion of fuel ranking, the weighting factors for each criterion may be changed. So, the decision maker has the capability to decide the weighting factor for each criterion to select the best alternative as appropriate to the goals set for improvement. The fuels were ranked and compared with the base case (equal weighting). Table 5.11 shows the PROMETHEE II complete ranking scheme to rank different fuel sources. If the decision maker or a stakeholder decides to double the weighting factor for the pellet production cost, the PROMETHEE II outranking changes into: 1) coal; 2) dry sawdust; 3) wet sawdust; 4) wood pellet; and 5) natural gas.

Table 5.11 Sensitivity analysis of selection criteria on PROMETHEE II fuel ranking[*].

Ranking	Base case (equal weight)	Double weighting for each criterion			
		Energy use	Enviro. impacts	Cost	Fuel quality
1	Natural gas (0.25)	Natural gas (0.5)	Natural gas (0.2)	Coal (0.15)	Natural gas (0.46)
2	Pellets (0.06)	Pellets (0.19)	Dry sawdust (0.11)	Dry sawdust (0.09)	Pellets (0.21)
3	Dry sawdust (0.02)	Coal (-0.06)	Pellets (-0.02)	Wet sawdust (0.06)	Dry sawdust (0.02)
4	Coal (-0.12)	Dry sawdust (-0.15)	Wet sawdust (-0.12)	Pellets (-0.13)	Wet sawdust (-0.31)
5	Wet sawdust (-0.22)	Wet sawdust (-0.48)	Coal (-0.17)	Natural gas (-0.17)	Coal (-0.37)

[*] the values in the paranthesis shows the netflow value.

110

Doubling the weighting factors for energy use and fuel quality does not change the ranking for wood pellet and natural gas, which is similar to the ranking of a base case. However, the ranking for coal, wet and dry sawdust is changed for each case. If the environmental regulation for the densification plant is the main concern, coal and wet sawdust may not be the better alternative, eventhough they are cheap fuels. The selection of the best alternative fuel is again a trade off and one should be careful in selecting the alternative based on the immediate concern for improvement. The preference-based rankings (both PROMETHEE I & II) will be helpful for decision makers to finalize the best alternative and to plan policy changes for a sustainable biomass pellet production system.

5.4 Summary

The biomass densification process has been analyzed using the environmental systems assessment tool to evaluate energy, emissions and economics of wood pellet production with different fuel options. From the energy consumption data, more than 80% of the energy was supplied for the drying process, which results in high energy cost of pelleting operation. Based on the emission inventory data, environmental impacts namely climate change, acid rain formation, smog formation and human toxicity were calculated for the best selection of alternatives. The environmental burden for the densification process is the highest if coal is used as a fuel among all other alternative fuels. Pellet production cost is high if natural gas or wood pellets is used as a fuel. The better fuel source would be dried sawdust or shavings due to low fuel cost. Selection of alternatives was performed using the multi-criteria decision making technique - PROMETHEE method.

CHAPTER 6

CONCLUSIONS AND RECOMMENDATIONS

6.1 Overall Conclusions

Biomass densification is the process of transforming loose biomass into dense solid products (pellets) for easy storage, handling and transportation. Densified biomass pellets have many advantages, which include uniform pellet moisture content, known pellet physical properties and easy handling and feeding attributes as a green fuel. The densification process consists of three key operations namely, biomass moisture control by rotary drum dryers, particle size reduction by hammer mills and densification by pellet mills. Secondary operations include pellet cooling, fines screening, pellet packaging and storage in the pelleting plant. Among the above operations, drying, size reduction and compaction are the major energy consuming operations, resulting in high cost of densified products. These unit operations have not been studied intensively in the context of biomass densification process. Flue gases produced from the direct combustion of natural gas are often used as a heating medium in the rotary dyer. Recent increase in natural gas price has impacted the operating cost of pelleting plants. The high pellet cost is the driving force for this research to determine the best alternative fuel for the sustainable operation of a densification process and to further understand the mechanics of the densification process. The alternative fuels studied in this research are wet sawdust, dry sawdust, wood pellets, coal and natural gas.

In order to reduce the operating cost, potential emissions generated due to the consumption of alternative fuels and energy consumptions of the plant, the present study is dedicated to investigate the entire biomass densification process by modeling three unit operations (drying, grinding and densification). In the modeling of drying operation the use of different alternative fuels: sawdust, wood pellets and coal to replace natural gas was investigated. The size reduction and the compaction of biomass operations were studied to understand the mechanics of the process and to determine the specific energy consumption of these operations. Systems analysis study focussed on the selection of the best process operations with low cost and environmentally friendly alternative fuel using PROMETHEE method as a multi-criteria decision making tool.

Biomass drying operation was investigated by developing models of direct contact co-current type rotary dryer with solid fuel combustion using lumped parameter approach. Two dryer models – single pass rotary drum dryer and triple pass rotary drum dryer, were developed along with the solid fuel burner to predict hot gas temperature and biomass moisture profiles, flue gas compositions and fuel requirement for drying operation. The predicted dryer results were validated with the industrial dryer data. The results were in close agreement with the commercial plant data. Among the different parameters evaluated, inlet hot gas temperature had the highest effect on exit gas temperature and biomass moisture content followed by hot gas flow rate. The developed model was used in the systems analysis study.

Size reduction of fibrous biomass species (straws, corn stover and switchgrass) was studied to determine the specific energy consumption of biomass using a laboratory hammer mill and the properties of the ground biomass particles were analyzed, as it is required for the compaction study. Specific energy consumption for grinding biomass was correlated to the hammer mill screen size to develop an empirical grinding energy model. Corn stover consumed the least specific energy during hammer mill grinding of all biomass species tested. Switchgrass used the highest specific energy requirement for grinding due to the fibrous nature of the material. The laboratory grinding energy results were compared with the commercial hammer mill energy data. In general, commercial hammer mill energy consumption that is reported in the published literature is about 1.5 to 2.0 times higher than that of laboratory hammer mill energy consumption data. The physical properties of biomass grind: particle size, particle size distribution, bulk density and particle density are useful data for storage and handling of biomass grinds in the energy conversion system. The physical properties of biomass grinds also influence the final quality of the densified products.

The compression characteristics of biomass particles were investigated using a single pelleter unit to understand the compaction mechanisms and the biomass compression and relaxation behaviors. The compaction mechanism of biomass particles was investigated by fitting the compression data into different compaction models. Among the five compaction models investigated, the Kawakita-Lüdde and Cooper-Eaton models fitted well with the compression data of all biomass grinds. The Cooper-Eaton

model parameters for biomass grinds showed that the prominent compaction mechanisms for biomass grinds are by particle rearrangement and elastic and plastic deformation. However, the mechanism of mechanical interlocking and ingredient melting phenomenon during compression of biomass must be further studied.

Pellets are produced by compression and extrusion of biomass particles using ring type pellet mills. Compression of biomass particles increases the particle density and forms a solid pellet, whereas the extrusion process does not really contribute to the pellet density and high energy is consumed to overcome wall friction. In order to determine the energy required for compressing and extruding biomass particles, an experiment was conducted using corn stover. In this study, the corn stover was densified up to a density range of 650 to 950 kg/m^3. The specific energy required to compress and extrude corn stover was in the range of 12 to 30 MJ/t. The extrusion (frictional) energy required to overcome the skin friction was high about 60% of the total energy consumption and it should be reduced or eliminated to minimize the energy consumption. Future research should be focussed on designing a new densification unit, which would completely eliminate the extrusion energy.

Finally, the entire biomass densification plant was analyzed to evaluate energy, emissions and economics of wood pellet production with different fuel options. From the energy consumption data, more than 80% of the energy was supplied for the drying process, which results in high energy cost of the pelleting operation. However, the operating cost of the dryer could be reduced by using dry sawdust or wood shavings. Based on the emission inventory data, environmental impacts namely climate change, acid rain formation, smog formation, and human toxicity were considered in evaluating the environmental burdens of different alternatives. The emission inventories and impact factors may be useful for developing emission standards for biomass densification plants and the foundation work for policy changes and strategic emission control measures. The environmental burden of the densification process is the highest if coal is used as a fuel among all other alternative fuels. Pellet production cost is high if natural gas or wood pellets are used as a fuel source. Since each alternative fuel has its own advantages and disadvantages, selection of the best alternative is difficult for decision makers using a single criterion. Therefore, a multi-criteria decision making tool, Preference Ranking

organization Method for Enrichment Evaluation (PROMETHEE) method was used to select the best alternative based on the four main criteria, namely total energy consumption, environmental impacts, cost of pellet production and fuel quality. The selection of the best alternative is purely on the hands of the decision makers, who decide the weighting factor for each criterion. It was found that wood pellet or dry sawdust may be the best alternative to natural gas followed by coal and wet sawdust, if all the criteria are weighed equally. If the decision maker or a stakeholder decides to double the weighting factor for the pellet production cost, the PROMETHEE outranking changes into: 1) coal; 2) dry sawdust; 3) wet sawdust; 4) wood pellet; and 5) natural gas. The study provided a comprehensive understanding of different unit operations to improve the biomass densification process with alternative fuel sources.

6.2 Recommendations for Future Work

The current study focussed on the investigation of different operations used in the densification process. However, there are many research works yet to be performed in the future to further improve the entire process and to reduce the densification cost of biomass. The following are the recommended future investigations evolving from the current study:

1. Although the current study has taken into consideration of the size and shape of the biomass particles during the modeling of drying process, further research is required to develop the drying kinetics of different biomass species by varying particle sizes, shapes and other process parameters.

2. The developed rotary dryer model results were validated with the inlet and exit conditions of a commercial rotary dryer. Future research is required to measure the temperature profiles of hot gases and feed material and the moisture contents of feed material along the path of the rotary dryer to validate the dryer model to fully understand the drying mechanisms. Such temperature and moisture profile data may be useful to determine the local volumetric heat transfer coefficient for the dryer. The current model also used the empirical relationship for the

115

volumetric heat transfer rate in the dryer. Future research may be required to develop a more comprehensive heat transfer rate relationship for rotary dryers.

3. The hydrodynamics of rotary drum dryers with different biomass particle sizes and shapes must be studied to further enhance the heat and mass transfer between the particles and the hot gas. Apart from convective heat transfer process, other modes of heat transfer: conduction and radiation may also be considered to improve the estimation of the heat and mass transfer rate during drying of biomass particles. The combined mode of heat transfer could be achieved by modifying the existing dryer or designing a new dryer altogether.

4. Since biomass drying is the most energy consuming process, other types of dryers may be considered to reduce both the capital and operating cost of the dryer. Interestingly, fluidized bed dryers are less expensive at small scales compared to rotary drum dryers. Research and development work is required to reduce the existing commercial dryer costs and improve energy efficiencies or to design a novel biomass dryer suitable for versatile biomass species. Research towards the application of solar energy for drying of biomass should also be considered as it may further reduce the pellet production cost.

5. Hammer mills are often used to reduce the particle size of biomass resulting in high energy consumption. They operate mainly on the principle of impact forces to produce new generation particles. If shear cutting forces are used for particle size reduction, the biomass grinding energy cost could be reduced considerably. The existing grinding energy models are more of empirical in nature and they may not be used for different biomass species with different physical properties. A more detailed research is required to develop a more comprehensive grinding energy model that would consider the material physical properties and other machine variables. The mechanism of size reduction may be further studied using population balance theory to understand the fundamentals of new biomass particle generation.

6. The existing pellet mills consume more than 60% of the energy during the extrusion process to overcome the wall friction. A novel pellet mill may be designed and developed to reduce the extrusion energy or to completely eliminate

116

the extrusion process during pelleting. Other alternative options to reduce energy consumption during the pelleting operation are: 1) biomass particles may be pre-treated to exploit the natural binding properties of the feedstock; 2) additional binding agents or processing aids: proteins and starch-based binding agents may be used to reduce the wall friction without losing the pellet density and quality.

7. Energy required to make pellets from different biomass species have not been studied intensively yet by incorporating biomass feed properties: moisture content, particle sizes and chemical composition of feed material. Such a study would play a major role in understanding the pelleting mechanism and the ways to design a novel pellet mill and the selection of feed particle characteristics for producing better quality pellets with the least energy consumption.

8. Biomass densification process consumes both the heat and electric energy for the production of biomass pellets. A combined heat and power generation system operated by biomass feedstock or biomass pellets may be useful to fulfill the electric energy and heat requirement of the densification plant. Economic and technical feasibility of such a system may be studied for the biomass densification plant.

9. In the environmental systems analysis of biomass densification process, the fuel emissions were considered on the life cycle basis. However, the densification process was analyzed on the gate-to-gate basis. Future research may be expanded to conduct the entire life cycle analysis of biomass densification process spanning the whole life cycle of biomass from harvesting to fuel utilization to further understand the environmental and economic impacts of the process. Such a comprehensive life cycle analysis of biomass may be useful in comparing different bioconversion technologies of produce heat and energy.

10. Ranking of different fuel sources may be performed using much more consistent multi-criteria decision making method. Analytical Hierarchy Process (AHP) may be explored for ranking different fuel sources. The main advantage of this method is that it calculates the inconsistency index as a ratio of the decision maker's inconsistency and randomly generated index. The index value assures the decision maker to selct the best alternative.

NOMENCLATURES

A	equipment heat transfer area, m^2
A_s	total heat transfer area of the solids/particles, m^2
[A]	ash content of the fuel in mass fraction.
AF_s	stoichiometric air to fuel ratio, kg of air/kg of fuel
AF_a	Actual air to fuel ratio, kg of air/kg of fuel
A_p	projected area of the particle, m^2
ARP_i	Acid Rainformation Potential of compound, i
a	number of moles of H^+ ion emitted
a, b	constants related to characteristic of the powder in Kawakita model
a_w	water activity of the feed, fraction.
a_0, b_0	empirical constants for the equation (2.29)
a_1, a_2	experimentally determined Copper-Eaton model constants
C	degree of volume reduction $(\dfrac{V_0 - V}{V_0})$ or engineering strain
C_c	total capital cost, $/y
C_D	drag coefficient, dimensionless
C_E	cost of electricity, $/kWh
C_{eq}	equipment cost, $
C_{eq1}	cost of the equipment, 1 having a capacity of C_1, $
C_{eq2}	cost of the equipment, 2 having a capacity of C_2, $
C_f	cost of the fuel, $/kg
C_{pa}	specific heat of air, kJ/kg C
C_{ps}	specific heat of sawdust, kJ/kg C
C_{op}	total operating cost, $/y
C_P	total production cost, $/kg
$C_{drywood}$	specific heat of dry wood, kJ/kg C
C_{pf}	specific heat of feed, kJ/kg C
C_{pv}	specific heat of water vapor, kJ/kg C
C_{pw}	specific heat of water, kJ/kg C
C_T	total annual cost, $/y

C_H	hammer mill capacity, t/h
c_{pf}	the specific heat of the dry fuel, kJ/kg C
c_{pm}	the specific heat of moisture in the fuel, kJ/kg C
c_{pw}	the specific heat of water, kJ/kg C
c_{pfg}	the specific heat of flue gas, kJ/kg C
c_{pa}	the specific heat of ash, kJ/kg C
D	dryer diameter, m
D_i	inner drum diameter, m
D_L	diffusivity of moisture in the solids, m^2/s
D_m	middle drum diameter, m
D_o	outer drum diameter, m
D_p	weighted average particle size of feed, μm
d_p	diameter of the feed particles, m
E	total electricity consumed, kWh
E	specific energy consumption, kWh/t
E_H	specific energy consumption of a hammer mill, kWh/t
E_i	mass emission rate of pollutant, i from the entire process, kg/hr
e	capital recovery factor, dimensionless
ex	exponent for the capacity of equipment, dimensionless
F	material flow rate per dryer cross section, kg of dry material/h m^2
F_D	drag force, N
F_g	gravitational force, N
FL	flight height, m
f	material feed rate kg/s
f_p	power factor, dimensionless
G	gas mass flow rate per dryer cross section, kg/h m^2
G_{fi}	inlet feed flow rate, kg/h
G_a	mass flow rate of a dry flue gas, kg/h
G_{ai}	inlet mass flow rate of a dry flue gas, kg/h
G_{fo}	outlet feed flow rate, kg/h
G_P	amount of product processed per hour, kg/h

GWP_i	Global Warming Potential of compound, i, fraction
g	gravitational force, m/s^2
H	humidity ratio of outlet air from a control volume, kg/kg db
H_d	drum hold up, kg
HHV	higher heating value, kJ/kg
HHV_d	higher heating value in dry basis, kJ/kg
H_i	humidity ratio of inlet air from a control volume, kg/kg db
h	convective heat transfer coefficient, $kW/m^2 K$
h_g	heat of vaporization of water, kJ/kg
i	interest rate, %
[i]	mass fraction of component, i in the fuel (eg. i = [C], [S], [H], [O])
I_i	infrared absorption band intensity of compound, i
I_{CO2}	infrared absorption band intensity of carbon dioxide,
k_1 & k_2	experimentally determined Copper-Eaton model constants
k	constant in eqn (2.25)
k	number of criteria, dimentionsless
k_d	drying constant, 1/s
L	dryer length, m
L_e	length of the drum at which the average particle progresses by cascade, m
LHV	lower heating value, kJ/kg
L_i	length of the inner drum, m
L_m	length of the middle drum, m
L_o	length of the outer drum, m
l	length of the stem, m
M_a	mass flow rate of dry air, kg db/h
M	moisture content of corn stover, % wet basis
M_{CO2}	molecular weight of carbon dioxide, g/mol
M_C	molecular weight of carbon, g/mol
M_S	molecular weight of sulphur, g/mol
M_H	molecular weight of hydrogen, g/mol
M_{H2O}	molecular weight of water, g/mol

M_{SO2}	molecular weight of sulphur dioxide, g/mol
MIR_i	maximum incremental reactivity of compound, i
MIR_{org}	average value for background reactive organic gases, the benchmark compound.
MW_i	molecular weight of the compound, i, kg/kmol
m_0, b_0	Heckel model constants.
m_1, b_1	experimentally determined Jones model constants.
m_2, b_2	experimentally determined Walkers model constants.
m_a	mass of the air in a control volume, kg db
m_f	feed retained on each control volume, kg db
m_{fuel}	the mass flow rate of the fuel consumed in the burner, kg/hr
m_{fm}	the moisture content of the fuel, dry basis
m_{fo}	mass fraction of oxygen in the air, fraction
$\dot{N}$	speed of rotation of the dryer, r/min
N_c	number of control volume, dimensionless
n	empirical constant in eqn (2.26).
n_{eq} & n_f	scaling factors for equipment and furnace, dimensionless
N_t	life time, year
N_t	number of heat transfer units based upon the gas, dimensionless
P	applied pressure, MPa
P_1	pressure reading after pressurizing the reference volume, Pa
P_2	pressure after including V_c, Pa
P_H	power consumed by the hammer mill, kW
P_m	machinery power, kW
Q	rate of heat transfer, kW
Q_l	heat loss from the control volume, kW
Q_{avg}	average diesel fuel consumption, l/h
Re	Reynolds number, dimensionless
Re_p	particle Reynolds number, dimensionless
RH	relative humidity of air, %
R_w	drying rate, kg of water/(kg of dry feed s)

S	slope of the dryer, m/m
S	hammer mill sieve opening size, mm
S_s	commercial hammer mill sieve opening size, mm
SFP_i	Smog formation potential of compound, i
T	temperature, °C
T_a	outlet temperature of air in a control volume, °C
T_{ai}	inlet temperature of air, °C
T_f	temperature of solids inside the control volume, °C
T_{fi}	inlet temperature of the solids, °C
t	time, s
t_c	cascading time, s
t_{clm}	cascading time for leaf in the middle drum , s
t_{clo}	cascading time for leaf in the outer drum , s
t_{csm}	cascading time for stem in the middle drum , s
t_{cso}	cascading time for stem in the outer drum , s
t_f	time of fall of particle, s
t_l	thickness of leaves, m
t_{op}	operation hours per year, h/y.
t_r	time taken by the particle in the flight, s
U_v	volumetric heat transfer coefficient, $W/m^3 K$
$U_v a$	volumetric heat transfer coefficient, $kW/m^{3}°C$
V	volume of compact at pressure P, m^3
V	volume of dryer control volume, m^3
V_∞	net volume of the powder, m^3
V_o	volume of compact at zero pressure, m^3
V_p	volume of the particle, m^3
V_c	volume of sample cell, m^3
V_R	packed volume ratio V/V_S or reference volume, m^3
V_S	void-free solid material volume, m^3
v_a	velocity of gases, m/s[1]
v_p	velocity of particle, m/s

v_{px}	velocity of particle along the X direction , m/s
w_i	weight assigned to each criteria, i, fraction
X	moisture content of solids in a control volume, kg/kg db
X_e	equilibrium moisture content of solids, kg/kg db
X_f	moisture content of the fuel, fraction wet basis
X_i	inlet moisture content of solids, kg/kg db
X_v	Water vapor content of flue gas, fraction wet basis
X_1, X_2	mass fraction of components of the mixture
x_c	cascading length, m
x_{clm}	cascading length for leaf in the middle drum, m
x_{clo}	cascading length for leaf in the outer drum, m
x_{csm}	cascading length for stem in the middle drum, m
x_{cso}	cascading length for stem in the outer drum, m
Y_f	the average height of fall particles in a cascade, m
Z	fuel flow rate kg/h

Greek symbols

θ	angle of repose of a particle, degree
ϕ	fraction of excess air, fraction
ρ	bulk density of compacted powder mixture, kg/m^3
ρ_a	air density, kg/m^3
ρ_{bl}	bulk density of alfalfa leaves, kg/m^3
ρ_{bs}	bulk density of alfalfa stems, kg/m^3
ρ_f	packing fraction or relative density of the material after particle rearrangement
ρ_p	particle density, kg/m^3
ρ_1, ρ_2	particle density of components of the mixture, kg/m^3
μ_a	viscosity of air, Pa s
η_c	overall combustion efficiency, fraction
τ	mean residence time of the material in a rotary dryer, s
τ_i	atmospheric life time of compound, i.

τ_{ri}	residence time of the material in a control volume, s
α	slope of the drum, degree
α_{eq}, α_f	unit cost of equipment and fuel
λ	latent heat of vaporization of water, kJ/kg
$\Delta T_f, \Delta T_a,$	the temperatures of fuel and air respectively, °C
$\Delta T_A, \Delta T_{fg}$	the temperatures of ash and flue gas respectively, °C
ΔT_m	true mean temperature difference between the got gases and material, K

REFERENCES

Abd-Elrahim, Y. M., A. S. Huzayyin and I. S. Taha. 1981. Dimensional analysis and wafering cotton stalks. Transactions of ASAE 24(4):829-832.

Adams, M. J., and R. McKeown. 1996. Micromechanical analyses of the pressure-volume relationships for powders under confined uniaxial compression. Powder Technology 88:155-163.

Albadvi, A. 2004. Formulating national technology strategies: a preference ranking model using PROMETHEE method. European Journal of Operations Research 153:290-296.

Alderborn, G., and M. Wikberg. 1996. Granule properties. In: Pharmaceutical powder compaction technology. G. Alderborn, and C. Nystrom. (Eds.) 323-373. New York: Marcel Dekker Inc.

Al-Rashdan, D., B. Al-Kloub, A. Dean and T. Al-Shemmeri. 1999. Environmental impact assessment and ranking the environmental projects in Jordan. European Journal of Operational Research 118:30-45.

Alvarez, P. I. and C, Shene. 1994a. Experimental determination of volumetric heat transfer coefficient in a rotary dryer. Drying Technology 12(7):1605-1627.

Alvarez, P. I. and C, Shene. 1994b. Experimental study of residence time in a direct rotary dryer. Drying Technology 12(7):1629-1651.

Al-Widyan, M. I., H. F. Al-Jalil, M. M. Abu-Zreig and N. H. Abu-Hamdeh. 2002. Physical durability and stability of olive cake briquettes. Canadian Biosystems Engineering 44:3.41-3.45.

Annoussamy M, G. Richard, S. Recous, and J. Guerif. 2000. Change in mechanical properties of wheat straw due to decomposition and moisture. Applied Engineering in Agriculture 16(6):657-664.

AOAC. 1990. AOAC Method 976.06 – Protein (crude) in animal feeds. In: Official method of analysis of the association of official analytical chemists, 15th ed., 72. Arlington, VA:Association of Official Analytical Chemists.

AOAC. 1990. AOAC Method 973.18 – Fiber (acid detergent) and lignin in animal feeds. In: Official method of analysis of the association of official analytical chemists, 15th ed., 82. Arlington, VA:Association of Official Analytical Chemists.

Aqa, S. and S. C. Bhattacharya. 1992. Densification of preheated sawdust for energy conservation. Energy 17:575-578.

Aquino, J. R. and R. R. Tan. 2004. Outranking matrix-based comparative streamlined environmental life cycle assessment of different packaging materials of an industrial system. In: LCA/LCM on-line conference paper, accessed on: July, 2004, The American Center for Life Cycle Assessment, http://www.lcacenter.org/InLCA2004/LC_green.html.

Arthur, J. F., R. A. Kepner, J. B. Dobie, G. E. Miller, and P. S. Parsons. 1982. Tub grinder performance with crop and forest residues. Transactions of ASAE 25(6):1488- 94.

ASAE Standards 47th Ed. 2001a. S424.1 –Method of determining and expressing particle size of chopped forage materials by screening. 576 - 578. St. Joseph, MI.:ASAE.

ASAE Standards 47th Ed. 2001b. S319.3 – Method of determining and expressing fineness of feed materials by sieving. 573-576. St. Joseph, MI.:ASAE.

ASAE Standards 47th Ed. 2001c. S358.2 – Moisture measurement-forages. 579. St. Joseph, MI.:ASAE.

ASAE Standards 49th Ed. 2003. ASAE Standard EP496.2 - Agricultural machinery management. St. Joseph, MI:ASAE.

Baker, C. G. J. 1992. Air solids drag in cascading rotary dryers. Drying Technology 10(2):365-393.

Balk, W. A. 1964. Energy requirements for dehydrating and pelleting coastal bermuda grass, Transactions of ASAE 7:349-351, 355

Barrefors, G and G. Petersson. 1993. Assessment of ambient volatile hydrocarbons from tobacco smoke and from vehicle emissions. Journal of Chromatography 643:71-76.

Basset-Mens, C. and H. M. G. van der Werf. 2005. Scenario-based environmental assessment of farming systems: the case of pig production in France. Agriculture, Ecosystems and Environment 105:127-144.

Bellinger, P. L. and H. H. McColly. 1961. Energy requirements for forming hay pellets, Agricultural Engineering 42(5):244-247.

Bhargava, A., B. Z. Dlugogorski and E. M. Kennedy. 2002. Emissions of polyaromatic hydrocarbons, polychlorinated biphenyls and polychlorinated dibenzo-p-dioxins and furans from fires of wood chips. Fire Safety Journal 37(7):659-672.

Bliss Industries Inc. 2003. Personal communication. Oklahoma, USA, www. www.bliss-industries.com.

Boateng, A. A. and P. V. Barr. 1996. A thermal model for the rotary kiln including heat transfer within the bed. International Journal of Heat and Mass Transfer 39(10):2131-2147.

Brans, J. P., Ph. Vincke, B. Mareschal. 1986. How to select and how to rank projects: The PROMETHEE method. European Journal of Operations Research 24:228-238.

Brans, J.P., and Ph. Vincke. 1985. A preference ranking organization method: (The PROMETHEE method for multiple criteria decision-making). Management Science 31(6):647-656.

Brentrup, F., J. Kusters, J. Lammel and H. Kuhlmann. 2004a. Environmental impact assessment of agricultural production systems using the life cycle assessment (LCA) methodology I. Theoretical concept of a LCA method tailored to crop production. European Journal of Agronomy 20:247-264.

Brentrup, F., J. Kusters, J. Lammel, P. Barraclough and H. Kuhlmann. 2004b. Environmental impact assessment of agricultural production systems using the life cycle assessment (LCA) methodology II. The application to N fertilizer use in winter wheat production systems. European Journal of Agronomy 20:265-279.

Burgess, A. A. and D. J. Brennan. 2001a. Application of life cycle assessment to chemical processes. Chemical Engineering Science 56:2589-2604.

Burgess, A. A. and D. J. Brennan. 2001b. Desulphurization of gas oil: A case study in environmental and economic assessment. Journal of Cleaner Production 9:465-472.

Cadoche L. and G. D. Lopez. 1989. Assessment of size reduction as a preliminary step in the production of ethanol from lignocellulosic wastes. Biological Wastes 30:153-157.

Cao, W. F. and T. A. G. Langrish. 2000. The development and validation of a systems model for a countercurrent cascading rotary dryer. Drying Technology, 18(1&2):99-115.

Carre, J., J. Hebert, L. Lacrosse, and Y. Schenkel. 1987. Briquetting agricultural and wood residues: experience gained with a heated die cylindrical screw press. Paper presented at the First FAO/CNRE Workshop on Handling and Processing of Biomass for Energy, Hamburg, FRG, pp. 14-15.

Carter, W.P.L. 1994. Development of ozone reactivity scales for volatile organic compounds. Air and Waste 44:881-899.

Consoli, F., I. Boustead, J. Fava, W. Franklin, A. Jensen, N. de Qude, R. Parish, D. Postlethwaite, B. Quay, J. Seguin and B. Vignon. 1993. Guidelines for life cycle assessment: A code of practice. Pensacola, FL:Society for Environmental Toxicology and Chemistry (SETAC).

Cooper, C. D. and F C. Alley. 2002. Air pollution control - A design approach, 3rd ed. Long Grove, IL:Waveland Press Inc.

Cooper, A. R., and L. E. Eaton. 1962. Compaction behavior of several ceramic powders. Journal of the American Ceramic Society 45(3):97-101.

Curran, M.A.1996. Environmental life cycle assessment. New York, NY:McGraw-Hill Companies

Datta, R. 1981. Energy requirement for lignocellulose pretreatment processes. Process Biochemistry 16(June/July):16-19, 42.

Demirbas, A. 1998a. Fuel properties and calculation of higher heating values of vegetable oils. Fuel 77:117-120.

Demirbas, A. 1998b. Determination of combustion heat of fuels by using non-calorimetric experimental data. Energy Education Science Technology 1:7-12.

Denny, P. J. 2002. Compaction equations: a comparison of the Heckel and Kawakita equations. Powder Technology 127:162-172.

Douglas, P. L., A. Kwade, P. L. Lee and S. K. Mallick. 1993. Simulation of rotary dryer for sugar crystalline. Drying Technology 11(1):129-155.

Drzymala Z. 1993. Industrial briquetting – Fundamentals and methods. Studies in Mechanical Engineering, 13. Warszawa : PWN-Polish Scientific Publishers.

Environmental Protection Agency (EPA). 1995. The compilation of air pollutant emission factor: stationary point and area sources. EPA No.: AP-42, Vol. 1 (5th edition). Washington, DC: U.S. Environmental Protection Agency.

Faborode, M. O. and J. R. O'Callaghan 1987. Optimizing the compression/briquetting of fibrous agricultural materials. Journal of Agricultural Engineering Research 38:245-262.

Fava, J. A., R. Denison, B. Jones, M. A. Curran, B. Vigon, S. Selke and J. Barnum. 1991. A technical framework for life cycle assessments. Pensacola, FL:Society for Environmental Toxicology and Chemistry (SETAC).

Fang, Q., E. Haque, C. K. Spillman, P. V. Reddy, and J. L. Steele. 1998. Energy requirement for size reduction of wheat using a roller mill. Transaction of the ASAE 41(6):1713-1720.

Forsberg, G. 2000. Biomass energy transport- analysis of bioenergy transport chains using life cycle inventory method. Biomass and Bioenergy 19:17-30.

Friedman, S. J. and W. R. Marshall. 1949a. Studies in rotary drying part I-holdup and dusting. Chemical Engineering Progress 45(8):482-493.

Friedman, S. J. and W. R. Marshall. 1949b. Studies in rotary drying part II-heat and mass transfer. Chemical Engineering Progress 45(9):573-588.

Garekani, H. A., J. L. Ford, M. H. Rubinstein, and A. R. Rajabi-Siahboomi. 2000. Highly compressible paracetamol – II. Compression properties. International Journal of Pharmaceutics 208:101-110.

Ghebre-Sellassie, I. 1989. Mechanism of pellet formation and growth, In Pharmaceutical Pelletization Technology, I. Ghebre-Sellassie, ed., pp.123- 143, New York, NY:Marcel Dekker, Inc.

Goumas, M. G. and V. Lygerou. 2000. An extension of the PROMETHEE method for decision making in fuzzy environment: ranking of alternative energy exploitation projects. European Journal of Operational Research 123:606-613.

Graedel, T.E., Allenby, B.R. and Comrie, P.R.1995. Matrix approaches to abridged life-cycle assessment. Environmental Science and Technology 29:134-139

Granstrom, K. 2003. Emissions of monoterpenes and VOCs during drying of sawdust in a spouted bed. Forest Products Journal 53(10):48-51.

Gray, W.A. 1968. Compaction after deposition, in the packing of solid particles, pp.89-107, New York, NY:Barnes & Noble.

Grieve, D. A., M. E. Holuszko and F. Goodarzi. 1996. British Columbia coal quality survey, Bulletin 96. Energy and Minerals Division, Geological survey branch, BC, Canada:Ministry of Employment and Investment.

Grover, P. D. and S. K. Mishra. 1996. Biomass briquetting: technology and practices. Regional Wood Energy Development program in Asia, Field document No. 46. Bangkok, Thailand: Food and Agriculture Organization of the United Nations.

Gustafson, A. S. and W. L. Kjelgaard. 1963. Hay pellet geometry and stability. Agricultural Engineering 44(8):442 - 445.

Guthrie, W. R. and E. B. Collins. 1965. Factors affecting sorption isotherms of alfalfa, West Virginia University Agricultural Experimental Station, Bulletin # 514T.

Haider, A. and O. Levenspiel. 1989. Drag coefficient and terminal velocity of spherical and non-spherical particles. Powder Technology 58:63-70.

Hann, S. A. and H. P. Harrison. 1976. Friction in and energy required for extruding alfalfa. Canadian Agricultural Engineering 18:21-25.

Haralambopoulos, D A. and H. Polatidis. 2003. Renewable energy projects: structuring a multi-criteria group decision making framework. Renewable energy 28:961-973.

Heckel, R. W. 1961. An analysis of powder compaction phenomena. Transaction of the Metallurgal Society of AIME 221:1001- 1008.

Heijungs, R., J. Guinee, G. Huppes, R. M. Lankreijer, H. A. Udo de Haes, S. A. Wegener, A. M. M. Ansems, P. G. Eggels, R. van Duin, and H. P. de Goede. 1992. Environmental life cycle assessment of products. Guides and backgrounds. CML, Leiden, The Netherlands:Leiden University.

Heller, M. C., G. A. Keoleian and T. A. Volk. 2003. Life cycle assessment of a willow Bioenergy cropping system. Biomass and Bioenerg, 25:147-165.

Hill, B. and D. A. Pulkinen. 1988. A study of the factors affecting pellet durability and pelleting efficiency in the production of dehydrated alfalfa pellets. A Special Report. Saskatchewan Dehydrators Association, Tisdale, SK, Canada.

Himmel, M., M. Tucker, J. Baker, C. Rivard, K. OH, and K. Grohmann. 1985. Comminution of biomass: hammer and knife mills. Biotechnology and Bioengineering Symposium15:39-58.

Holtzapple, M. T., A. E. Humphrey, and J. D. Taylor. 1989. Energy requirements for the size reduction of poplar and aspen wood. Biotechnology and Bioengineering 33:207-210.

Huijbregts, M. A. J., U. Thissen, J. B. Guinee, T. Jager, D. Kalf, D. van de Meent, A. M. J. Ragas, A. W. Sleeswijk and L. Reijnders. 2000. Priority assessment of toxic substances in life cycle assessment. Part 1: Calculation of toxicity potentials for 181 substances with the nested multi-media fate, exposure and effects model USES-LCA. Chemosphere 41:541-573.

Iguaz, A., A. Esnoz, G. Martínez, A. López and P. Vírseda. 2003. Mathematical modeling and simulation for the drying process of vegetable wholesale by-products in a rotary dryer. Journal of Food Engineering 59:151-160.

Iguaz, A., H. Budman and P. L. Douglas. 2002. Modeling and control of an alfalfa rotary dryer. Drying Technology 20(9):1869-1887.

Intergovermental Panel on Climate Change (IPCC). 1996. Climate change 1995. In: The science of climate change, J. T. Houghton, Y. Ding, D.J. Griggs, M. Noguer, P. J.

van der Linden and D. Xiaosu (Eds.). (eds). Cambridge, UK: Cambridge University Press.

Jannasch, R., Y. Quan, and R. Samson. 2001. A process and energy analysis of pelletizing switchgrass. Final report. Website: http://www.reap-canada.com/Reports/PelletSG.htm ; accessed on August 2002

Jayas, D. S. and S. Sokhansanj. 1989. Thin layer drying of barley at low temperatures. Canadian Agricultural Engineering 31:21-23.

Johansson, B. and G. Alderborn. 1996. Degree of pellet deformation during compaction and its relationship to the tensile strength of tablets formed of microcrystalline cellulose. International Journal of Pharmaceutics 132:207-220.

Johansson, B., M. Wikberg, R. Ek, and G. Alderborn. 1995. Compression behavior and compactability of microcrystalline cellulose compacts in relationship to their pore structure and mechanical properties. International Journal of Pharmaceutics 117:57-73.

Jokob, H. 2002. Densified biomass fuels in Sweden: country report for the EU/INDEBIF project. Department of Forest Management and Products, Uppsala, Sweden:Swedish University of Agricultural Sciences.

Jones, W. D. 1960. Fundamental principles of powder metallurgy. 242 – 370; London: Edward Arnold Publishers.

Kakareka, S. V., T. I. Kukharchyk and V. S. Khomich. 2005. Study of PAH emission from the solid fuels combustion in residential furnaces. Environmental Pollution 133:383-387.

Kamke, F. A. 1984. Engineering analysis of a rotary dryer: drying of wood particles. Ph.D. Thesis, Department of Forest Products, Oregon State University, Corvallis, OR.

Kamke, F. A. and J. B. Wilson. 1986a. Computer simulation of a rotary dryer Part I: Residence time. AIChE Journal 32:263-269.

Kamke, F. A. and J. B. Wilson. 1986b. Computer simulation of a rotary dryer Part II: Heat and mass transfer. AIChE Journal 32:269-275.

Kawakita, K., and K.-H. Lüdde. 1971. Some considerations on powder compression equations. Powder Technology 4:61-68.

Kelly, J. J. 1995. Rotary drying In: Handbook of industrial drying, A. S. Mujumdar (ed), 2nd Ed., pp. 161-183, New York:Marcel Dekker.

Kinoshita, C. M. 1988. A theoretical analysis of pre-drying of solid fuels with flue gas. Journal of Energy Resources Technology 110:119-123.

Kiranoudis, C. T., Z. B. Maroulis and D. Marinos-Kouris. 1996. Drying of solids-selection of some continuous operation dryer types. Computers in Chemical Engineering 20:S177-S182.

Kiranoudis, C. T., Z. B. maroulis, D. Marinos-Kouris. 1997. Modeling and optimization of fluidized bed and rotary dryers. Drying Technology 15(3&4):735-763.

Kjallstrand, J and M. Olsson. 2004. Chimney emissions from small-scale burning of pellets and fuel wood – examples referring to different combustion appliances. Biomass and Bioenergy 27(6):557-561.

Koch, F. H. 2000. Hydropower-internalized costs and externalized benefits. International Energy Agency (IEA)-Implementing Agreement for Hydro Power Technologies and Programme, Ottawa, Canada.

Krokida, M. K., Z. B. Maroulis and C. Kremalis. 2002. Process design of rotary dryers for olive cake. Drying Technology 20(4&5):771-788.

Kurttio, P., P. Kalliokoski, S. Lampelo and M. J. Jantunen. 1990. Mutagenic compounds in wood-chip drying fumes. Mutation research/Genteic Toxicology 242(1):9-15.

Lashof, D. A. and D. R. Ahuja. 1990. Relative contributions of greenhouse gas emissions to global warming. Nature 344(6266):529-531.

Lewandowski, I and A. Heinz. 2003. Delayed harvest of miscanthus – influence on biomass quality and quantity and environmental impacts of energy production. European Journal of Agronomy 19:45-63.

Li, J., J. Gifford and K. Senelwa. 2001. Prediction of combustion characteristics for woody biomass fuels – heat output. In: Progress in thermo chemical biomass conversion, A. V. Bridgwater (ed), Vol. 1. pp. 630-640. Oxford, UK: Blackwell Science Inc.

Lopo P. 2002. The right grinding solution for you: roll, horizontal or vertical. Feed Management 53(3):23- 26.

Luthe, C., I. Karidio and V. Uloth. 1997. Towards controlling dioxins emissions from power boilers fuelled with salt-laden wood wastes. Chemosphere 35:557 – 574.

Luthe, C., I. Karidio and V. Uloth. 1998. Dioxins formation in salt-laden power boilers: a mass balance. Chemosphere 36:231-249.

Macharis, C., J. Springael, K. De Brucker and A. Verbeke. 2004. PROMETHEE and AHP: The design of operational synergies in multi-criteria analysis. Strengthening PROMETHEE with ideas of AHP. European Journal of Operational Research 153:307-317.

Mani, S., L. G. Tabil and S. Sokhansanj. 2004. Grinding performance and physical properties of wheat and barley straws, corn stover and switchgrass. Biomass and Bioenergy 27(4):339-352

Mani, S., L. G. Tabil, and S. Sokhansanj. 2002. Compaction behavior of some biomass grinds. CSAE Paper No. 02-305. Canadian Society of Agricultural Engineers Mansonville, QC.

Mani, S., L. G. Tabil, and S. Sokhansanj. 2003. An overview of compaction of biomass grinds. Powder Handling and Processing 15(3):160-168.

Matchett, A. J. and C. G. J. Baker. 1987. Residence times in cascading rotary dryers. Part 1- derivation of the two-stream model. Journal of Separation Process Technology 8:11-17

Matchett, A. J. and C. G. J. Baker. 1988. Residence times in cascading rotary dryers. Part 2- Application of the two-stream model to experimental and industrial data. Journal of Separation Process Technology 9:5-13.

Matchett, A.J. and M. S. Sheikh. 1990. An improved model of particle motion in cascading rotary dryers. Transactions of the Institute of Chemical Engineers 68:139-148.

McCormick, P. Y. 1962. Gas velocity effects on heat transfer in direct heat rotary dryers. Chemical Engineering Progress 58(6):57-61.

Mewes, E. 1959a. Berechung der druckverteilung an stroh-und heupressen (Calculation of the pressure distribution in straw and hay balers). Landtechnische Forschung 9(6):160-170.

Mewes, E. 1959b. Verdichtungsgesetzmassigkeiten nach presstopfversuchen (Compression relationships as a result of experiments in pressure chambers). Landtechnische Forschung 9(3):68-76.

Miles, T. R. and T. R. Miles, Jr. 1980. Densification systems for agricultural residues. In: Thermal conversion of solid wastes and biomass, American Chemical Society, Washington DC, pp.179-191.

Mohsenin, N. and J. Zaske 1975. Stress relaxation and energy requirements in compaction of unconsolidated materials, Journal of Agricultural Engineering Research 11:193- 205.

Mujumdar, A. S. 2000. Innovation in drying techniques and future trends. In: Mujumdar's practical guide to industrial drying, S. Devahastin (ed), pp. 99-113, Energex Corporation.

Myklestad, O. 1963a. Heat and mass transfer in rotary dryers. Chemical Engineering Progress Symposium Series 59(41):129-137.

Myklestad, O. 1963b. Moisture control in rotary dryer. Chemical Engineering Progress Symposium Series 59(41):138-144.

Neale, M. A. 1986. Straw compaction research. Agricultural Engineer 4(4):126-130.

Nellist, M. E. 1976. Exposed layer drying of ryegrass seeds. Journal of Agricultural Engineering Research 21(1):49-66.

Nelson, R. M. 1983. A model for sorption of water vapor by cellulosic materials. Wood and Fiber Science 15(1):8-22.

Netherlands Agency for Energy and Environment (NOVEM). 1996. Pretreatment technologies for energy crops. Report No. 9525. BTG biomass Technology Group BV, Enschede, The Netherlands.

Nevers De, N. 2000. Pollution control engineering. New York, NY:McGraw Hill Publications.

Nonhebel, G and A. A. H. Moss. 1971. Drying of solids in the chemical industry. Toronto, ON:Butter Worths & Co.

O'Dogherty, M. J. and J. A. Wheeler 1984. Compression of straw to high densities in closed cylindrical dies, Journal of Agricultural Engineering Research 29(1):61-72.

Ollet, A.L., A. R. Kirrby, P. Parker, and A. C. Smith. 1993. A comparative study of the effects of water content on the compaction behavior of some food materials. Powder Technology 75:59- 65.

Olsson, M. and J. Kjallstrand. 2004. Emissions from burning of softwood pellets. Biomass and Bioenergy 27(6):613-620.

Olsson, M., J. Kjallstrand and G. Petersson. 2003. Specific chimney emissions and biofuel characteristics of softwood pellets for residential heating in Sweden. Biomass and Bioenergy 24(1):51-57.

Pasikatan, M. C., G. A. Milliken, J. L. Steele, C. K. Spillman and E. Haque. 2001. Modeling the size properties of first break ground wheat. Transactions of ASAE 44(6):1727-1735.

Payne, F. A. 1984. Energy and mass flow computation in biomass combustion systems. Transaction of ASAE 27:1532-1537, 1541.

Payne, J. D. 1997. Troubleshooting the pelleting process. Technical Bulletin, American Soyabean Association, Singapore.

Perry, R. H. and D.W. Green. 1999. Perry's chemical engineers' handbook. New York, NY: McGraw Hill Inc.

Pietsch, W. 1997. Size enlargement by agglomeration. In:Handbook of powder science and technology, pp.202-377, 2nd ed. Fayed, M.E. and L. Otten, ed., Florence, KY:International Thomson Publishing.

Plump, O. A., P. C. Malte, R. W. Cox and R. J. Robertus. 1978. Convective drying of small wood particles. Proceedings of the first international symposium on drying, Science Press, Princeton.

Pohekar, S. D., and M. Ramachandran. 2004. Application of multi-criteria decision making to sustainable energy planning – A review. Renewable and Sustainable Energy Review 8:365-381.

136

Pordesimo, L. O., W. C. Edens, and S. Sokhansanj S. 2004. Distribution of aboveground biomass in corn stover. Biomass Bioenergy 26:337-343

Preto, F., R. McCleave, D. McLaughlin and J. Wang. 2005. Dioxins/furans emissions from fluidized bed combustion of salt-laden hog fuel. Chemosphere, 58: 935-941.

Reed, T. B. and B. Bryant. 1978. Densified biomass: A new form of solid fuel. SERI – 35, Solar Energy Research Institute, Golden, CO, p. 30.

Reed, T. B., G. Trezek and L. Diaz. 1980. Biomass densification energy requirements. In: Thermal conversion of solid wastes and biomass, pp.169- 177, Washington DC:American Chemical Society.

Renaud, M., J. Thibault and A. Trusiak. 2000. Solids transportation model of an industrial rotary dryer. Drying Technology 18(4&5):843-865.

Renaud, M., J. Thibault and P. I. Alvarez. 2001. Influence of solids moisture content on the average residence time in a rotary dryer. Drying Technology 19(9):2131-2150.

Robinson, R. 1984. Pelleting. In: Manufacure of animal feed, Ed. Beaven, D. A., 50-53. Herts, England: Turrent-Wheatland Ltd.

Rodrigues, G. S., C. Campanhola and P. C. Kitamura. 2003. An environmental impact assessment system for agricultural R & D. Environmental Impact Assessment Review 23:219-244.

Rosa, L. P. and R. Schaeffer. 1995. Global warming potentials- The case of emissions from dams. Energy Policy 23(2):149-158.

Rumpf, H. 1962. The strength of granules and agglomerates, in Agglomeration, pp. 379-419. W. A. Knepper, ed. New York, NY:John Wiley and Sons.

Rypma J. A.1983. What the European feed manufacturer requires in particle reduction equipment and systems. In: Proceedings First International Symposium on Particle Size Reduction in the Feed Industry, B-11. Manhattan, KS, USA: Kansas State University.

Saeman, W. C. and T. R. Mitchel. 1954. Analysis of rotary dryer and cooler performance. Chemical Engineering progress 50:467-475.

Samson, P., P. Duxbury, M. Drisdelle and C. Lapointe. 2000. Assessment of pelletized biofuels. http://reap.ca/Reports/pelletaug2000.html. accessed on June 20, 2001.

SAS. 1999. SAS User's Guide: Statistics. Ver. 8. Cary, NC:SAS Institute Inc.

Sastry, K.V.S. and D.W. Fuerstenau 1973. Mechanisms of Agglomerate Growth in Green Pelletization, Powder Technology 7:97-105.

Schell, D. J. and C. Harwood. 1994. Milling of lignocellulosic biomass: results of pilot-scale testing. Applied Biochemistry and Biotechnology 45/46:159-168.

Schofield, F. R. and G. Glikin. 1962. Rotary dryers and coolers for granular fertilizers. Transactions of the Institute of Chemical Engineers 40:183.

Senior, C. L., A. F. Sarofim, T. Zeng, J. J. Helblec and R. Mamani-Pacoc. 2000. Gas-phase transformations of mercury in coal-fired power plants. Fuel Processing Technology 63(2-3):197-213.

Sharples, K., P. G. Glikin and R. Warne. 1964. Computer simulation of rotary dryers. Transactions of the Institute of Chemical Engineers 42:275-284.

Sheehan, J., V. Camobreco, J. Duffield, M. Graboski and H. Shapouri. 1998. Life cycle inventory of biodiesel and petroleum diesel for use in an urban bus. Final report, NREL/SR-580-24089. National Renewable Energy Laboratory, Golden, CO.

Shene, C., P. I. Álvarez, F. Cubillos and J. R. Pérez-Correa. 1996. Modeling and simulation of a direct control rotary dryer. Drying Technology 14(10):2419-2436.

Shepperson, G. and W. T. B. Marchant. 1978. Production of grass and alfalfa cubes using an experimental ring die press, Proceedings 2nd International Green Crop Drying Conference, Saskatoon, SK, pp. 264-270.

Sherritt, R. G., R. Caple, L. A. Behie and A. K. Mehrotra. 1993. The movement of solids through flighted rotating drums. Part I: Model formulation. Canadian Journal of Chemical Engineering 71:337-346.

Sherritt, R. G., R. Caple, L. A. Behie and A. K. Mehrotra. 1994. The movement of solids through flighted rotating drums. Part II: Solids-gas interaction and model validation. Canadian Journal of Chemical Engineering 72:240-248.

Shivanand, P, O. L. and Sprockel. 1992. Compaction behavior of cellulose polymers. Powder Technology 69:177- 184.

Siskos, J. and P. H. Hubert. 1983. Multi-criteria analysis of the impacts of energy alternatives: A survey and a comparative approach. European Journal of Operational Research 13:278-299.

Sitkei G. 1986. Mechanics of agricultural materials. Amsterdam: Elsevier Publishing Ltd.

Skodras, G., P. Grammelis, E. Kakaras and G. P. Sakellaropoulos. 2004. Evaluation of the environmental impacts of waste wood co-utilization for energy production. Energy 29:2181 – 2193.

Smith, E., S. Probert, R. Stokes and R. Hansford. 1977. The briquetting of wheat straw. Journal of Agricultural Engineering Research 22:105-111.

Sokhansanj, S. and R. T. Patil. 1996. Kinetics of dehydration of green alfalfa. Drying Technology 14(5):1197-1234

Sokhansanj, S., E. A. Arinze and G. J. Schoenau 1993. Forage drying and storage, A Technical Report, Department of Agricultural and Bioresource Engineering, University of Saskatchewan, Saskatoon, SK, Canada.

Sonnemann, G., F. Castells and M. Schuhmacher. 2004. Integrated life cycle and risk assessment for industrial processes. Boca Raton, FL:CRC Press Co.

Spath, P. L. and M. K. Mann. 2001. Life cycle assessment of hydrogen production via natural gas steam reforming. Technical Report, NREL/TP-570-27637. National Renewable Energy Laboratory, Golden, CO.

Spath, P. L., M. K. Mann and D. R. Kerr. 1999. Life cycle assessment of coal-fired power production. Technical Report, NREL/TP-570-25119. National Renewable Energy Laboratory, Golden, CO.

Stahl, M., K. Granstrom, J. Berghel and R. Renstrom. 2004. Industrial processes for biomass drying and their effects on the quality properties of wood pellets. Biomass and Bioenergy 27:621-628.

Stanzel, W. 1994. Combustion simulation of a woodchip furnace. In: Advances in thermo chemical conversion of biomass. A. V. Bridgwater (ed). Vol. 1, pp. 590-604. Oxford, UK: Blackie Academic and Professional.

Sun, D. W. and J. L. Woods. 1994. Low temperature moisture transfer characteristics of barley: Thin layer models and equilibrium isotherms. Journal of Agricultural Engineering Research 59(4):273-283.

Tabil, L. G. 1996. Binding and pelleting characteristics of alfalfa. Ph.D diss. Saskatoon, Saskatchewan, Canada: University of Saskatchewan, Department of Agricultural and Bioresource Engineering.

Tabil, L.G. Jr. and S. Sokhansanj 1996. Compression and Compaction Behavior of Alfalfa Grinds, Part 1: Compression Behavior, Powder Handling and Processing 8(1):17-23.

Teno, T. F. L. and B. Marseschal. 1998. An interval version of PROMETHEE for comparison of building products design with ill defined data on environmental quality. European Journal of Operational Research 109:522-529.

Throne, B. and J. J. Kelly. 1980. Mathematical modeling of rotary dryers. In: International Symposium on Solid Separation Processes. Institute of Chemical Engineering Symposium Series, 59

Todd, J. A. and M. A. Curran. 1999. Streamlined life cycle assessment: A final report from the SETAC North American streamlined LCA workgroups. Society of Environmental Toxicology and Chemistry, Pensacola, FL.

Tripathi, A. K., P. V. R. Iyer and T. C. Kandpal. 1998. A techno-economic evaluation of biomass briquetting in India. Biomass and Bioenergy 14(5-6):479-488.

Twidell, J. 1998. Biomass energy. Renewable Energy World 3:38-39.

Ulrich, G. D. 1984. A guide to chemical engineering process design and economics. John Wiley & Sons, New York, USA.

van Dam, J.E.G., M.J.A. van den Oever, W. Teunissen, E.R.P. Keijsers and A.G. Peralta. 2004. Process for production of high density/high performance binderless boards from whole coconut husk - Part 1: Lignin as intrinsic thermosetting binder resin. Industrial Crops and Products 19:207-216.

Van der Werf, H. M. G., J. Petit and J. Sanders. 2005. The environmental impacts of the production of concentrated feed: the case of pig feed in Bretagne. Agricultural Systems 83(2):153-177.

Visual Decision Inc. 2003. Decision lab 2000 – Executive edition, Getting started guide. Montreal, QC, Canada.

Walas, S. M. 1990. Chemical process equipment – selection and design. New York, NY:Elsevier publication.

Walker, E. E. 1923. The properties of powders. Part VI. The compressibility of powders. Transactions of the Faraday Society 19(1):73-82.

Walker, S. 2000. Major coalfields of the world, CCC/32, London, UK: IEA Coal Research – The clean coal center.

Wamukonya, L. and B. Jenkins. 1995. Durability and relaxation of sawdust and wheat straw briquettes as a possible fuels for Kenya. Biomass and Bioenergy 8(3):75-179.

Wang, F. Y., I. T. Cameron, J. D. Litster and P. L. Douglas. 1993. A distributed parameter approach to the dynamics of rotary drying processes. Drying Technology 11(7):1641-1656.

Wood, H. C. and S. Sokhansanj. 1990. Heat treatment of chopped alfalfa in rotary drum dryers. Drying Technology 8(3):533-541.

Yang, W., S. Sokhansanj, W. J. Crerar and S. Rohani. 1996. Size and shape related characteristics of alfalfa grind. Canadian Agricultural Engineering 38(3):201-205.

APPENDICES

Appendix I - Summary of previous work on modeling of rotary dryers

Researchers	Year	Modeling approach	Dryer type	Inlet temp. (C)	Inlet moisture (%)	material use	Comments
Myklestad	1963b	Lumped parameter	Counter-current	50	26	Pumice	Particle transport was considered
Sharples et al	1964	Lumped parameter	Both type	350	5	Fertilizers	Dynamic behavior of the dryer was analyzed
Kamke & Wilson	1986	Lumped parameter	Co-current	270	60	Wood chips	Model error 22.2%. However, particle transport was considered.
Wood & Sokhansanj	1990	Distributed parameter	Co-current 3 -pass dryer	600	70	Alfalfa	Model developed for inspecting the heat treatment of Hessian fly on the alfalfa chops.
Douglas et al.	1993	Lumped parameter	Counter current	50	2.2	Sugar	Model error 10%. Operating range was narrow.
Wang et al.	1993	Distributed parameter	current Counter current	30	2.2	Sugar	More rigorous model, not much improvement on the simulation results.
Shene et al.	1996	Lumped parameter	Co-current	200	30	Soya and fish meal	Simulation result did not agree with expt. Data
Cao & Langrish	2000	Lumped parameter	Counter-current	120	---	Sorghum grain	- do -
Iguaz et al.	2002	Lumped parameter	Co-current	450	65	Alfalfa	Simulation results had good agreement with the end conditions
Iguaz et al.	2003	Lumped parameter	Co-current	200	70	Vegetable waste	Empirical relations were used for particle transportation

Appendix II –Summary of residence time calculation for a triple pass rotary dryer.

	Inner drum	Middle drum	Outer drum
For leaves			
Particle shape	Disk	Disk	Disk
Cascading length	$x_{cil} = \dfrac{K_{il} Y_{fi} v_{ai}^2}{g}$	$x_{cml} = \dfrac{1}{2} K_{ml} t_{mf}^2 v_{ma}^2$	$x_{col} = \dfrac{1}{2} K_{ol} t_{of}^2 v_{oa}^2$
	where, $K_{il} = \dfrac{1}{2} C_{iD} \dfrac{\rho_a}{\rho_p t_1}$	where, $K_{ml} = \dfrac{1}{2} C_{mD} \dfrac{\rho_a}{\rho_p t_1}$	where, $K_{ol} = K_{ml}$
Cascading time	$t_{cil} = \sqrt{\dfrac{2Y_{fi}}{g}} + \dfrac{90+\theta}{360N}$	$t_{cml} = \dfrac{\pi+\theta}{360N} + \sqrt{\dfrac{2y_{ml}}{g}} + \sqrt{\dfrac{2y_{m2}}{g}} + \dfrac{\pi+\theta}{360N}$	$t_{col} = \dfrac{\pi+\theta}{360N} + \sqrt{\dfrac{2y_{ol}}{g}} + \sqrt{\dfrac{2y_{o2}}{g}} + \dfrac{\pi+\theta}{360N}$
	$Y_{fi} = \dfrac{D_i}{2} + \left(\dfrac{D_i}{2} - FL\right)\sin\theta$	$y_{ml} = \left(\dfrac{D_m}{2} - \dfrac{D_i}{2} - \dfrac{FL}{2}\right)\sin\theta$	$y_{ol} = \left(\dfrac{D_o}{2} - \dfrac{D_m}{2} - \dfrac{FL}{2}\right)\sin\theta$
		$y_{m2} = \left(\dfrac{D_m}{2} - \dfrac{FL}{2}\right)$	$y_{o2} = \left(\dfrac{D_o}{2} - \dfrac{FL}{2}\right)$
For stems			
Particle shape	Cylindrical	Cylindrical	Cylindrical
Cascading length	$x_{cis} = \dfrac{K_{is} Y_{fi} v_{ai}^2}{g}$	$x_{cms} = \dfrac{1}{2} K_{ms} t_{mf}^2 v_{ma}^2$	$x_{cos} = \dfrac{1}{2} K_{os} t_{of}^2 v_{oa}^2$
	where, $K_{is} = \dfrac{1}{2} C_{iD} \dfrac{\rho_a}{\rho_p l_s}$	$K_{ms} = K_{is}$	where, $K_{os} = K_{ms}$
Cascading time	$t_{cis} = t_{cil}$	$t_{cms} = t_{cml}$	$t_{cos} = t_{col}$

Appendix III – MATLAB program codes.

1. Single pass Rotary drum dryer model

```
% Heat and mass transfer (co-current type) model for a single pass rotary dryer to saw dust
% Written by Sudhagar Mani
clc
global D L S N CVRT Tr Gfin Gain Tfin Tain Yin Uh Tair Aw Mf Win Ma Uva eqdia
global Cpa Cpw Cpv V rowp rowf Aw ncv lstem dstem pie g mu alpha FL mfin decay tecay
ncv = 10; % number of control volume
% Air properties
Cpa= 1.01; Cpv = 1.805; Cpw= 4.186;  mu = 0.000025;
% feed material properties
decay = 0.19;  tecay = -248; eqdia = 0.0015;
% dryer dimentions
L = 12.8;  D = 3.8; N = 8.75; % drum speed in rpm
S = 0; alpha = 0; FL = 0.25;
Nf = 30; % number of flights
Area = pie*D^2/4;
V = (pie*D^2*L)/4;
% operating conditions
Gain = 11.06; % kg/s dry basis
Gfin = 1.16;  % kg/s dry basis
rowf = 250; Tair = 255; % constants
pie = 3.143; g = 9.81;
rowa = air_density(Tair);
Aw = 0.02; Uh = 0.02; % Over all heat loss coefficient
%Residence time calculation
Tr = residence_time;
CVRT = Tr/ncv;
%Resa = L*rowa*A/(Gain*ncv);
```

```matlab
%Ma = Gain*Resa;
%Ma = 0.96*V*rowa/ncv;
Ma = Gain*CVRT;
%Mf = 0.04*V*250/ncv;
Mf = Gfin*CVRT;
Uva= vol_heat;
options = odeset('RelTol',1e-4,'AbsTol',[1e-6 1e-6 1e-6 1e-6], 'MaxOrder',[5]);
Win = zeros(10,1); Yin = zeros(10,1); Tfin = zeros(10,1); Tain = zeros(10,1);


% section 1
RT1 = [0:0.01:CVRT];    Win(1,1)= 0.67;    Yin(1,1)=0.02;    Tfin(1,1)= 25;    Tain(1,1)= 250;
[t1,P1] = ode15s(@sec1,[RT1],[Win(1,1) Yin(1,1) Tfin(1,1) Tain(1,1)],options);


% dryer section 2
pp1=length(RT1); RT2 = [CVRT:0.01:2*CVRT]; Win(2,1) = P1(pp1,1); Yin(2,1) =P1(pp1,2); Tfin(2,1) =P1(pp1,3);
Tain(2,1) =P1(pp1,4);
[t2,P2] = ode15s(@sec2,[RT2],[Win(2,1) Yin(2,1) Tfin(2,1) Tain(2,1)],options);


% dryer section 3
pp2=length(RT2);  RT3 = [2*CVRT:0.01:3*CVRT]; Win(3,1) =P2(pp2,1);  Yin(3,1) =P2(pp2,2);  Tfin(3,1) =P2(pp2,3);
Tain(3,1) =P2(pp2,4);
 [t3,P3] = ode15s(@sec3,[RT3],[Win(3,1) Yin(3,1) Tfin(3,1) Tain(3,1)],options);


% dryer section 4
pp3=length(RT3); RT4 = [3*CVRT:0.01:4*CVRT];  Win(4,1) =P3(pp3,1); Yin(4,1) =P3(pp3,2);  Tfin(4,1) =P3(pp3,3);
Tain(4,1) =P3(pp3,4);
[t4,P4] = ode15s(@sec4,[RT4],[Win(4,1) Yin(4,1) Tfin(4,1) Tain(4,1)],options);


% dryer section 5
pp4=length(RT4); RT5 = [4*CVRT:0.01:5*CVRT];  Win(5,1) =P4(pp4,1); Yin(5,1) =P4(pp4,2); Tfin(5,1) =P4(pp4,3);
Tain(5,1) =P4(pp4,4);
```

```
[t5,P5] = ode15s(@sec5,[RT5],[Win(5,1) Yin(5,1) Tfin(5,1) Tain(5,1)],options);

% dryer section 6
pp5=length(RT5); RT6 = [5*CVRT:0.01:6*CVRT]; Win(6,1) =P5(pp5,1); Yin(6,1) =P5(pp5,2); Tfin(6,1) =P5(pp5,3);
Tain(6,1) =P5(pp5,4);
 [t6,P6] = ode15s(@sec6,[RT6],[Win(6,1) Yin(6,1) Tfin(6,1) Tain(6,1)],options);

% dryer section 7
pp6=length(RT6); RT7 = [6*CVRT:0.01:7*CVRT]; Win(7,1) =P6(pp6,1); Yin(7,1) =P6(pp6,2); Tfin(7,1) =P6(pp6,3);
Tain(7,1) =P6(pp6,4);
 [t7,P7] = ode15s(@sec7,[RT7],[Win(7,1) Yin(7,1) Tfin(7,1) Tain(7,1)],options);

% dryer section 8
pp7=length(RT7); RT8 = [7*CVRT:0.01:8*CVRT]; Win(8,1) =P7(pp7,1); Yin(8,1) =P7(pp7,2); Tfin(8,1) =P7(pp7,3);
Tain(8,1) =P7(pp7,4);
 [t8,P8] = ode15s(@sec8,[RT8],[Win(8,1) Yin(8,1) Tfin(8,1) Tain(8,1)],options);
% dryer section 9
pp8=length(RT8); RT9 = [8*CVRT:0.01:9*CVRT];  Win(9,1) =P8(pp8,1); Yin(9,1) =P8(pp8,2); Tfin(9,1) =P8(pp8,3);
Tain(9,1) =P8(pp8,4);
 [t9,P9] = ode15s(@sec9,[RT9],[Win(9,1) Yin(9,1) Tfin(9,1) Tain(9,1)],options);
% dryer section 10
pp9=length(RT9);  RT10 = [9*CVRT:0.01:10*CVRT];  Win(10,1) =P9(pp9,1); Yin(10,1) =P9(pp9,2); Tfin(10,1) =P9(pp9,3);
Tain(10,1) =P9(pp9,4);
 [t10,P10] = ode15s(@sec10,[RT10],[Win(10,1) Yin(10,1) Tfin(10,1) Tain(10,1)],options);
fid = fopen('drytime1.xls','w');
fprintf(fid,'Rotary drying data\n\n');
fprintf(fid,'%10.5f\n    %10.5f\n     %10.5f\n    %10.5f\n    %10.5f\n    %10.5f\n    %10.5f\n    %10.5f\n    %10.5f\n    %10.5f\n
',t1,t2,t3,t4,t5,t6,t7,t8,t9,t10);
fidmf = fopen('moisture1.xls','w');
fprintf(fidmf,'%10.5f\n    %10.5f\n     %10.5f\n    %10.5f\n    %10.5f\n    %10.5f\n    %10.5f\n    %10.5f\n    %10.5f\n    %10.5f\n
',P1(:,1),P2(:,1),P3(:,1),P4(:,1),P5(:,1),P6(:,1),P7(:,1),P8(:,1),P9(:,1),P10(:,1));
```

```matlab
fidW = fopen('humidity1.xls','w');
fprintf(fidW,'%10.5f\n     %10.5f\n     %10.5f\n     %10.5f\n     %10.5f\n     %10.5f\n     %10.5f\n     %10.5f\n     %10.5f\n     %10.5f\n
',P1(:,2),P2(:,2),P3(:,2),P4(:,2),P5(:,2),P6(:,2),P7(:,2),P8(:,2),P9(:,2),P10(:,2));
fidY = fopen('Feed_temp1.xls','w');
fprintf(fidY,'%10.5f\n     %10.5f\n     %10.5f\n     %10.5f\n     %10.5f\n     %10.5f\n     %10.5f\n     %10.5f\n     %10.5f\n     %10.5f\n
',P1(:,3),P2(:,3),P3(:,3),P4(:,3),P5(:,3),P6(:,3),P7(:,3),P8(:,3),P9(:,3),P10(:,3));
fidTf = fopen('Air_temp1.xls','w');
fprintf(fidTf,'%10.5f\n     %10.5f\n     %10.5f\n     %10.5f\n     %10.5f\n     %10.5f\n     %10.5f\n     %10.5f\n     %10.5f\n     %10.5f\n
',P1(:,4),P2(:,4),P3(:,4),P4(:,4),P5(:,4),P6(:,4),P7(:,4),P8(:,4),P9(:,4),P10(:,4));
status = fclose('all');
figure(1);
plot(t1,P1(:,1), t2,P2(:,1),t3,P3(:,1),t4,P4(:,1),t5,P5(:,1),t6,P6(:,1),t7,P7(:,1),t8,P8(:,1),t9,P9(:,1),t10,P10(:,1));
figure(2);
plot(t1,P1(:,2), t2,P2(:,2),t3,P3(:,2),t4,P4(:,2),t5,P5(:,2),t6,P6(:,2),t7,P7(:,2),t8,P8(:,2),t9,P9(:,2),t10,P10(:,2));
figure(3);
plot(t1,P1(:,3),              t2,P2(:,3),t3,P3(:,3),t4,P4(:,3),t5,P5(:,3),t6,P6(:,3),t7,P7(:,3),t8,P8(:,3),t9,P9(:,3),t10,P10(:,3),t1,P1(:,4),
t2,P2(:,4),t3,P3(:,4),t4,P4(:,4),t5,P5(:,4),t6,P6(:,4),t7,P7(:,4),t8,P8(:,4),t9,P9(:,4),t10,P10(:,4));
%figure(3);
%plot(t1,P1(:,4), t2,P2(:,4),t3,P3(:,4),t4,P4(:,4),t5,P5(:,4),t6,P6(:,4),t7,P7(:,4),t8,P8(:,4),t9,P9(:,4),t10,P10(:,4));


fprintf('******************************************************************************************\n');
fprintf('***********                                                              *********** \n');
fprintf('***********          Single Pass Rotary Drum Dryer Simulation Model           *********** \n');
fprintf('***********                                                              *********** \n');
fprintf('******************************************************************************************\n');
fprintf('***********                   Developed by Sudhagar Mani                  *********** \n');
fprintf('***********          Department of Chemical & Biological Engineering           *********** \n');
fprintf('***********              University of British Columbia              *********** \n');
fprintf('***********                      October, 2004                  *********** \n');
fprintf('******************************************************************************************\n\n');
```

147

```
fprintf('Rotary dryer dimentions:\n');
fprintf('Dryer length (m)-----------------------------------------------%10.2f\n',L);
fprintf('Dryer diameter (m)---------------------------------------------%10.2f\n',D);
fprintf('Dryer drum speed (rpm)-----------------------------------------%10.2f\n',N);
fprintf('Drum slope (degree)--------------------------------------------%10.2f\n',S);
fprintf('Dryer flight length (m)----------------------------------------%10.2f\n',FL);
fprintf('Inlet gas conditions:\n');
fprintf('Hot gas inlet temperature (deg. C)-----------------------------%10.2f\n',Tair);
fprintf('Hot gas inlet humidity (kg water/kg air)-----------------------%10.2f\n',Yin(1,1));
fprintf('Hot gas flow rate (kg/s)---------------------------------------%10.2f\n',Gain);
fprintf('Feed Temperature (Deg. C)--------------------------------------%10.2f\n',Tfin(1,1));
fprintf('Feed moisture content (db)-------------------------------------%10.2f\n',Win(1,1));
fprintf('Feed flow rate (kg/s)------------------------------------------%10.2f\n',Gfin);
fprintf('Feed particle residence time (s)-------------------------------%10.2f\n',Tr);
fprintf('Dryer simulation results:\n');
fprintf('Dryer section    Feed Moisture(db)    gas humidity(kg/kg)    Feed Temp (C)    Gas Temp (C)\n');
%for i = 1:1800
%fprintf('%10.2f %10.2f %10.2f %10.2f %10.2f\n', t1,    P1(i,1),    P1(i,2),    P1(i,3),    P1(i,4));
%end
```

■■■

Sub function 1 – Residence time calculations

```
% residence time of particles (For saw dust particles)
function p = residence_time
global D L FL N mu rowp pie g eqdia rowp Tair Gain alpha
% avenrage particle diameter
Dp = eqdia;
% Dryer dimentions
Adryer = pie*D^2/4;
Vdryer = Adryer*L;
```

```
% length of fall of particles
y = D/2 + (D/2 - FL)* 0.707;
% Air properties and measurements
rowa = air_density(Tair);
Airflow = Gain/rowa;
vela = Airflow/Adryer;
Re = (rowa*vela*Dp)/mu;

% Particles travelled in x direction due to drag force
 kk = 0.4373/(1+(7185/Re));
Cd = (24/Re)*(1+0.1858*Re^(0.6529))+ kk;
pp = Cd;
J = 1.5*rowa*Cd/(Dp*rowp);
x = y*(sin(alpha)+ J*vela^2/g)
% Particle time in the flight
tr = 60/(2.67*N);
% particle time to fall
tf = (2*y/g)^0.5;

% Particle residence time in the dryer
p = (L/x)*(tr+tf);
cascade = L/x;
return
```

****

Sub function 2 - Air density prediction
```
function y = air_density(temp)
global Tair
y = 1.293*(273/(temp+273));
return
```

▪▪

Sub function 3 - Volumetric heat transfer coefficient

```
function y = vol_heat
global Gain D pie
Area = pie*D^2/4;
y= (425*(Gain/Area)^0.8)/1000;
return
```

■■

Sub function 4 – solving differential equations simultaneously

```
function dP = sec1(t,P)
global D L S N CVRT Tr Gfin Gain Win  Uh  Mf Tain  Ma Uva V Yin Cpa Cpw Cpv Dp Tfin rowf Aw ncv decay tecay
% calculation of equilibrium moisture content for grasses
Wm = 0.00039229*exp(1858.8/(P(4)+273.13));
C= 323.1769*exp(-974.55/(P(4)+273.13));
denom = (1-Aw)*(1+((C-1)*Aw));
Num=Wm*C*Aw;
We= Num/denom;
%We = 0.005; % Equilibrium moisture content
Drate = (decay*exp(tecay/P(4))); % drying rate is in 1/s
%Mf = Gfin*CVRT; % feed rate leaving the control volume
M1 = Gfin*(Win(1,1)-P(1));
M2 = Drate*(P(1)-We)*Mf;
A1 = Gain*(Yin(1,1)-P(2));
A2 = M2;

%calculation of latent heat and specific heat
Cpfin = 1.7 + 1.81*(Win(1,1));
Cpf= 1.7 + 1.81*(P(1));
```

```
Lw=2260;
Qst = (1.6018*We^(0.8540))/(0.0068+We^(2.5758));
lamda= Lw+Qst;

% calculation of components for feed heat balance
C1=Gfin*Cpfin*(Tfin(1,1));
C2 = Gfin*Cpf*P(3);
%V_F =P(1)/rowf;
%Volume = A*t*L/Tr;
vol = V/ncv;
%SSK = wetbulb(P(2),P(4));
%SS= SSK-273.13;
C3 =Uva*vol*(P(4)-P(3)) ;
C4 = M2*lamda;
C5 = M2*Cpv*(P(4)-P(3));
C6 = (Uh*(3.14*D*L)*(P(4)-20))/ncv;
%C7 = Cpf*P(3)*P(1);

%calculation of component heat for air heat balance
Cpain = Cpa+Cpv*Yin(1,1);
Cpao = Cpa+Cpv*P(2);
%Ein = Cpa*Tain(1,1)+(Cpv*Tain(1,1)+2500)*Yin(1,1);
%Eo = Cpa*P(4)+(Cpv*P(4)+2500)*P(2);
C8= Gain*Cpain*Tain(1,1);
C80= Gain*Cpao*P(4);
%tlmn = (Tain(1,1)-Tfin(1,1))
%tlmd=(P(4)-P(3))
%psk =log(tlmn/tlmd)
%delta=(tlmn-tlmd)/(psk)
%C3 = Uva*vol*delta;
C9 = C3;
```

```
C10= M2*Cpv*P(4);
%C11 = Ma*(Cpao)*P(4)

% simultaneous differential equations
dP = zeros(4,1); % column vector
dP(1) = (M1-M2)/Mf;
dP(2) = (A1+A2)/Ma;
dP(3)=(C1-C2+C3-C4-C5-C6)/(Mf*Cpfin);
dP(4)=(C8-C80-C9+C10)/(Ma*Cpain);
```

****

****

2. Solid fuel burner model

```
% Simple burner model developed by Sudhagar
% The model provides the flue gas composition of given fuel and estimates
% the fuel requirement for the burner for the given gas temperature and gas
% flow rate.
clc
global HHV flue_totalv flue_vper temp air_comp fuel_comp air_tin fuel_tin fuel_moist air_hin air_cp
% Composition of fuel
fuel_comp = ones(6,1);
air_comp = ones(4,1);
air_cdry = ones(3,1);
fprintf(' Enter the ultimate analysis of the fuel in weight basis \n');
fuel_comp(1,1) = input ('Enter the amount of carbon in the fuel in fraction (wt)=' );
fuel_comp(2,1) = input ('Enter the amount of hydrogen in the fuel in fraction (wt)=' );
fuel_comp(3,1) = input ('Enter the amount of oxygen in the fuel in fraction(wt)=');
fuel_comp(4,1) = input ('Enter the amount of nitrogen in the fuel in fraction (wt)=');
fuel_comp(5,1) = input ('Enter the amount of sulpur in the fuel in fraction (wt)=');
```

```
fuel_comp(6,1) = input ('Enter the amount of ash in the fuel in fraction (wt)=' );
fuel_heatingvalue= input ('Enter the higher heating value of the fuel in kJ/kg =');
flue_gas = input('Enter the amount of hot gas required to dry the materials in kg/s =');
fuel_tin = 20;
flue_temp = input ('Enter the expected flue gas temperature for drying process, C = ');
fuel_moist = input(' Enter the percent moisture in the fuel = ');
Comb_eff = input ('Enter the combustion efficiency of the fuel (recoverable heat) =');

% Composition of air
%fprintf ('\n Enter the composition of air in dry weight basis\n');
air_comp(1,1) =  0.23; %input ('Enter the percent oxygen in the air in % (wt)=');
air_comp(2,1) = 0.759; %input ('Enter the percent nitrogen in the air in % (wt)=');
air_comp(3,1) = 0.003; %input ('Enter the percent carbon dioxide in the air % =');
air_comp(4,1) = 0.008;

% air properties
air_tin = 20; %input ('Enter the inlet temperature of the air in celcius =');
air_hin = 0.008; %input ('Enter the inlet humidity of the air in kg of water/kg dry air =');
air_cp = 1.06; %input ('Enter the specific heat of the air in kJ/kg C =');
air_den = 1.0; %input ('Enter the density of the air in kg/m3 =');

for i = 1:3
    air_cdry(i,1) = air_comp(i,1)*(1-air_comp(4,1));
end
% determination of stoichiometric air requirement for the fuel
HHV = fuel_heatingvalue*(1-fuel_moist/100)*Comb_eff;
temp = flue_temp+273.13;
air_required = air_req
fluegas_required = air_req + (1-fuel_comp(6,1));
fuel_required = flue_gas*3600/fluegas_required;
oxygen_use = fuel_comp(1)*32/12 + fuel_comp(2)*32/4 + fuel_comp(5) - fuel_comp(3);
```

```
stoichio_air = oxygen_use/air_comp(1);
flue_comp = ones(5,1);

% determination of flue gas composition
flue_comp(1,1) = fuel_comp(1,1)*(1+(32/12))+ air_comp(3,1)*air_required; % amount of CO2 in the flue gas
flue_comp(2,1) = fuel_comp(2,1) *(1+ (32/4)) + air_comp(4,1)*air_required + fuel_moist/100; % amount of water vapor in wet basis
flue_comp(3,1) = (air_required-stoichio_air)*air_comp(1,1)   ; % amount of O2
flue_comp(4,1) = air_required*air_comp(2,1)+ fuel_comp(4,1);% nitrogen
flue_comp(5,1) = fuel_comp(5,1)*2;% amount of sox
flue_wtotal = flue_comp(1,1)+flue_comp(2,1)+flue_comp(3,1)+flue_comp(4,1)+flue_comp(5,1);

%flue_cmw = ones(5,1);
flue_cvol = ones(5,1);
flue_vper = ones(5,1);
flue_cmw = [44 18 32 28 64];
flue_vtotal = 0;
flue_mw = 0.0;

for i = 1:5
    flue_cvol(i,1) = flue_comp(i,1)/flue_cmw(i);
    flue_vtotal = flue_vtotal + flue_cvol(i,1);
    flue_mw = flue_mw + (flue_cmw(i)*flue_comp(i,1)/flue_wtotal);
end

flue_totalv = flue_wtotal/flue_mw*1000; % total flue gas in mol/kg of fuel
for i = 1:5
    flue_vper(i,1) = flue_cvol(i,1)/flue_vtotal;
end
fprintf('Amount of fuel required for drying, kg/h = %10.6f \n', fuel_required);
fprintf('Composition of fuel gases generated during combustion in percent volume \n');
```

```
for i = 1:5
    fprintf('flue gas composition,  percent vol = %10.6f \n', flue_vper(i,1));
end


*******************************************************************************************
```

Sub function 1

```
function T = air_req()
global LHV flue_totalv flue_cper
        tol = 1e-6;
        xi = 0; xf = 2273.13;  dx = 0.01; x1 = xi;
        y1=heatbalance(x1);
        if y1==0
                T = x1;
        else
                while(x1<xf)

                        x2 = x1 + dx;
                        y2 = heatbalance(x2);
                        if (y1*y2)>0
                                        x1=x2;
                                        y1=y2;
        else
                                while((x2-x1)>tol)
                                        x3=(x1+x2)/2.0;
        y3=heatbalance(x3);

                                        if(y1*y3)>0
                                                x1=x3;
                                                y1=y3;
        else

                                                x2=x3;
```

```
                    y2=y3;
                end
            end
                    T = x3;
                    return
        end


    end
end
```

****

Sub function 2
```
function y = heatbalance(actual_air)
global air_comp temp air_tin fuel_tin fuel_moist air_hin HHV air_cp fuel_comp

fuel_cp = 1.7; % kJ/kg k
W_cp = 4.184; %kJ/kg k
oxygen_use = fuel_comp(1)*32/12 + fuel_comp(2)*32/4 + fuel_comp(5) - fuel_comp(3);
stoichio_air = oxygen_use/air_comp(1);
flue_comp = ones(5,1);

% determination of flue gas composition
flue_comp(1,1) = fuel_comp(1,1)*(1+(32/12))+ air_comp(3,1)*actual_air; % amount of CO2 in the flue gas
flue_comp(2,1) = fuel_comp(2,1) *(1+ (32/4)) + air_comp(4,1)*actual_air + fuel_moist/100; % amount of water vapor in wet basis
flue_comp(3,1) = (actual_air-stoichio_air)*air_comp(1,1)   ; % amount of O2
flue_comp(4,1) = actual_air*air_comp(2,1)+ fuel_comp(4,1);% nitrogen
flue_comp(5,1) = fuel_comp(5,1)*2;% amount of sox
flue_wtotal = flue_comp(1,1)+flue_comp(2,1)+flue_comp(3,1)+flue_comp(4,1)+flue_comp(5,1);
%flue_cmw = ones(5,1);
flue_cvol = ones(5,1);
```

```
flue_vper = ones(5,1);
flue_cmw = [44 18 32 28 64];
flue_vtotal = 0;
flue_mw = 0.0;

for i = 1:5
    flue_cvol(i,1) = flue_comp(i,1)/flue_cmw(i);
    flue_vtotal = flue_vtotal + flue_cvol(i,1);
    flue_mw = flue_mw + (flue_cmw(i)*flue_comp(i,1)/flue_wtotal);
end
flue_totalv = flue_wtotal/flue_mw*1000; % total flue gas in mol/kg of fuel

for i = 1:5
    flue_vper(i,1) = flue_cvol(i,1)/flue_vtotal;
end
flue_vtoalper = flue_wtotal/flue_vtotal;Cp = ones(5,1);
Cp(1,1) = 0.004184*(10.34+0.00274*temp-(195500/temp^2));% in kJ/mol K
Cp(2,1) = 0.004184*(8.22+0.00015*temp+0.00000134*temp^2);
Cp(3,1) = 0.004184*(8.27+0.000258*temp-(187700/temp^2));
Cp(4,1) = 0.004184*(6.5+0.001*temp);
Cp(5,1) = 0.004184*(7.7+0.00530*temp-0.00000083*temp^2);
Entotal = 0.0;
for i = 1:5
    ethal(i,1) = Cp(i,1)*flue_vper(i,1);
    Entotal = Entotal + ethal(i,1);
end
LHV = HHV-(fuel_comp(2,1)*(1+ (32/4)))*2442;
H1 = (1-fuel_moist)*fuel_cp*fuel_tin;
H2 = fuel_moist*W_cp*fuel_tin;
H3 = actual_air*(air_cp*air_tin + (1.88*air_tin + 2500)*air_hin);
H4 = flue_totalv*Entotal*(temp-273.13);
```

157

```
H5 = fuel_comp(6,1)*1*(temp-273.13);
y = H1 + H2 + LHV + H3 - H4 - H5;
return
```

****

Sub function 3

```
function y = value(temp)
global LHV flue_totalv flue_vper
Cp = ones(5,1);
Cp(1,1) = 0.004184*(10.34+0.00274*temp-(195500/temp^2));% in kJ/mol K
Cp(2,1) = 0.004184*(8.22+0.00015*temp+0.00000134*temp^2);
Cp(3,1) = 0.004184*(8.27+0.000258*temp-(187700/temp^2));
Cp(4,1) = 0.004184*(6.5+0.001*temp);
Cp(5,1) = 0.004184*(7.7+0.00530*temp-0.00000083*temp^2);
Entotal = 0.0;
for i = 1:5
    ethal(i,1) = Cp(i,1)*flue_vper(i,1);
    Entotal = Entotal + ethal(i,1);
end
y = flue_totalv*Entotal*(temp-298.13) - LHV;
return
```

****

3. Triple pass rotary drum dryer model

```
% Heat and mass transfer (co-current type) model for a triple pass rotary dryer written by Sudhagar Mani
clc
global Do Lo S N Aream Areai Areao CVRT Tr Gfin Gain RH Win Tain We Drate Mf
global Ma Uvai pd Ul Uvam Uvao kd Vi Vm Vo Yin Cpa Cpw Cpv Di Tfin rowf Aw ncv
```

```
ncv = 12; % number of control volume
% Air properties
Cpa= 1;
Cpv = 1.805; Cpw= 4.186;
Gain = 16.67;Gfin = 1.2;rowf =350;Li = 12;Lm = 12;Lo = 12;Di = 1;Dm = 1.75;
Do = 2.5;N = 8;pie = 3.14;kd = 0.074;pd = -236; Ul = 0.02; Tr = RTS;
Areai = pie*Di^2/4; Vi = Areai*Li;
Aream = (pie/4)*(Dm^2-Di^2); Vm = Aream*Lm;
Areao = (pie/4)*(Do^2-Dm^2);
Vo = Areao*Lo;
CVRT = Tr/ncv;
Aw = 0.05;
%Ma = V*Rowain/ncv;
Ma = Gain*CVRT;
Mf = Gfin*CVRT;
Uvai = vol_heat1; Uvam = vol_heat2; Uvao = vol_heat3;
options = odeset('RelTol',1e-4,'AbsTol',[1e-6 1e-6 1e-6 1e-6], 'MaxOrder',[5]);
Win = zeros(12,1);
Yin = zeros(12,1);
Tfin = zeros(12,1);
Tain = zeros(12,1);
% section 1
RT1 = [0.0001:0.1:CVRT]; Win(1,1)=1.5;Yin(1,1)=0.01; Tfin(1,1)=25; Tain(1,1)=400;
[t1,P1] = ode45(@drying1,[RT1],[Win(1,1) Yin(1,1) Tfin(1,1) Tain(1,1)],options);

% dryer section 2
pp1=length(RT1); RT2 = [CVRT:0.1:2*CVRT]; Win(2,1) =P1(pp1,1); Yin(2,1) =P1(pp1,2);
Tfin(2,1) =P1(pp1,3); Tain(2,1) =P1(pp1,4);
[t2,P2] = ode45(@drying2,[RT2],[Win(2,1) Yin(2,1) Tfin(2,1) Tain(2,1)],options);
```

```
% dryer section 3
pp2=length(RT2); RT3 = [2*CVRT:0.1:3*CVRT];Win(3,1) =P2(pp2,1);Yin(3,1) =P2(pp2,2);
Tfin(3,1) =P2(pp2,3); Tain(3,1) =P2(pp2,4);
 [t3,P3] = ode45(@drying3,[RT3],[Win(3,1) Yin(3,1) Tfin(3,1) Tain(3,1)],options);
% dryer section 4
pp3=length(RT3); RT4 = [3*CVRT:0.1:4*CVRT]; Win(4,1) =P3(pp3,1);Yin(4,1) =P3(pp3,2);
Tfin(4,1) =P3(pp3,3); Tain(4,1) =P3(pp3,4);
 [t4,P4] = ode45(@drying4,[RT4],[Win(4,1) Yin(4,1) Tfin(4,1) Tain(4,1)],options);

% dryer section 5
pp4=length(RT4);RT5 = [4*CVRT:0.1:5*CVRT];Win(5,1) =P4(pp4,1);Yin(5,1) =P4(pp4,2);
Tfin(5,1) =P4(pp4,3); Tain(5,1) =P4(pp4,4);
 [t5,P5] = ode45(@drying5,[RT5],[Win(5,1) Yin(5,1) Tfin(5,1) Tain(5,1)],options);

% dryer section 6
pp5=length(RT5); RT6 = [5*CVRT:0.1:6*CVRT]; Win(6,1) =P5(pp5,1);Yin(6,1) =P5(pp5,2);
Tfin(6,1) =P5(pp5,3); Tain(6,1) =P5(pp5,4);
[t6,P6] = ode45(@drying6,[RT6],[Win(6,1) Yin(6,1) Tfin(6,1) Tain(6,1)],options);

% dryer section 7
pp6=length(RT6); RT7 = [6*CVRT:0.1:7*CVRT]; Win(7,1) =P6(pp6,1); Yin(7,1) =P6(pp6,2);
Tfin(7,1) =P6(pp6,3); Tain(7,1) =P6(pp6,4);
 [t7,P7] = ode45(@drying7,[RT7],[Win(7,1) Yin(7,1) Tfin(7,1) Tain(7,1)],options);

% dryer section 8
pp7=length(RT7); RT8 = [7*CVRT:0.1:8*CVRT]; Win(8,1) =P7(pp7,1);Yin(8,1) =P7(pp7,2);
Tfin(8,1) =P7(pp7,3); Tain(8,1) =P7(pp7,4);
 [t8,P8] = ode45(@drying8,[RT8],[Win(8,1) Yin(8,1) Tfin(8,1) Tain(8,1)],options);

% dryer section 9
pp8=length(RT8); RT9 = [8*CVRT:0.1:9*CVRT]; Win(9,1) =P8(pp8,1);Yin(9,1) =P8(pp8,2);
```

```
Tfin(9,1) =P8(pp8,3); Tain(9,1) =P8(pp8,4);
 [t9,P9] = ode45(@drying9,[RT9],[Win(9,1) Yin(9,1) Tfin(9,1) Tain(9,1)],options);


% dryer section 10
pp9=length(RT9); RT10 = [9*CVRT:0.1:10*CVRT]; Win(10,1) =P9(pp9,1); Yin(10,1) =P9(pp9,2);
Tfin(10,1) =P9(pp9,3); Tain(10,1) =P9(pp9,4);
 [t10,P10] = ode45(@drying10,[RT10],[Win(10,1) Yin(10,1) Tfin(10,1) Tain(10,1)],options);


% dryer section 11
pp10=length(RT10); RT11 = [10*CVRT:0.1:11*CVRT];Win(11,1) =P10(pp10,1); Yin(11,1) =P10(pp10,2);
Tfin(11,1) =P10(pp10,3); Tain(11,1) =P10(pp10,4);
 [t11,P11] = ode45(@drying11,[RT11],[Win(11,1) Yin(11,1) Tfin(11,1) Tain(11,1)],options);


% dryer section 12
pp11=length(RT11); RT12 = [11*CVRT:0.1:12*CVRT]; Win(12,1) =P11(pp11,1); Yin(12,1) =P11(pp11,2);
Tfin(12,1) =P11(pp11,3); Tain(12,1) =P11(pp11,4);
 [t12,P12] = ode45(@drying12,[RT12],[Win(12,1) Yin(12,1) Tfin(12,1) Tain(12,1)],options);


fid = fopen('drytime.xls','w');
fprintf(fid,'Rotary drying data\n\n');
fprintf(fid,'%10.5f\n %10.5f\n %10.5f\n %10.5f\n %10.5f\n %10.5f\n %10.5f\n %10.5f\n %10.5f\n %10.5f\n %10.5f\n %10.5f\n
',t1,t2,t3,t4,t5,t6,t7,t8,t9,t10,t11,t12);
fidmf = fopen('moisture.xls','w');
fprintf(fidmf,'%10.5f\n %10.5f\n %10.5f\n %10.5f\n %10.5f\n %10.5f\n %10.5f\n %10.5f\n %10.5f\n %10.5f\n %10.5f\n %10.5f\n
',P1(:,1),P2(:,1),P3(:,1),P4(:,1),P5(:,1),P6(:,1),P7(:,1),P8(:,1),P9(:,1),P10(:,1), P11(:,1), P12(:,1));
fidW = fopen('humidity.xls','w');
fprintf(fidW,'%10.5f\n %10.5f\n %10.5f\n %10.5f\n %10.5f\n %10.5f\n %10.5f\n %10.5f\n %10.5f\n %10.5f\n %10.5f\n %10.5f\n
',P1(:,2),P2(:,2),P3(:,2),P4(:,2),P5(:,2),P6(:,2),P7(:,2),P8(:,2),P9(:,2),P10(:,2),P11(:,2), P12(:,2));
fidY = fopen('Feed_temp.xls','w');
fprintf(fidY,'%10.5f\n %10.5f\n %10.5f\n %10.5f\n %10.5f\n %10.5f\n %10.5f\n %10.5f\n %10.5f\n %10.5f\n %10.5f\n %10.5f\n
',P1(:,3),P2(:,3),P3(:,3),P4(:,3),P5(:,3),P6(:,3),P7(:,3),P8(:,3),P9(:,3),P10(:,3),P11(:,3), P12(:,3));
```

```
fidTf = fopen('Air_temp.xls','w');
fprintf(fidTf,'%10.5f\n %10.5f\n %10.5f\n %10.5f\n %10.5f\n %10.5f\n %10.5f\n %10.5f\n %10.5f\n %10.5f\n %10.5f\n %10.5f\n
',P1(:,4),P2(:,4),P3(:,4),P4(:,4),P5(:,4),P6(:,4),P7(:,4),P8(:,4),P9(:,4),P10(:,4),P11(:,4), P12(:,4));
status = fclose('all');
figure(1);
plot(t1,P1(:,1), t2,P2(:,1),t3,P3(:,1),t4,P4(:,1),t5,P5(:,1),t6,P6(:,1),t7,P7(:,1),t8,P8(:,1),t9,P9(:,1),t10,P10(:,1),t11,P11(:,1),t12,P12(:,1));
figure(2);
plot(t1,P1(:,2), t2,P2(:,2),t3,P3(:,2),t4,P4(:,2),t5,P5(:,2),t6,P6(:,2),t7,P7(:,2),t8,P8(:,2),t9,P9(:,2),t10,P10(:,2),t11,P11(:,2),t12,P12(:,2));
figure(3);
plot(t1,P1(:,3), t2,P2(:,3),t3,P3(:,3),t4,P4(:,3),t5,P5(:,3),t6,P6(:,3),t7,P7(:,3),t8,P8(:,3),t9,P9(:,3),t10,P10(:,3),t11,P11(:,3),t12,P12(:,3));
figure(4);
plot(t1,P1(:,4), t2,P2(:,4),t3,P3(:,4),t4,P4(:,4),t5,P5(:,4),t6,P6(:,4),t7,P7(:,4),t8,P8(:,4),t9,P9(:,4),t10,P10(:,4),t11,P11(:,4),t12,P12(:,4));
```

****

Sub function 1 – Stem residence time calculation

```
% residence time model for alfalfa stems
function p = RTS()
%Residence time of stems in the inner drum
% leaves are assumed as disk particles
pie = 3.143;
Di = 1;Dm = 1.75;Do = 2.5;Li = 12;Lm = 12;Lo = 12;
ls = 0.075; % stem length
ds = 0.003; % stem diameter
Gain = 16.67;Tair = 600;mu = 0.000033;g = 9.81;rowp = 1200;
theta = 45;N = 8;alpha = 0;FL = 0.2;
 % avenrage particle diameter
Dp = ds;
 % Dryer dimentions
Adryer = pie*Di^2/4;
Vdryer = Adryer*Li;
```

```
% angle of repose of the material was assumed as 45 degree
% length of fall of particles
y = Di/2 + (Di/2 - FL)* 0.707;
% Air properties and measurements
rowa = air_density(Tair);
Airflow = Gain/rowa;
vela = Airflow/Adryer;
Re = (rowa*vela*Dp)/mu;
% Particles travelled in x direction due to drag force
% drag coefficient for disc particles are similar to the spherical
% particles

 if Re <2.0
    Cd= 24*Re^1.0;
else if Re >2 && Re <100
      Cd = 18.5*Re^(-0.6);
else if Re > 100 && Re <1000
      Cd = 1.5;
else if Re > 1000
      Cd = 1.2;% Cd for disc shaped leaves from Cooper and Alley (2002)
   end
end
end
end
J = 0.5*rowa*Cd/(ls*rowp);
xi = y*(sin(alpha)+ J*vela^2/g);
% Particle time in the flight
tr = 60/(2.67*N);

% particle time to fall
tf = (2*y/g)^0.5;
```

```
% leaf residence time in the inner dryer
rti = (Li/xi)*(tr+tf)

% RT for the second middle section
denam = air_density(Tair-200);
Amiddle = pie*(Dm^2 - Di^2)/4;
vam = Gain/(Amiddle*denam);
ym1 = 0.5*(Dm-Di-FL)*sin(theta);
ym2 = 0.5*(Dm-Di);
trm = (90+theta)/(360*N);
tfm = (2*ym1/g)^0.5 + (2*ym2/g)^0.5 + trm;
Rem = (denam*vam*ds)/mu;

if Rem <2.0
    Cdm= 24*Rem^1.0;
else if Rem >2 && Rem <100
     Cdm = 18.5*Rem^(-0.6);
else if Rem > 100 && Rem <1000
     Cdm = 2;
else if Rem > 1000
     Cdm = 1.2;% Cd for disc shaped leaves from Cooper and Alley (2002)
   end
end
end
end
Jsm = 0.5*denam*Cdm/(ls*rowp);
xsm = 0.5*Jsm*vam^2*tfm^2
tcm = trm + tfm;
rtm = Lm*tcm/xsm % residence time of leaves in the middle drum
```

```
    % RT for the outer section
denao = air_density(Tair-450);
Aouter = pie*(Do^2 - Dm^2)/4;
vao = Gain/(Aouter*denao);
yo1 = 0.5*(Do-Dm-FL)*sin(theta);
yo2 = 0.5*(Do-Dm);
tro = trm;
tfo = (2*yo1/g)^0.5 + (2*yo2/g)^0.5 + tro;
Reo = (denao*vao*ds)/mu;

if Reo <2.0
   Cdo= 24*Reo^1.0;
else if Reo >2 && Reo <100
      Cdo= 18.5*Reo^(-0.6);
else if Reo > 100 && Reo <1000
      Cdo = 1.5;
else if Reo > 1000
      Cdo= 1.2;% Cd for disc shaped leaves from Cooper and Alley (2002)
   end
end
end
end
Jlo = 0.5*denao*Cdo/(ls*rowp);
xlo = 0.5*Jlo*vao^2*tfo^2;
tco = tro + tfo;
rto = Lo*tco/xlo % residence time of leaves in the outer drum
 rtto = rti + rtm + rto;
p = rtto;
return


***********************************************************************************************
```

Sub function 2 – Leaf residence time calculation

```
% residence time model for alfalfa leaves
function p = RTL()
%Residence time of leaves in the inner drum
% leaves are assumed as disk particles
pie = 3.143;Di = 1;Dm = 1.75;Do = 2.5;Li = 12;Lm = 12;Lo = 12;
la = 0.025;lb = 0.015;lt =0.005;Gain = 16.67;Tair = 600;mu = 0.000033;
g = 9.81;rowp = 1400;theta = 45;N = 8;alpha = 0;FL = 0.25;
% stem equivalent diameter
Aleaf = pie*la*lb/4;
%    Vleaf = pie*dstem^2*lstem/4;
%Deqs = (4*Astem/pie)^0.5;
% avenrage particle diameter
Dp = (la+lb)/2;
% Dryer dimentions
Adryer = pie*Di^2/4;
Vdryer = Adryer*Li;
% angle of repose of the material was assumed as 45 degree
% length of fall of particles
y = Di/2 + (Di/2 - FL)* sin(theta);

% Air properties and measurements
rowa = air_density(Tair);
Airflow = Gain/rowa;
vela = Airflow/Adryer;
Re = (rowa*vela*Dp)/mu;
% Particles travelled in x direction due to drag force
% drag coefficient for disc particles are similar to the spherical particles
```

```
if Re <2.0
   Cd= 24*Re^1.0;
else if Re >2 && Re <100
     Cd = 18.5*Re^(-0.6);
else if Re > 100 && Re <1000
     Cd = 1.8;
else if Re > 1000
     Cd = 1.2;% Cd for disc shaped leaves from Cooper and Alley (2002)
   end
end
end
end
 pp = Cd;
J = 0.5*rowa*Cd/(Dp*rowp);
xi = y*(sin(alpha)+ J*vela^2/g);
% Particle time in the flight
tr = 60/(2.67*N);
% particle time to fall
tf = (2*y/g)^0.5;
% leaf residence time in the inner dryer
rti = (Li/xi)*(tr+tf);

% RT for the second middle section
denam = air_density(Tair-200);
vam = Gain/(0.25*pie*(Dm^2-Di^2)*denam);
ym1 = 0.5*(Dm-Di-FL)*sin(theta);
ym2 = 0.5*(Dm-Di);
trm = (90+theta)/(360*N);
tfm = (2*ym1/g)^0.5 + (2*ym2/g)^0.5 + trm;
Rem = (denam*vam*Dp)/mu;
if Rem <2.0
```

```
            Cdm= 24*Rem^1.0;
        else if Rem >2 && Rem <100
            Cdm = 18.5*Rem^(-0.6);
        else if Rem > 100 && Rem <1000
            Cdm = 1.8;
        else if Rem > 1000
            Cdm = 1.2;% Cd for disc shaped leaves from Cooper and Alley (2002)
        end
    end
    end
    end
    Jlm = 0.5*denam*Cdm/(Dp*rowp);
    xlm = 0.5*Jlm*vam^2*tfm^2;
    tcm = trm + tfm;
    rtm = Lm*tcm/xlm; % residence time of leaves in the middle drum
    % RT for the outer section
    denao = air_density(Tair-400);
    vao = Gain/(0.25*pie*(Do^2-Dm^2)*denao);
    yo1 = 0.5*(Do-Dm-FL)*sin(theta);
    yo2 = 0.5*(Do-Dm);
    tro = trm;
    tfo = (2*yo1/g)^0.5 + (2*yo2/g)^0.5 + tro;
    Reo = (denao*vao*Dp)/mu;

    if Reo <2.0
        Cdo= 24*Reo^1.0;
    else if Reo >2 && Reo <100
        Cdo= 18.5*Reo^(-0.6);
    else if Reo > 100 && Reo <1000
        Cdo = 1.8;
    else if Reo > 1000
```

```
Cdo= 1.2;% Cd for disc shaped leaves from Cooper and Alley (2002)
    end
end
end
end
 Jlo = 0.5*denao*Cdo/(Dp*rowp);
 xlo = 0.5*Jlo*vao^2*tfo^2;
 tco = tro + tfo;
 rto = Lo*tco/xlo; % residence time of leaves in the outer drum
 rtto = rti + rtm + rto;
 p = rtto;
 return
```

****

Sub function 3 – Volumetric heat transfer coefficient
```
% Inner drum section
function S = vol_heat1()
global Gain Di
innerarea = 3.143*Di^2/4;
y= (425*(Gain/innerarea)^0.8)/1000;
S = y;
return
% Outer drum section
function S = vol_heat1()
global Gain Areao
y= (425*(Gain/Areao)^0.8)/1000;
S = y;
return
% Middle drum section
function S = vol_heat1()
global Gain Aream
```

```
y= (425*(Gain/Aream)^0.8)/1000;
S = y; Return
```

****

Sub function 4 – solving differential equations
```
function dP = drying1(t,P)
global S N CVRT Tr Gfin Gain Win Tain Mf Ma Uvai Vi Yin Cpa Cpw Cpv Tfin rowf Aw ncv kd pd
% calculation of equilibrium moisture content
Wm = 0.00039229*exp(1858.8/(P(4)+273.13));
C= 323.1769*exp(-974.55/(P(4)+273.13));
denom = (1-Aw)*(1+((C-1)*Aw));
Num=Wm*C*Aw;
We= Num/denom;
% calculation of drying rate
Drate= kd*exp(pd/(P(4)));
%calculation of latent heat and specific heat
Cpfin = 1.382+2.805*(Win(1,1));
Cpf=1.382+2.805*(P(1));
Lw=2260;
Qst = (1.6018*We^(0.8540))/(0.0068+We^(2.5758));
lamda= Lw+Qst;
% calculation of components for feed heat balance
C1=Gfin*Cpfin*(Tfin(1,1))
C2 = Gfin*Cpf*P(3)
%V_F =P(1)/rowf;
vol = Vi/4;
M1 = Drate*(P(1)-We);
M2 = Gfin*(Win(1,1)-P(1));
M3 = Gain*(Yin(1,1)-P(2));
Cpain = Cpa+Cpv*Yin(1,1);
Cpao =Cpa+Cpv*P(2);
```

```
C8 =Gain*Cpain*(Tain(1,1));
SSK = wetbulb(P(2),P(4));
SS= SSK-273.13;
C3=Uvai*vol*(P(4)-P(3))
C4=M1*Mf*lamda
C5=M1*Mf*Cpv*(P(4)-P(3))
%C6 = (0.20*(3.14*D*L)*(P(4)-25))/ncv;
C7 = Cpf*P(3)*Mf;
%calculation of component heat for air heat balance
C80 =Gain*Cpao*(P(4));
%tlmn = ((P(4)-P(3)));
%SSK = wetbulb(P(2),P(4));
%SS= SSK-273.13;
%tlmd=(P(4)-SS);
%delta=(tlmn-tlmd)/(log(tlmn/tlmd));
%C9 = Uva*vol*delta;
C9 = C3;
C10 = M1*Mf*Cpv*P(4);
%C11 = Ma*(Cpao)*P(4);
% simultaneous differential equations
dP = zeros(4,1); % column vector
dP(1) = (M2/Mf)-M1;
dP(2) = (1/Ma)*(M3+M1*Mf);
dP(3)=(1/(Mf*Cpf))*(C1-C2+C3-C4-C5);
dP(4)=(1/(Ma*Cpao))*(C8-C80-C9+C10);
```

****

****

Appendix IV – Emission factors

Table 1 Emission factors for producing fossil fuels

Pollutants	Natural gas[1], g/kg	Coal[2], g/kg	Diesel[3], g/l
CO_2	487.16	20.14	3129.56
CO	1.88	0.02	6.28
SO_x	2.01	0.15	4.58
NO_x	3.44	0.10	24.75
CH_4	20.54	1.90	1.00
NH_3	nd	0.21	nd
VOCs	4.68	0.17	0.65
PM	0.16	0.03	1.06
N_2O	nd	nd	0.03
HCl	nd	nd	0.02
HF	nd	nd	nd
Benzene	0.48	nd	nd
Formaldehyde	nd	nd	nd

nd – no data available

[1] Data extracted from Spath and Mann (2001).

[2] Data extracted from Spath et al. (1999)

[3] Data extracted from Sheehan et al (1998)

Table 2 Emission factors from life cycle analysis of different electricity generation systems (Koch, 2000).

Pollutants	Natural gas power plant	Hydro power plant	Coal power plant	Biomass power plant
GHG, g CO_2 eqt./kWh	389 – 511	2.0 – 48	790 – 1182	15 – 101
SO_2, mg/kWh	4 - 15000	5.0 - 60	700 - 32321	12.0 - 140
NO_x, mg/kWh	13 - 1500	3.0 - 42	700 - 5273	701-1950
NMVOCs, mg/kWh	72 – 164	0	18 - 29	0
PM, mg/kWh	1.0 - 10	5	30 - 663	217 -320

NMVOCs – Non Methane Volatile Organic Compounds

Table 3 Emission data from natural gas combustion (EPA, 1995)

Pollutant	Emission factor (kg/10^6 m^3)
CO_2	1920000
N_2O (uncontrolled)	35.2
N_2O (controlled – low NO_x burner)	10.24
PM (Total)	121.6
PM (Condensable)	91.2
PM (Filtered)	30.4
SO_2	9.6
Methane	36.8
TOC (Total Organic Compounds)	176
VOC (Volatile Organic Compounds)	88
Lead	0.008

Table 4 Emission factors[1] for combustion of bituminous coal and wood residues (EPA, 1995)

Pollutants	wet wood, lb/mmbtu	Dry wood, lb/mmbtu	Bituminous coal, lb/ton
CO_2	195	195	72.6C
CO	0.6	0.6	0.5
SO_2	0.025	0.025	38S
NO_x	0.49	0.22	33
N_2O	0.013	0.013	0.09
VOCs	0.017	0.017	5.90E-05
PM	0.22	0.3	10A
PM_{10}	0.2	0.27	2.3A
$PM_{2.5}$	0.12	0.16	-
HCl	1.90E-02	1.90E-02	1.2
HF	nd	nd	0.15
CH_4	2.10E-02	2.10E-02	0.01
Dioxin, PCDD	2E-09	2E-09	4.28E-08
Furans, PCDF	2.40E-10	2.40E-10	2.01E-07

C – Carbon percentage in the fuel

A – Ash percentage in the fuel

S – Sulfur percentage in the fuel

nd – data not available

[1] Emission factors for the cyclonic fuel combustor

Table 5 Emission factors for the alfalfa dehydration plant (EPA, 1995).

Source	Emission factors (kg/t of pellet produced)	
	Particulate matters (PM)	
	Filterable	Condensable
Triple-pass dryer & cyclone		
- Gas-fired	2.4	0.5
Single-pass dryer & cyclone		
- Gas-fired	2.05	0.33
- Wood-fired	1.55	0.65

Table 6. Trace elements emissions from combustion of coal (Spath et al., 1999)

Trace elements	Emission factors, kg/kg of coal	Human toxicity potential to air
Antimony	1.84E-09	6.70E+03
Arsenic	2.20E-08	3.50E+03
Barium	5.83E-09	7.60E+02
Beryllium	7.17E-10	2.30E+05
Boron	7.62E-06	-
Cadmium	1.84E-09	1.50E+05
Chromium	2.64E-08	6.50E+02
Cobalt	3.09E-09	1.70E+04
Copper	1.03E-08	4.30E+03
Lead	1.34E-08	4.70E+02
Manganese	1.93E-08	-
Mercury	1.66E-08	6.00E+03
Molybdenum	1.70E-08	5.40E+03
Nickel	2.60E-08	3.50E+04
Selenium	1.84E-07	4.80E+04
Vanadium	3.94E-08	6.20E+03

Appendix V – Environmental and human impact potentials for some pollutants.

Table 1 Global Warming Potential (GWP) for greenhouse gases (IPCC, 1996)

Greenhouse Gas	GWP
Carbon dioxide (CO_2)	1
Methane (CH_4)	21
Nitrogen oxide (NOx)	40
Nitrous oxide (N_2O)	310

Table 2 Acid rain formation potential for some compounds (Heijungs et al., 1992)

Compound	a	MW_i (mol/kg)	η_i (mol H^+/kg i)	ARP_i
SO_2	2	0.064	31.25	1.00
NO	1	0.030	33.33	1.07
NO_2	1	0.046	21.74	0.70
NH_3	1	0.017	58.82	1.88
HCl	1	0.0365	27.40	0.88
HF	1	0.020	50.00	1.60

Table 3 Maximum incremental reactivities (MIR) for smog formation. (Carter, 1994).

Compound	MIR
Methane	0.015
Ethane	0.25
Propane	0.48
Alkanes(normal)	0.55
Alkanes(cyclic)	2.06
Acetylenes	2.3
Ketones	0.87
Alcohols & Ethers	1.32
Alkenes (primary)	5.66
Alkenes (secondary)	6.75
Alkenes (branched)	1.2
Alkenes (others- terpenes)	6.85
Aromatic oxygenates	0.95
Aromatics (avg)	4.34
Benzenes	0.42
Toluenes	2.7
Naphthalenes	1.17
Styrenes	2.2

Table 4 Human toxicity potentials for some metals and other pollutants (Huijbregts et al., 2000).

Trace elements & other pollutants[1]	Human toxicity potential to air
Trace elements	
Antimony	6.70E+03
Arsenic	3.50E+03
Barium	7.60E+02
Beryllium	2.30E+05
Cadmium	1.50E+05
Chromium	6.50E+02
Cobalt	1.70E+04
Copper	4.30E+03
Lead	4.70E+02
Mercury	6.00E+03
Molybdenum	5.40E+03
Nickel	3.50E+04
Selenium	4.80E+04
Vanadium	6.20E+03
Other pollutants	
Ammonia	0.1
Hydrogen sulfide	0.22
Hydrogen chloride	0.5
Sulfur dioxide	0.31
Nitrogen dioxide	1.2
PM10	0.096
Formaldehyde	0.64
Benzene	1900
Toluene	0.33
Phenol	0.52
Naphthalene	8.1
Carcinogenic PAHs	570,000
2,3,7,8 – TCDD	1.9E09

[1]Human toxicity potential to air for additional trace elements and other toxic pollutants can be obtained from Huijbregts et al. (2000).

Appendix VI – Description of PROMETHEE outranking approach.

The PROMETHEEE method (Preference Ranking Organization METHod for Enrichment Evaluation) outranks the set of actions or scenarios based on the value of criteria selected for those actions. Let us consider the multi-criteria problem

$$\text{Max or Min}\{f_1(a),............f_k(a); a \in K\}$$

where, K is the finite set of actions and $f_{i...k}$ are k criteria to be minimized or maximized. In order to outrank the actions, the PROMETHEE method uses a valued outranking relation based on a generalization of the notion of criterion is considered.

Let us compare two actions a and b with i number of criteria, a preference function, P is defined and evaluated in terms of preference. The preference function, P translates the difference between the evaluations obtained by two actions or alternatives in terms of a particular criterion into a preference degree ranging from 0 to 1.

P: K x K → (0,1) representing the intensity of preference of action a over b and such that

1. P(a, b) = 0 means no preference of a over b

2. P(a, b) ~ 0 means weak preference of a over b

3. P(a, b) ~ 1 means strong preference of a over b

4. P(a, b) = 1 means strict preference of a over b.

In practice, this preference function will be a function of the difference between the two evaluations. For each criterion f, a generalized criterion is defined by f and a corresponding preference function, P as

$$P(a, b) = G_f(f(a) - f(b)) \qquad 0 \leq P(a,b) \leq 1$$

Where G_f is a non-decreasing function of the observed deviation (d) between f(a) and f(b).

In order to facilitate the selection of a specific preference function, there are six types of generalized criteria function that are proposed in the PROMETHEE method (Brans et al., 1986). Among them only two of the criteria function is defined here.

1. Criterion with linear preference:

$$H(d) = \begin{cases} d/p & \text{if } -p \le d \le p \\ 1 & \text{if } d < -p \text{ or } d > p \end{cases}$$

where, d is the difference between two action criteria, p is a preference threshold. As long as d is lower than p, the preference of the decision maker increases linearly with d. If d becomes greater than p, the actions has strict preference situation. The linear criterion function is shown in figure 1.
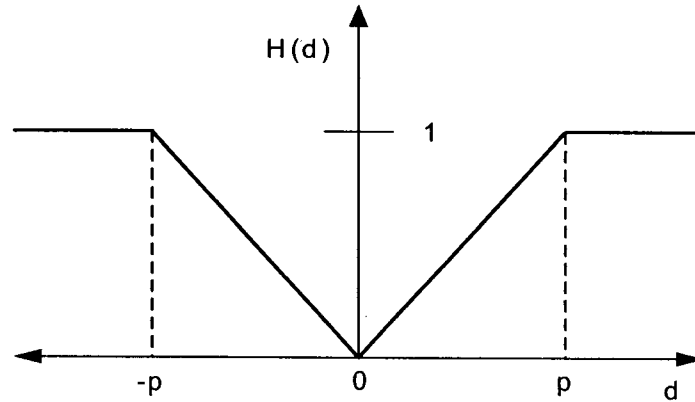

Figure 1. Criterion with linear preference function.

2. Level criterion

$$H(d) = \begin{cases} 0 & \text{if } |d| \le q, \\ 0.5 & \text{if } q < |d| \le p \\ 1 & \text{if } p < |d| \end{cases}$$

where, q is the indifference threshold. If d lies between q and p, there is a weak preference situation (H(d) = 0.5). The function is represented by Figure 2. Now, the decision maker has two thresholds to define. This criterion function is often used in evaluating qualitative criterion. Other criterion preference function can be found in Brans et al., (1986).
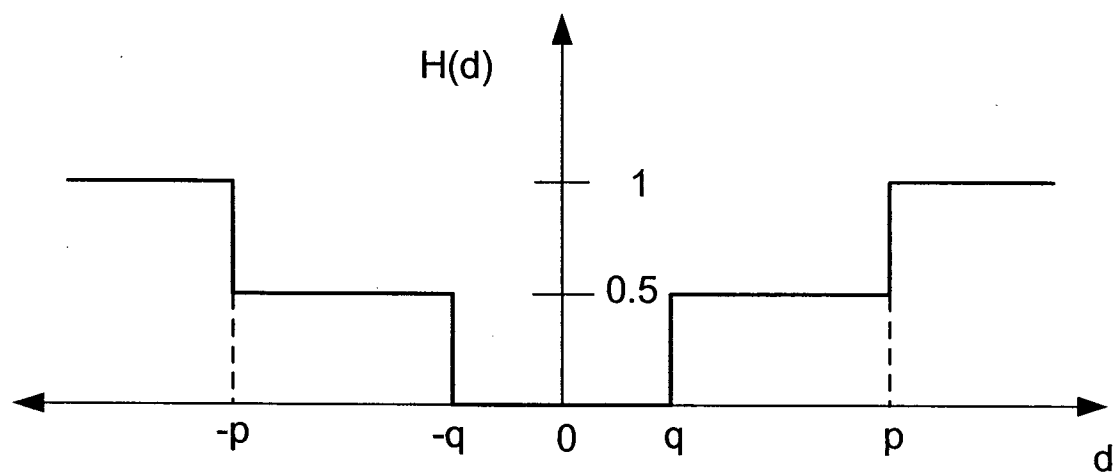
Figure 2. Level criterion function.

Appendix VII –Example of engineering cost calculations.

Table 1. List of parameters used in the calculations of the wood pellet production cost for the Princeton Pellet Plant (Scenario 7).

Parameters	Values
Plant capacity, t/h	11.5
Hours of operation per day, h	24
Total number of production days per year, days	310
Electricity cost, USD/kWh	0.05
Interest rate, %	6
Average equipment utilization period, y	10
Labor wage, USD	16
No. of shifts	3

Table 2. Details of engineering cost calculations in US dollars.

Equipment	Purchase cost ($)	Installation cost ($)	Equipment life (y)	Total equipment cost ($)	Capital cost ($/y)	Operating cost ($/y)	Total cost ($/y)
Solifd fuel burner	156858.98	78429.49	10	235288.47	31968.16	198202.79	230170.95
Rotary dryer	501005.27	300603.16	10	801608.43	108912.90	7856.64	116769.54
Dryer fan	25144.07	37716.11	10	52802.55	7174.18	39283.20	46457.38
Multicyclone	25359.89	10143.95	10	35503.84	4823.83	0.00	4823.83
Hammer mill	27242.61	8172.78	10	35415.39	4811.82	32862.90	37674.71
Pellet mill	797438.40	398719.20	10	1196157.60	162519.49	107635.97	270155.46
Pellet cooler	49709.34	24854.67	10	74564.01	10130.86	13213.44	23344.30
Pellet shaker	33085.64	19851.38	10	52937.02	7192.44	2624.83	9817.28
Bagging unit	131353.37	65676.69	10	197030.06	26770.07	4821.12	31591.19
Storage bin for fuel	9746.93	5848.16	15	15595.09	2118.87	0.00	2118.87
Front end loader	200000.00	0.00	10	200000.00	27173.59	383379.96	410553.55
Fork lift	82000.00	0.00	10	82000.00	11141.17	183287.40	194428.57
Truck	400000.00	0.00	10	400000.00	54347.18	280095.20	334442.38
Labor cost	0.00	0.00	-	0.00	0.00	1190400.00	1190400.00
Miscell Conveyors	42100.10	16840.04	8	58940.13	9491.48	13124.16	22615.64
Bucket elevators	35790.74	14316.30	8	50107.03	8069.03	2624.83	10693.87
Bottom bin	37629.85	22577.91	15	60207.76	7181.40	0.00	7181.40
Building	95875.08	0.00	20	95875.08	8358.83	7142.40	15501.23
Feeding system	16747.40	8373.70		25121.10	3413.15	3571.20	6984.35